BIOCHEMISTRY
including biophysical chemistry & molecular biology

Article

pubs.acs.org/biochemistry

Specific Stabilization of *c-MYC* and *c-KIT* G-Quadruplex DNA Structures by Indolylmethyleneindanone Scaffolds

K. V. Diveshkumar,[†] Saaz Sakrikar,[†] Frédéric Rosu,[‡,§] S. Harikrishna,[†] Valérie Gabelica,[*,§,⊥] and P. I. Pradeepkumar[*,†]

[†]Department of Chemistry, Indian Institute of Technology Bombay, Mumbai 400076, India
[‡]CNRS, UMS3033/US001, Institut Européen de Chimie et Biologie, 33607 Pessac, France
[§]Université de Bordeaux, U869 ARNA Laboratory, 33600 Pessac, France
[⊥]Inserm, U869 ARNA Laboratory, 33000 Bordeaux, France

Supporting Information

ABSTRACT: Stabilization of G-quadruplex DNA structures by small molecules has emerged as a promising strategy for the development of anticancer drugs. Since G-quadruplex structures can adopt various topologies, attaining specific stabilization of a G-quadruplex topology to halt a particular biological process is daunting. To achieve this, we have designed and synthesized simple structural scaffolds based on an indolylmethyleneindanone pharmacophore, which can specifically stabilize the parallel topology of promoter quadruplex DNAs (*c-MYC*, *c-KIT1*, and *c-KIT2*), when compared to various topologies of telomeric and duplex DNAs. The lead ligands (**InEt2** and **InPr2**) are water-soluble and meet a number of desirable criteria for a small molecule drug. Highly specific induction and stabilization of the *c-MYC* and *c-KIT* quadruplex DNAs ($\Delta T_{1/2}$ up to 24 °C) over telomeric and duplex DNAs ($\Delta T_{1/2} \sim 3.2$ °C) by these ligands were further validated by isothermal titration calorimetry and electrospray ionization mass spectrometry experiments ($K_a \sim 10^5$ to 10^6 M^{-1}). Low IC_{50} (~2 μM) values were emerged for these ligands from a *Taq* DNA polymerase stop assay with the *c-MYC* quadruplex forming template, whereas the telomeric DNA template showed IC_{50} values >120 μM. Molecular modeling and dynamics studies demonstrated the 5′- and 3′-end stacking modes for these ligands. Overall, these results demonstrate that among the >1000 quadruplex stabilizing ligands reported so far, the indolylmethyleneindanone scaffolds stand out in terms of target specificity and structural simplicity and therefore offer a new paradigm in topology specific G-quadruplex targeting for potential therapeutic and diagnostic applications.

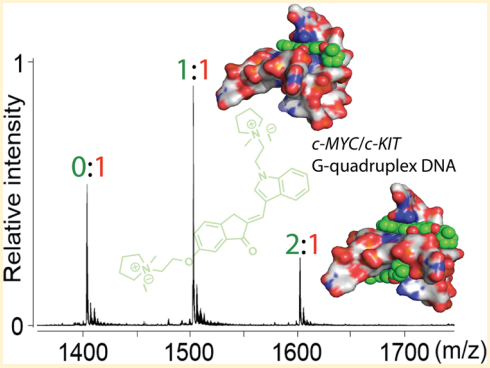

Tetrameric DNA structures formed by guanine-rich sequences in the presence of monovalent metal ions are called G-quadruplexes.[1,2] These structures consist of planar arrangements called G-quartets, formed by the association of four guanine bases through the hydrogenbonding interactions of Hoogsteen and Watson−Crick faces of the adjacent guanines. Putative G-quadruplex forming sequences have been identified in the various parts of human genome such as in telomeres,[3,4] promoter regions of various oncogenes,[5] introns,[6] and the immunoglobulin switch regions.[7]

G-quadruplex structures present in the telomeric and the promoter regions have emerged as attractive drug targets due to their biological relevance.[5] Promoter regions of many proto oncogenes such as *c-MYC*, *c-KIT*, *BCL-2*, *k-RAS*, *VEGF*, *HIF-1α*, and *PDGF-A* possess G-rich sequences that have the propensity to form G-quadruplex structures.[8−13] In such regions, molecular crowding conditions due to the high concentration of macromolecules and the dynamic forces evolved from negative superhelicity promote the formation of G-quadruplex structures from duplex DNAs.[5,14] The identification of proteins that have a crucial role in unwinding the quadruplex structures further validates the existence of such G-quadruplex structures *in vivo*.[15]

Small molecules that can stabilize the quadruplex structures present in the promoter regions can effectively inhibit the transcription process.[5] Recently, such approaches have been touted as promising new directions in the anticancer drug discovery.[5] Major challenges in G-quadruplex mediated anticancer drug development are to achieve selectivity toward the G-quadruplexes over the duplex DNAs, to impart specificity among the different topologies of Gquadruplexes, and moreover to engineer drug-like properties to the stabilizing ligands.[16]

G-quadruplex structures can exhibit different topologies depending on the nature and length of the sequence, size/length of the loops, presence of metal ions, and conformations of the glycosidic bonds.[17,18] Telomeric quadruplex DNAs are

Received: February 11, 2016
Revised: May 23, 2016
Published: May 25, 2016

DOI: 10.1021/acs.biochem.6b00120
Biochemistry 2016, 55, 3571−3585

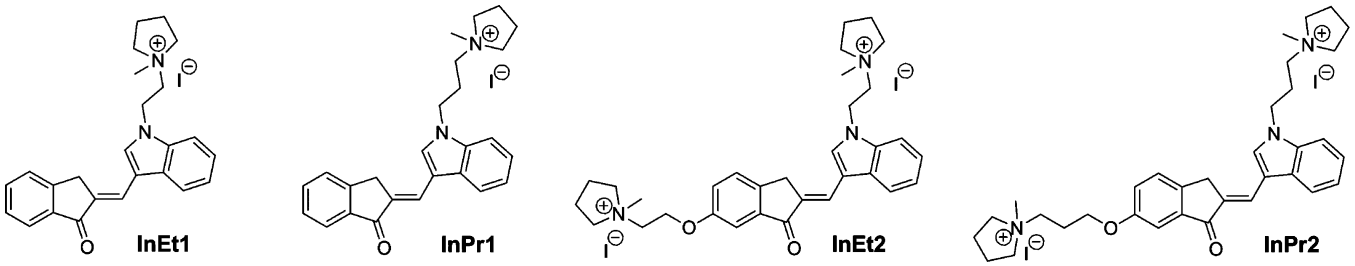

Figure 1. Structures of indolylmethyleneindanone based scaffolds used to achieve topology specific stabilization of *c-MYC* and *c-KIT* promoter G-quadruplex DNAs.

highly polymorphic in nature and exist in different topologies including antiparallel, hybrid, and mixed hybrid, whereas promoter quadruplex DNAs mostly exist in parallel topology with propeller loops.[19] Since all the G-quadruplexes have identical G-quartet interfaces in their structures, achieving specificity toward a particular topology is a daunting task. However, subtle differences in the quartet surface area, size/length of the loops, and nature of the grooves of the different quadruplex topologies can be harnessed to design topology specific ligands. There are only limited reports in the literature describing those ligands, which are able to achieve topology specific stabilization of quadruplex structures. Among those, most of the ligands have shown a moderate preference for one of the topologies of telomeric quadruplex DNA as revealed from a few biophysical screening assays.[20−24] The ligands, which show preferential stabilization toward *c-MYC* quadruplex DNA over duplex DNA, include furan based cyclic oligopeptides,[25] ellipticine derivatives,[26] piperazinylquindoline derivatives,[27] and metallorectangles with terpyridine ligands.[28] However, these molecules were found to have affinity toward telomeric quadruplex DNAs as well. Diethynylpyridine derivatives were reported for their selective stabilization toward various promoter quadruplexes over duplex DNAs.[29] Similarly, bisaryldiketene derivatives were studied for their preferential affinity toward promoter quadruplexes over duplex DNAs and telomeric quadruplex DNAs.[30] Recently, a new class of small molecules has been reported as a strong inhibitor of *c-MYC* expression via quadruplex stabilization, which was identified using small molecule microarray.[31] None of these ligands were reported to have specificity toward parallel topology of promoter quadruplex DNAs over various topologies of telomeric and duplex DNAs. An exception to this is the peptidomimetic ligands that have shown marginal specificity toward the *c-KIT1* quadruplex structure.[32]

Recently, our group has reported indenopyrimidine derivatives and bisbenzimidazole carboxamide derivatives of naphthiridine and phenanthroline that can specifically stabilize *c-MYC* and *c-KIT* quadruplex DNAs having parallel topology over telomeric quadruplex and duplex DNAs.[33,34] Even though these ligands were able to achieve specificity toward a particular topology, weak stabilization property for indenopyrimidine derivatives and poor druglike properties due to the presence of multiple aromatic rings and heteroatoms for the latter one weaken the therapeutic index of these molecules. Apart from achieving high specificity toward a particular G-quadruplex topology, for clinical success, development of anticancer molecules having druglike properties is highly warranted.[16] To fill this lacuna, herein, we report a new qudruplex stabilizing ligand family having simple scaffolds based on an indolylmethyleneindanone skeleton (**InEt1**, **InEt2**, **InPr1**, and **InPr2**, Figure 1). Topology specific stabilization of these ligands with *c-MYC* and *c-KIT* quadruplex DNAs having parallel topologies was unambiguously validated using various biophysical, biochemical, and molecular modeling and dynamics studies.

MATERIALS AND METHODS

General Methods. Dry solvents (DMF, $CHCl_3$, toluene) were obtained from commercial suppliers and CH_3CN and DCM were dried using calcium hydride. Thin layer chromatography (TLC) was performed on silica gel plates precoated with fluorescent indicator with visualization by UV light (260 nm). Silica gel (100−200 mesh) or basic alumina was used for column chromatography. ^{13}C NMR (100 and 125 MHz) and ^{1}H NMR (400 and 500 MHz) were recorded on 400 and 500 MHz instruments, respectively. The chemical shifts in parts per million (ppm) were referenced to the residual signal of deuteriated solvents or TMS: TMS (0 ppm), CD_3OD (3.31 ppm), and DMSOd_6 (2.5 ppm) for ^{1}H NMR spectra; and $CDCl_3$ (77.2 ppm), CD_3OD (49.1 ppm), and DMSOd_6 (39.5 ppm) for ^{13}C NMR spectra. Multiplicities of ^{1}H NMR spin couplings are reported as s (singlet), d (doublet), t (triplet), q (quartet), dd (doublet of doublets), and (q) quintet or m (multiplet and overlapping spin systems). Values for apparent coupling constants (J) are reported in Hz. High resolution mass spectra (HRMS) were obtained in positive ion electrospray ionization (ESI) mode using a QTOF analyser. The molecular structures of all the compounds described below are shown in Scheme 1.

Method A: General Procedure for Bromination. Aldol product (1 equiv) was dissolved in dry DMF (7 mL/mmol), and to this anhydrous K_2CO_3 (2 equiv) and corresponding dibromoalkane (2 equiv) were added under nitrogen at 0 °C. After being stirred at room temperature for 24 h, water was added and extracted with EtOAc. The organic layer was dried over anhydrous Na_2SO_4, evaporated under reduced pressure, and purified by column chromatography (12% EtOAc in pet ether) using silica gel as a stationary phase to afford the brominated compounds.

Method B: General Procedure for Bromine Displacement. Brominated compound (1 equiv) was dissolved in dry ACN (6 mL/mmol) and to this pyrrolidine (3−10 equiv) was added, and the mixture was refluxed for 3−4 h. Solvent was evaporated under reduced pressure, and the crude product was purified by column chromatography (0−1% MeOH in DCM) using basic alumina as a stationary phase.

Method C: General Procedure for Methylation. Compound (1 equiv) was dissolved in dry ACN (6 mL/mmol), and to this excess methyl iodide (16−32 equiv) was added and the mixture was refluxed for 12 h. Solvent was evaporated, and the solid product was washed with chloroform

DOI: 10.1021/acs.biochem.6b00120
Biochemistry 2016, 55, 3571−3585

for removing the impurities to afford the methylated iodide salts.

Method D: General Procedure for Aldol Condensation. Aldehyde (1 equiv) and ketone (1 equiv) were dissolved in acetic acid (8 mL/mmol). To this, 4 or 5 drops of concentrated HCl was added and the mixture was refluxed for 3−4 h. The reaction mixture was poured into water and extracted with EtOAc. The organic layer was dried over anhydrous Na_2SO_4, evaporated under reduced pressure, and purified by column chromatography (15−20% EtOAc in pet ether) using silica gel as the stationary phase to yield the condensed aldol products.

*(E)-2-((1-(2-Bromoethyl)-1H-indol-3-yl)methylene)-2,3-dihydro-1H-inden-1-one (**2**).* Method A was followed using compound **1** (320 mg, 1.23 mmol), in dry DMF (6 mL), anhydrous K_2CO_3 (341 mg, 2.46 mmol) and 1,2-dibromoethane (0.21 mL, 2.46 mmol) to afford compound **2** as a yellow solid (351 mg, 78%). M. p. 167−169 °C. ^{1}H NMR (400 MHz, $CDCl_3$): δ 8.00 (s, 1H), 7.88 (dd, J = 14.6, 7.0 Hz, 2H), 7.47−7.56 (m, 3H), 7.37 (t, J = 7.6 Hz, 1H), 7.21−7.32 (m, 3H), 4.55 (t, J = 6.4 Hz, 2H), 3.75 (br, 2H), 3.70 (t, J = 6.4 Hz, 2H). ^{13}C NMR (100 MHz, $CDCl_3$): δ 193.8, 148.7, 139.1, 135.8, 134.0, 130.6, 130.0, 128.8, 127.5, 126.1, 124.9, 124.1, 123.5, 121.6, 119.6, 113.1, 109.4, 48.5, 33.2, 29.7. HRMS (ESI): Calcd for $C_{20}H_{17}NOBr$ $[(M + H)]^+$ 366.0494; found, 366.0484 (Δm −0010 and error −2.7 ppm).

*(E)-2-((1-(3-Bromopropyl)-1H-indol-3-yl)methylene)-2,3-dihydro-1H-inden-1-one (**3**).* Method A was followed using compound **1** (305 mg, 1.18 mmol) in dry DMF (6 mL), anhydrous K_2CO_3 (325 mg, 2.35 mmol), and 1,3-dibromopropane (0.24 mL, 2.35 mmol) to afford compound **3** as a yellow solid (356 mg, 79%). M.p. 165−166 °C. ^{1}H NMR (400 MHz, $CDCl_3$): δ 8.06 (s, 1H), 7.91 (dd, J = 15.2, 7.36 Hz, 2H), 7.52−7.59 (m, 3H), 7.40 (t, J = 8.5 Hz, 2H), 7.267.32 (m, 2H), 4.42 (t, J = 6.4 Hz, 2H), 3.83 (br, 2H), 3.34 (t, J = 6.1 Hz, 2H), 2.41 (q, J = 6.1 Hz, 2H). ^{13}C NMR (100 MHz, $CDCl_3$): δ 193.9, 148.7, 139.2, 136.0, 134.0, 130.3, 130.2, 128.9, 127.6, 126.1, 125.2, 124.1, 123.4, 121.5, 119.6, 112.9, 109.9, 44.7, 33.3, 32.2, 30.4. HRMS (ESI): Calcd for $C_{21}H_{19}NOBr$ $[(M + H)]^+$ 381.0623; found, 381.0620 (Δm −0003 and error −0.8 ppm).

*(E)-2-((1-(2-Cyclopentylethyl)-1H-indol-3-yl)methylene)-2,3-dihydro-1H-inden-1-one (**4**).* Method B was followed using compound **2** (84 mg, 0.23 mmol) in dry ACN (2 mL), pyrrolidine (0.06 mL, 0.69 mmol) to afford compound **4** as a yellow sticky solid (60 mg, 74%). ^{1}H NMR (400 MHz, $CDCl_3$): δ 8.06 (s, 1H), 7.90 (dd, J = 12.9, 7.3 Hz, 2H), 7.60 (s, 1H), 7.49−7.57 (m, 2H), 7.22−7.39 (m, 4H), 4.31 (t, J = 7.0 Hz, 2H), 3.80 (br, 2H), 2.93 (t, J = 7.0, 2H), 2.57 (br, 4H), 1.80 (br, 4H). ^{13}C NMR (100 MHz, $CDCl_3$): δ 193.9, 148.7, 139.4, 136.3, 133.9, 130.5, 129.9, 128.7, 127.5, 126.1, 125.5, 124.1, 123.2, 121.3, 119.4, 112.7, 109.9, 55.6, 54.5, 46.5, 33.3, 23.7. HRMS (ESI): Calcd for $C_{24}H_{25}N_2O$ $[(M+H)]^+$ 357.1961; found, 357.1966 (Δm +0005 and error +1.3 ppm).

*(E)-2-((1-(3-Cyclopentylpropyl)-1H-indol-3-yl)methylene)-2,3-dihydro-1H-inden-1-one (**5**).* Method B was followed using compound **3** (175 mg, 0.46 mmol) in dry ACN (4 mL) and pyrrolidine (0.15 mL, 1.83 mmol) to afford compound **5** as a yellow sticky solid (140 mg, 82%). ^{1}H NMR (400 MHz, $CDCl_3$): δ 8.10 (s, 1H), 7.92 (dd, J = 12.0, 7.48 Hz, 1H), 7.527.61 (m, 3H), 7.38−7.42 (m, 2H), 7.247.31 (m, 2H), 4.30 (t, J = 6.7 Hz, 2H), 3.83 (br, 2H), 2.50 (br, 4H), 2.43 (t, J = 6.7 Hz, 2H), 2.08 (q, J = 6.7 Hz, 2H), 1.82 (q, J = 3.2 Hz, 4H). ^{13}C NMR (100 MHz, $CDCl_3$): δ 194.0, 148.7, 139.4, 136.4, 133.9, 130.6, 129.7, 128.8, 127.5, 126.1, 125.7, 124.1, 123.1, 121.2, 119.4, 112.5, 110.1, 54.2, 52.8, 44.9, 33.4, 29.2, 23.7. HRMS (ESI): Calcd for $C_{25}H_{27}N_2O$ $[(M + H)]^+$ 371.2196; found, 371.2192 (Δm −0004 and error −1.2 ppm).

(E)-1-Methyl-1-(2-(3-((1-oxo-1H-inden-2(3H)-ylidene)-methyl)-1H-indol-1-yl)ethyl)pyrrolidinium Iodide (InEt1). Method C was followed using compound **4** (30 mg, 0.08 mmol), in dry ACN (2 mL) and excess methyl iodide (1 mL, 16 mmol) to afford the final methylated iodide salt **InEt1** as a yellow solid (35 mg, 89%). M. p. 251253 °C. ^{1}H NMR (500 MHz, DMSOd_6): δ 8.24 (s, 1H), 7.96 (d, J = 7.74 Hz, 1H), 7.89 (s, 1H), 7.67−7.79 (m, 4H), 7.49 (t, J = 7.2 Hz, 1H), 7.36 (t, J = 7.5 Hz, 1H), 7.28 (t, J = 7.2 Hz, 1H), 4.87 (t, J = 7.5 Hz, 2H), 4.00 (br, 2H), 3.88 (t, J = 7.2 Hz, 2H), 3.19 (s, 3H), 2.13 (br, 4H). ^{13}C NMR (125 MHz, DMSOd_6): δ 192.6, 149.0, 138.6, 135.8, 134.5, 131.8, 130.4, 128.1, 127.8, 126.5, 124.2, 123.5, 123.3, 121.6, 118.9, 112.1, 110.9, 64.3, 61.0, 48.1, 40.7, 32.9, 21.2. HRMS (ESI): Calcd for $C_{25}H_{27}N_2O$ $[M - I]^+$ 371.2118; found, 371.2122 (Δm −0004 and error −1.2 ppm).

(E)-1-Methyl-1-(3-(3-((1-oxo-1H-inden-2(3H)-ylidene)-methyl)-1H-indol-1-yl)propyl)pyrrolidinium Iodide (InPr1). Method C was followed using compound **5** (35 mg, 0.09 mmol)in dry ACN (3 mL) and excess methyl iodide (1 mL, 16 mmol) to afford the final methylated iodide salt **InPr1** (42 mg, 87%). M.p. 251−252 °C. ^{1}H NMR (400 MHz, DMSOd_6): δ 8.13 (s, 1H), 7.94 (d, J = 7.52 Hz, 1H), 7.90 (s, 1H), 7.77 (d, J = 7.52 Hz, 1H), 7.64−7.73 (m, 3H), 7.49 (d, J = 6.45 Hz, 1H), 7.30−7.36 (m, 1H), 7.26 (d, J = 7.52 Hz, 1H), 4.41 (t, J = 6.98 Hz, 2H), 4.00 (s, 2H), 2.98 (s, 3H), 2.34 (br, 2H), 2.07 (br, 4H). ^{13}C NMR (100 MHz, DMSO-d_6): δ 192.0, 148.5, 138.2, 135.6, 133.9, 131.4, 129.4, 127.7, 127.3, 126.0, 124.1, 123.0, 122.6, 120.9, 118.3, 111.0, 110.3, 63.4, 60.2, 47.3, 32.4, 23.9, 20.7. HRMS (ESI): Calcd for $C_{26}H_{29}N_2O$ $[M - I]^+$ 385.2273; found, 385.2274 (Δm +0001 and error +0.3 ppm).

*(E)-6-(2-Bromoethoxy)-2-((1-(2-bromoethyl)-1H-indol-3-yl)methylene)-2,3-dihydro-1H-inden-1-one (**10**).* Method D was followed using compound **6** (140 mg, 0.55 mmol) and compound **8** (130 mg, 0.55 mmol) in acetic acid (4 mL) to yield compound **10** as a yellow solid (210 mg, 78%). M.p. 178−180 °C. ^{1}H NMR (400 MHz, $CDCl_3$): δ 8.05 (s, 1H), 7.96 (d, J = 7.3 Hz, 1H), 7.58 (s, 1H), 7.45 (d, J = 8.2 Hz, 1H), 7.287.39 (m, 4H), 7.19 (dd, J = 5.8, 2.3 Hz, 1H), 4.63 (t, J = 6.7 Hz, 2H), 4.36 (t, J = 6.1 Hz, 2H), 3.81 (s, 2H), 3.73 (t, J = 6.4 Hz, 2H), 3.68 (t, J = 5.8 Hz, 2H). ^{13}C NMR (100 MHz, $CDCl_3$): δ 193.6, 158.1, 142.0, 140.5, 135.8, 131.4, 130.1, 128.9, 127.1, 125.1, 123.6, 121.7, 119.7, 113.1, 109.5, 106.8, 68.2, 48.6, 32.7, 29.8, 29.6, 29.2. HRMS (ESI): Calcd for $C_{22}H_{20}Br_2$ NO_2 $[(M + H)]^+$ 489.9831; found, 489.9831.

*(E)-6-(3-Bromopropoxy)-2-((1-(3-bromopropyl)-1H-indol-3-yl)methylene)-2,3-dihydro-1H-inden-1-one (**11**).* Method D was followed using compound **7** (105 mg, 0.39 mmol) and compound **9** (104 mg, 0.39 mmol) in acetic acid to yield compound **11** as a yellow solid (150 mg, 74%). M.p. 176−178 °C. ^{1}H NMR (400 MHz, $CDCl_3$): δ 8.03 (s, 1H), 7.94 (d, J = 7.5 Hz, 1H), 7.57 (s, 1 H), 7.26−7.43 (m, 5H), 7.15 (d, J = 6.5 Hz, 1H), 4.42 (t, J = 6.0 Hz, 2H), 4.16 (t, J = 5.5 Hz, 2H), 3.76 (br, 2H), 3.62 (t, J = 6.2 Hz, 2H), 3.34 (t, J = 5.7 Hz, 2H), 2.39 (q, J = 6.0 Hz, 2H), 2.35 (t, J = 5.7 Hz, 2H). ^{13}C NMR (100 MHz, $CDCl_3$): δ 193.7, 158.6, 141.6, 140.5, 136.0, 131.2, 130.2, 128.9, 126.9, 125.1, 123.4, 123.3, 121.5, 119.5, 112.9, 109.9, 106.7, 65.8, 44.7, 32.6, 32.4, 32.3, 30.4, 30.0. HRMS (ESI): Calcd for $C_{24}H_{23}Br_2NO_2$ $[(M + H)]^+$ 518.0149; found, 518.0152 (Δm +0003 and error +0.5 ppm).

DOI: 10.1021/acs.biochem.6b00120
Biochemistry 2016, 55, 3571−3585

*(E)-6-(2-(Pyrrolidin-1-yl)ethoxy)-2-((1-(2-(pyrrolidin-1-yl)-ethyl)-1H-indol-3-yl)methylene)-2,3-dihydro-1H-inden-1-one (**12**).* Method B was followed using compound **10** (50 mg, 0.1 mmol) in dry ACN (2 mL) and pyrrolidine (0.08 mL, 1 mmol) to afford compound **12** as a yellow sticky solid (40 mg, 85%). ^{1}H NMR (400 MHz, $CDCl_3$): δ 8.05 (s, 1H), 7.93 (d, J = 7.5 Hz, 1H), 7.60 (s, 1H), 7.17−7.30 (m, 3H), 7.357.47 (m, 3H), 4.31(t, J = 7.0 Hz, 2H), 4.17 (t, J = 5.7 Hz, 2H), 3.74 (s, 2H), 2.90−2.98 (m, 4H), 2.65 (br, 4H), 2.58 (br, 4H), 1.80 (br, 8H). ^{13}C NMR (100 MHz, $CDCl_3$): δ 193.8, 158.8, 141.4, 140.5, 136.2, 130.8, 130.5, 128.7, 126.7, 125.4, 123.5, 123.1, 121.2, 119.4, 112.7, 109.9, 106.6, 67.5, 55.5, 55.1, 54.8, 54.5, 46.4, 32.7, 23.7, 23.6. HRMS (ESI): Calcd for $C_{30}H_{36}N_3O_2$ [(M + H)]$^+$ 470.2802; found, 470.2804 (Δm +0002 and error +0.5 ppm).

*(E)-6-(3-(Pyrrolidin-1-yl)propoxy)-2-((1-(3-(pyrrolidin-1-yl)-propyl)-1H-indol-3-yl)methylene)-2,3-dihydro-1H-inden-1-one (**13**).* Method B was followed using compound **11** (60 mg, 0.11 mmol) in dry ACN (2 mL) and pyrrolidine (0.1 mL, 1.16 mmol) to afford compound **13** as a yellow sticky solid (48 mg, 88%). ^{1}H NMR (400 MHz, $CDCl_3$): δ 8.03 (s, 1H), 7.90 (dd, J = 4.4, 2.0 Hz, 1H), 7.51 (s, 1H), 7.21−7.36 (m, 5H), 7.12 (dd, J = 5.5, 2.6 Hz, 1H), 4.24 (t, J = 6.4 Hz, 2H), 4.05 (t, J = 6.4 Hz, 2H), 3.67 (br, 2H), 2.63 (t, J = 7.6 Hz, 2H), 2.54 (br, 4H), 2.48 (br, 4H), 2.41 (t, J = 6.7 Hz, 2H), 1.97−2.09 (m, 4H), 1.79 (br, 8H). ^{13}C NMR (100 MHz, $CDCl_3$): δ 193.8, 158.9, 141.2, 140.5, 136.3, 130.6, 130.5, 128.7, 126.7, 125.4, 123.2, 123.0, 121.1, 119.2, 112.4, 110.0, 106.6, 66.8, 54.3, 54.1, 53.1, 52.8, 44.8, 32.6, 29.1, 28.8, 23.6, 23.5. HRMS (ESI): Calcd for $C_{32}H_{40}N_3O_2$ [(M + H)] $^+$ 498.3115; found, 498.3117 (Δm +0002 and error +0.5 ppm).

*(E)-1-Methyl-1-(2-(3-((6-(2-(1-methylpyrrolidinium-1-yl)-ethoxy)-1-oxo-1H-inden-2(3H)-ylidene)methyl)-1H-indol-1-yl)ethyl)pyrrolidinium Iodide (**InEt2**).* Method C was followed using compound **12** (30 mg, 0.06 mmol) in dry ACN (2 mL) and excess methyl iodide (2 mL, 32 mmol) to yield the final methylated iodide salt **InEt2** as a yellow solid (43 mg, 90%). M.p. 262−263 °C. ^{1}H NMR (500 MHz, DMSOd_6): δ 8.28 (s, 1H), 7.98 (d, J = 7.9 Hz, 1H), 7.90 (s, 1H), 7.77 (d, J = 8.2 Hz, 1H), 7.63 (d, J = 8.2 Hz, 1H), 7.33−7.40 (m, 3H), 7.29 (d, J = 7.78 Hz, 1H), 4.90 (t, J = 7.3 Hz, 2H), 4.59 (t, J = 4.5 Hz, 2H), 3.98 (s, 2H), 3.87−3.94 (m, 4H), 3.63 (br, 8H), 3.22 (s, 3H), 3.14 (s, 3H), 2.14 (br, 8H). ^{13}C NMR (125 MHz, DMSOd_6): δ 192.6, 157.7, 142.5, 140.2, 136.2, 132.2, 131.4, 128.4, 127.7, 124.6, 123.6, 123.5, 121.9, 119.2, 112.3, 111.3, 107.4, 64.7, 64.6, 63.0, 62.1, 61.3, 48.5, 48.4, 48.3, 32.7, 21.5, 21.4. HRMS (ESI): Calcd for $C_{32}H_{41}N_3O_2$ [(M/2)]$^+$ 249.6591; found, 249.6594 (Δm +0003 and error +1 ppm).

*(E)-1-Methyl-1-(3-(3-((6-(3-(1-methylpyrrolidinium-1-yl)-propoxy)-1-oxo-1H-inden-2(3H)-ylidene)methyl)-1H-indol-1-yl)propyl)pyrrolidinium Iodide (**InPr2**).* Method C was followed using compound **13** (25 mg, 0.05 mmol) in dry ACN (2 mL) and excess methyl iodide (2 mL, 32 mmol) to afford the final methylated iodide salt **InPr2** as a yellow solid (32 mg, 82%). M.p. 258−260 °C. ^{1}H NMR (500 MHz, DMSOd_6): δ 8.13 (s, 1H), 7.94 (d, J = 7.9 Hz, 1H), 7.88 (s, 1H), 7.71 (d, J = 8.2 Hz, 1H), 7.60 (d, J = 7.9 Hz, 1H), 7.23−7.35 (m, 4H), 4.42 (t, J = 7.0 Hz, 2H), 4.17 (t, J = 5.8 Hz, 2H), 3.94 (s, 2H), 3.40−3.56 (m, 12H), 3.05 (s, 3H), 2.99 (s, 3H), 2.33 (q, J = 7.6 Hz, 2H), 2.25 (q, J = 6.1 Hz, 2H), 2.082.12 (m, 8H). ^{13}C NMR (125 MHz, DMSOd_6): δ 192.3, 158.0, 141.5, 139.8, 135.9, 131.7, 130.4, 128.0, 127.2, 124.4, 122.9, 122.7, 121.1, 118.6, 111.2, 110.7, 106.6, 65.2, 63.7, 63.6, 60.5, 60.4, 47.7, 47.6, 43.3, 33.5, 32.1, 24.3, 23.3, 21.1. HRMS (ESI): Calcd for $C_{34}H_{45}N_3O_2$ [(M/2)]$^+$ 263.6750; found, 263.6753 (Δm +0003 and error +0.9 ppm).

Oligonucleotides. Oligonucleotides used for CD titration, melting, ESI-MS, and ITC experiments are listed in Table S1. Oligonucleotides except for those used for ESI-MS experiments were synthesized using a Mermade-4 DNA/RNA synthesizer and were purified by 20% PAGE using standard protocols. Integrity of all the oligonucleotides was confirmed by MALDI-TOF/TOF (Brucker autoflex speed) spectrometry. The concentration of all the oligonucleotides was measured at 260 nm in UV−Vis spectrophotometer (PerkinElmer-Lamda Bio$^+$) using appropriate molar extinction coefficients (ε). For the ESIMS experiments oligonucleotides (Table S1) were purchased from Eurogentec (Seraing, Belgium) with RP Cartridge-Gold purification and reconstituted in water as received.

CD Titration Studies. CD spectra were recorded on a Jasco J-815 CD spectrophotometer in the wavelength range of 220−320 nm using a quartz cuvette with 1.0 mm path length. The scanning speed of the instrument was set to 100 nm/min, and the response time was 2 s. Baseline was measured using 50 mM Tris buffer, pH 7.2, and the strand concentration of oligonucleotide used was 12.5 μM. Each spectrum is an average of three measurements at 25 °C. All spectra were analyzed using Origin 8.0 software.

CD Melting Studies. For the melting studies, 10 μM strand concentration of oligonucleotide for quadruplex, and 15 μM for duplex DNAs in 10 mM lithium cacodylate (pH 7.2), the required amount of monovalent salts (LiCl and KCl) and 5 mol equiv of ligands were used. *c-MYC* DNA (10 μM in 1 mM KCl and 99 mM LiCl), *c-KIT1* DNA (10 μM DNA in 10 mM KCl and 90 mM LiCl), *c-KIT2* DNA (10 μM in 1 mM KCl and 99 mM LiCl), telomeric DNA (10 μM DNA in 10 mM KCl and 90 mM LiCl), and duplex DNA (15 μM in 10 mM KCl and 90 mM LiCl) were annealed by heating at 95 °C for 5 min followed by gradual cooling to room temperature. Ligands (5 equiv) were added to the annealed DNAs, and samples were kept at 4 °C for overnight. Thermal melting was monitored at 295, 263, and 242 nm for telomeric, promoter, and duplex DNAs respectively at a heating rate of 1 °C/min. The melting temperatures were determined from the sigmoidal curve fit using the Boltzmann function in Origin 8.0 software.

Native Electrospray Ionization Mass Spectrometry. Electrospray ionization mass spectrometry (ESI-MS) experiments were performed on an Agilent 6560 DTIMS-Q-TOF spectrometer (Agilent Technologies, Santa Clara, CA), with the dual-ESI source operated in negative ion mode. Duplex and quadruplex solutions were prepared in 100 mM NH_4OAc, pH 7.0. The drug−nucleic acids complexes were analyzed at a concentration 5 μM in 100 mM ammonium acetate. The trapping funnel was tuned to avoid energizing of the complexes (RF lower than 200 V for the ion funnel, and low extraction potentials). The data were analyzed using the Agilent MassHunter software (version B.07).

Isothermal Titration Calorimetry. Calorimetric experiments were carried out using a MicroCal iTC-200. All the DNA samples (50 μM in 100 mM KCl and 10 mM Lithium cacodylate buffer, pH 7.2) were preannealed by heating at 95 °C for 5 min and then gradual cooling to room temperature over 3−4 h. Titrations were carried out by overfilling the DNA samples (50 μM) in the sample cell ∼300 μL and by titrating with ligand solution (2.5 mM under similar salt and buffer

DOI: 10.1021/acs.biochem.6b00120
Biochemistry 2016, 55, 3571−3585

conditions) over 35−40 injections. During the experiment the temperature of the sample and reference cells was maintained at 25 °C. Volume for each ligand injection was 1 μL for 2 s, and the time interval between successive injection was 120 s. To nullify the heats of dilution, the same concentration of ligand was titrated against the buffer under similar conditions and was subtracted from the raw data prior to the curve fitting. The dilution corrected data were fitted using a sequential binding model in Origin 7 to derive the thermodynamic parameters for the DNA−ligand interactions.

5′-End-Radiolabeling of Oligonucleotides. Labeling of the primer was performed by following the previously reported protocol.[35] DNA (10 pmol) was 5′ end labeled by T4 polynucleotide kinase (PNK) enzyme (5 U) in 1× PNK buffer for the forward reaction [50 mM Tris-HCl, pH 7.6, 10 mM $MgCl_2$, 5 mm DTT, 0.1 mM each spermidine and 0.1 mM EDTA] and [γ-^{32}P]ATP (30 μCi) in a total volume of 10 μL for 1 h at 37 °C followed by deactivation of the enzyme by heating at 70 °C for 3 min. The end labeled DNA was then purified using a QIAquick Nucleotide removal kit by employing protocol provided by the manufacturer.

Electrophoretic Shift Mobility Assay. The appropriate amount of labeled oligonucleotides (∼18 000 CPM) was mixed with corresponding cold oligonucleotides (5 μM in 10 mM Tris buffer, pH 7.2) and was annealed by heating at 95 °C followed by gradual cooling to room temperature over 3−4 h. Various amounts (0−10 equiv) of ligands were incubated with the annealed DNA at 4 °C for overnight (final volume 10 μL). 1 μL of 10× glycerol dye [60% glycerol (v/v), 0.1% each bromophenol blue, and xylene cyanol (w/v)] was added prior to loading the reaction mixture onto the gel. Analysis was carried out in 15% native PAGE at 22 °C in which 1× TBE (89 mM of each Tris and boric acid and 2 mM of EDTA, pH 8.3) was used as running buffer, and gels were autoradiographed using a phosphorimager, Storm 825. Quantification of gels was performed using ImageQuant 5.2 software.

***Taq* DNA Polymerase Stop Assay.** This assay was performed using reported procedures.[36,37] An appropriate amount of labeled primer (∼20 000 CPM) was mixed with cold primer (50 nM) and template (100 nM), and they were annealed in an annealing buffer [5 mM Tris (pH 8), 10 mM NaCl, 0.1 mM EDTA] by heating at 95 °C for 5 min and then gradual cooling to room temperature over 3−4 h. The annealed primer−template was mixed with 1× polymerase buffer [50 mM Tris, 0.5 mM DTT, 0.1 mM EDTA, 5 mM $MgCl_2$, 5 mM KCl for *c-MYC* template and 10 mM KCl for telomeric template], 1 μg/μL BSA in 5% glycerol (v/v), and 0.2 mM dNTPs. The ligands in the appropriate concentration were added to the reaction mixture (10 μL total volume), and incubated for 30 min at room temperature. Finally, the primer extension reaction was initiated by adding *Taq* DNA polymerase enzyme (0.5 U) and incubating at 50 °C for *c-MYC*, and at 40 °C for telomeric DNA for 30 min. The extension reaction was stopped by adding 10 μL of 2× stop buffer (10 mM EDTA, 10 mM NaOH, 0.1% each bromophenol blue (w/v) and xylene cyanole (w/v) in formamide). Samples were analyzed in 15% denaturing PAGE in which 1× TBE (89 mM of each Tris and boric acid and 2 mM of EDTA, pH 8.3) was used as the running buffer, and gels were autoradiographed using a phosphorimager (Storm 825). Quantification of gels was performed using ImageQuant 5.2 software.

Molecular Modeling and Dynamics Studies. The coordinates of *c-MYC* (PDB entry: 2L7V),[38] *c-KIT1* (PDB entry: 2O3M)[39] telomeric parallel (PDB ID: 1KF1),[40] telomeric antiparallel (PDB ID: 143D),[41] and telomeric hybrid (PDB ID: 2MB3)[42] G-quadruplex DNA structures were retrieved and prepared for docking. The ligand structures were optimized using Gaussian 09[43] (HF/6-31G* level). Docking was carried out using AutoDock 4.2[44] and Autodock Vina,[45] with a grid size enough to encompass the full receptor molecule. Hence, all possible binding modes, intercalation, end-stacking, and groove-binding, could be revealed by docking studies. For AutoDock 4.2, the Lamarckian genetic algorithm was used by following the procedure developed for G-quadruplex DNA and ligand docking.[46] To facilitate the docking to *c-KIT1* DNA, the terminal 5′-nucleotide dA1 was removed from the PDB file. Subsequent to the docking studies, MD simulations were carried out using AMBER14. The procedure for MD simulations was derived from the methods reported by Haider and Neidle.[46] Briefly, RESP[47] charge fitted ligands was complexed with G-quadruplex DNAs. Generalized AMBER force field (GAFF)[48] was used for the ligands and force field parm99 with parmbsc0 and parm$_{\chi OL4}$ refinement was used for the DNA.[49,50] The system was then solvated using TIP3P water molecules extended up to 10 Å in an octahedral box. The system was then neutralized by adding K^+ ions. The solvated system was then subjected to equilibration (700 ps) followed by 100 ns of MD simulation at a constant temperature of 300 K (using Langevin coupling) and a constant pressure at 1 atm. The nonbonded cutoff was set to 8 Å, and the periodic boundary conditions were attained by PME algorithm. The coordinates were saved for each ps. Binding free energy of ligands was estimated using MM-PB/GBSA methods.[51] The last 15 ns of the MD run (85−100 ns) was used for this since the complexes were stabilized by this time of the simulations. RMSDs of the heavy atoms, Hoogsteen hydrogen bonding occupancies, and dihedral angles were calculated using the ptraj and cpptraj modules. Trajectory analysis was carried out with UCSF Chimera (http://www.cgl.ucsf.edu/chimera), and figures were rendered using PyMOL (http://www.pymol.org).

RESULTS AND DISCUSSION

Ligand Design and Synthesis. Indole and indanone moieties are one of the major components in the core structures of various natural products and FDA approved drugs.[52,53] To make a quadruplex stabilizing indolylmethyleneindanone skeleton, indanone and indole rings were connected through a conjugating double bond thereby extending the delocalization. Fully conjugated indolylmethyleneindanone core perfectly match in size with the two guanine bases, and thereby it can very well stack onto the G-quartet. These core structures were tuned into DNA G-quadruplex stabilizing ligands by introducing suitable side chains at appropriate positions. We have designed four indolylmethyleneindanone based molecules (**InEt1**, **InPr1**, **InEt2**, and **InPr2**; Figure 1) that fulfill the criteria for G-quadruplex stabilizing ligands. A minimum number of hydrogen bond acceptors and donors, low molecular weights, and lower number of aromatic rings/heteroatoms impart drug like properties to these ligands. Ethyl and propyl cationic pyrrolidine side chains in these molecules can increase the water solubility and stability of quadruplexes through their interaction with the phosphate groups present in the loops and grooves.

Synthesis of **InEt1** and **InPr1** was achieved from a common intermediate aldol (**1**) (Scheme 1), which was prepared by using reported procedures with slight modifications.[54] *N*-

DOI: 10.1021/acs.biochem.6b00120
Biochemistry 2016, 55, 3571−3585

Scheme 1. Synthesis of Indolylmethyleneindanone Derivatives[a]

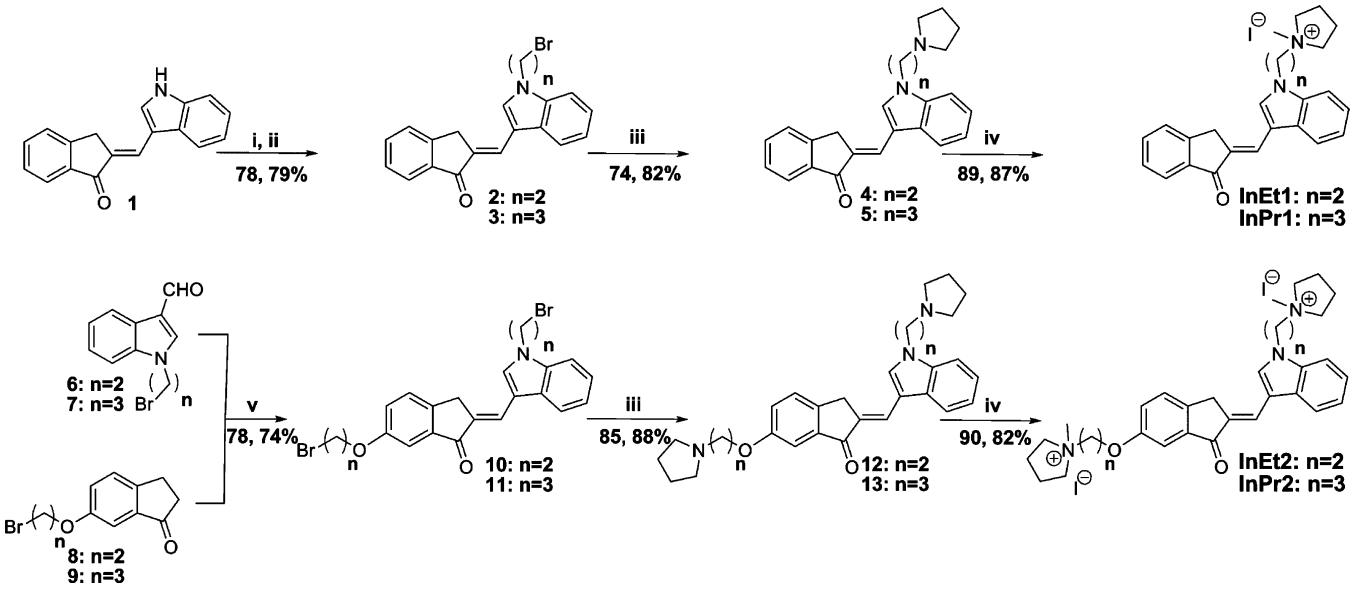

[a]Reagents and conditions: (i) 1,2-dibromoethane, K_2CO_3, DMF, RT, 24 h; (ii) 1,3-dibromopropane, K_2CO_3, DMF, RT, 24 h; (iii) pyrrolidine, ACN, reflux, 3 h; (iv) MeI, ACN, reflux, 12 h; and (v) AcOH, conc. HCl, 90 °C, 4 h.

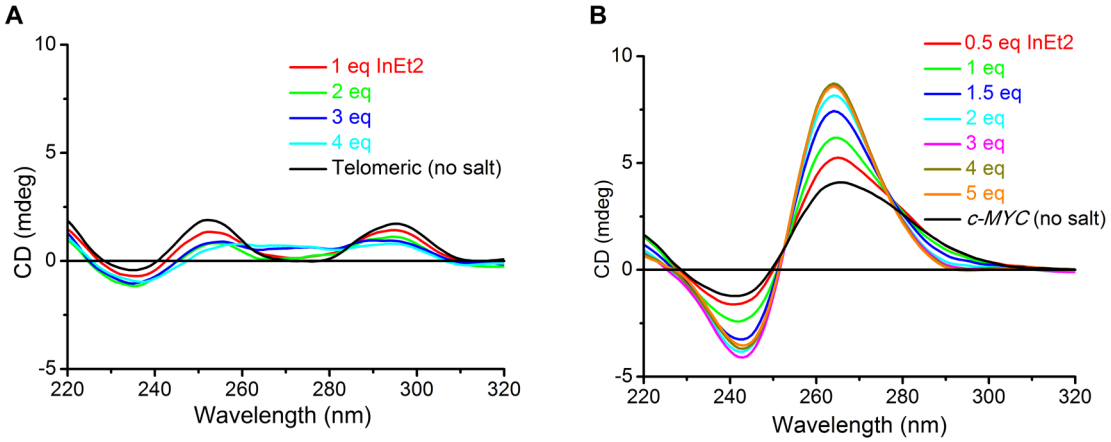

Figure 2. CD titration spectra of telomeric and *c-MYC* DNA with **InEt2** in the absence of added metal ions (12.5 μM DNA in 50 mM Tris-HCl buffer, pH 7.2). (A) Telomeric DNA; and (B) *c-MYC* DNA.

Alkylation of the aldol product was carried out by using 1,2-dibromoethane and 1,3-dibromopropane under basic medium to give alkyl bromides **2** with 78% and **3** with 79% yields. Bromine was displaced by using pyrrolidine to get compounds **4** in 74% and **5** in 82% yields. Finally, the amino groups were methylated by refluxing with MeI to afford the target compounds **InEt1** and **InPr1** in 89% and 87% yields, respectively. The target molecules **InEt1** and **InPr1** were synthesized from the common intermediate aldol (**1**) with overall yields of 51% and 56% respectively.

Similarly, synthesis of **InEt2** and **InPr2** was achieved from alkylated intermediates **6**, **7**, **8**, and **9**, which were prepared by using reported procedures (Scheme 1).[55,56] Alkylated compounds **6**, **8**, and **7**, **9** were coupled by employing acid mediated aldol condensation to yield the products **10** with 78% and **11** with 74% yields. Compounds **10** and **11** were refluxed with pyrrolidine to generate the compounds **12** with 85% and **13** with 88% yields. Finally, compounds **12** and **13** were methylated by refluxing with MeI to furnish the target molecules **InEt2** and **InPr2** in 90% and 82% yields, respectively. The ligands **InEt2** and **InPr2** were synthesized from compounds **6**, **7**, **8**, and **9** with overall yields of 60% and 53% respectively.

Circular Dichroism (CD) Titration Studies and Electrophoretic Mobility Shift Assay (EMSA). CD spectroscopy is a useful technique to study the conformation of nucleic acid structures, especially G-quadruplex nucleic acids in solution.[57−59] CD titration studies were performed with telomeric and promoter quadruplex DNAs (*c-MYC* and *c-KIT*) to elucidate the ability of the ligands to induce a particular topology in the quadruplex DNAs. Telomeric DNA in the absence of added metal ions (Tris-HCl buffer, pH 7.2) exhibit a small positive peak around 295 and 251 nm, which do not correspond to any defined topology (Figure 2A and Figure S1, Supporting Information). Upon titration with 4−5 equiv of ligands, there was no induction of any characteristic peaks for a particular topology of the telomeric quadruplex DNA (Figure 2A and Figure S1, Supporting Information). Promoter

DOI: 10.1021/acs.biochem.6b00120
Biochemistry 2016, 55, 3571−3585

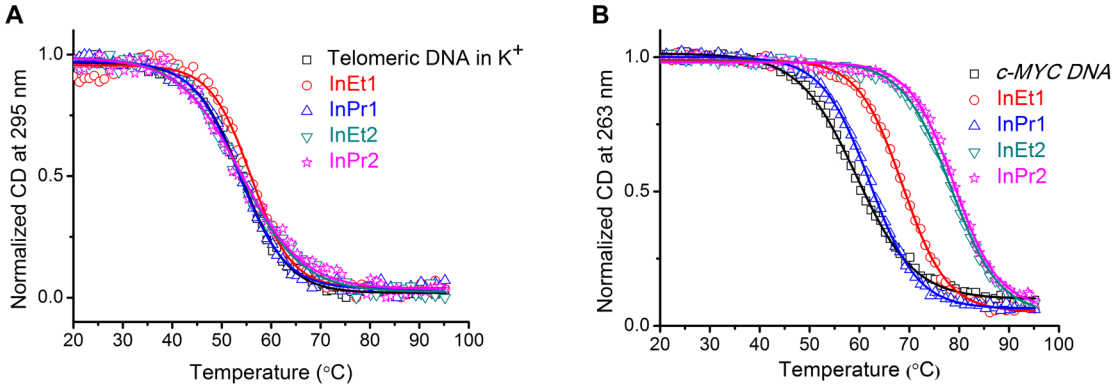

Figure 3. CD melting curves for the telomeric and the *c-MYC* quadruplex DNAs (10 μM DNA in 10 mM lithium cacodylate buffer, pH 7.2) in the absence and in the presence of 5 equiv of ligands. (A) Telomeric DNA (10 mM KCl and 90 mM LiCl); and (B) *c-MYC* DNA (1 mM KCl and 99 mM LiCl).

Table 1. Thermal Stability of Quadruplex and Duplex DNAs (Sequences are Shown in Table S1, Supporting Information) with the Ligands Measured by CD Melting Experiments

	$\Delta T_{1/2}$[a] (°C)				
ligands	*c-MYC*	*c-KIT1*	*c-KIT2*	telomeric (K^+)	duplex-17 (DS17)
InEt1	8.6 ± 0.6	14.1 ± 0.6	7.2 ± 0.6	1.4 ± 0.4	3.2 ± 0.1
InPr1	2.9 ± 0.7	4.4 ± 0.5	2.6 ± 0.1	−0.6 ± 0.1	0.5 ± 0.1
InEt2	18.7 ± 0.2	22 ± 0.1	11.6 ± 0.5	−0.2 ± 0.1	2.4 ± 0.9
InPr2	19.5 ± 0.1	24.3 ± 0.1	12.4 ± 0.5	−0.4 ± 0.3	2.8 ± 0.7

[a] $\Delta T_{1/2}$ represents difference in thermal melting [$\Delta T_{1/2} = T_{1/2}$ (DNA + 5 mol equiv ligand) − $T_{1/2}$ (DNA)]. All the experiments were carried out in 10 mM lithium cacodylate buffer, pH 7.2 with DNA concentration 10 μM for quadruplex and 15 μM for duplex DNAs. $T_{1/2}$ values in the absence of ligands are 59 ± 0.2 °C (*c-MYC* DNA in 1 mM KCl and 99 mM LiCl); 44.8 ± 0.1 °C [*c-KIT1* DNA in 10 mM KCl and LiCl 90 mM); 54.4 ± 0.3 °C (*c-KIT2* DNA in 1 mM KCl and 99 mM LiCl); 54.2 ± 0.2 °C (telomeric DNA in 10 mM KCl and 90 mM LiCl); and 62.8 ± 0.2 °C (DS17 in 10 mM KCl and 90 mM LiCl). $\Delta T_{1/2}$ values are reported as the average with standard deviations from three independent experiments.

quadruplex DNAs such as *c-MYC* and *c-KIT* were reported to adopt parallel topology even in the absence of added metal ions.[29] As expected, CD spectra for the *c-MYC*, *c-KIT1*, and *c-KIT2* DNAs in the absence of added metal ions showed a positive peak around 260 nm and a negative peak around 240 nm, which are characteristic peaks for the parallel topology.[29] For the *c-MYC* DNA, upon titration with increasing concentration of ligands, intensities of the characteristic peaks were dramatically increased, and there was a saturation after the addition of 3−4 equiv of the ligands (Figure 2B and Figure S2, Supporting Information).

Similarly, titration experiments for the *c-KIT1* DNA with all the ligands showed an increase in the intensity for characteristic peaks of parallel quadruplex DNAs indicating further induction of existing parallel topology (Figure S3, Supporting Information). *c-KIT2* DNA showed very strong characteristic peaks for the parallel topology even in the absence of ligands and added metal ions.[29] Upon titration with ligands, the intensities of the characteristic peaks were retained, indicating the retention of the prefolded parallel topology for *c-KIT2* quadruplex DNA (Figure S4, Supporting Information). Overall, from the CD titration experiments, it is evident that the ligands are able to further induce or retain the existing parallel topology for the *c-MYC* and the *c-KIT* quadruplex DNAs and are not able to induce any particular topology of telomeric DNAs.

To further support these findings from CD titration studies, an electrophoretic mobility shift assay (EMSA) was carried out with telomeric quadruplex DNAs. G-quadruplex structures are more compact in nature and migrate faster in the non-denaturing gel than nonquadruplex forms.[60] Ligand induced quadruplex formation can be detected by the faster migration of DNAs treated with ligands as compared to the untreated DNAs.[35] Telomeric DNA was studied for the ligand induced quadruplex formation with all the four ligands. A strong G-quadruplex inducer **3AQN** reported from our lab was used as a standard in these experiments.[35] All the ligands together with the standard were incubated with the telomeric DNA in the absence of any added metal ions in a concentration dependent manner (0−10 equiv). Telomeric DNA treated with **3AQN** (5 equiv) migrated faster in the gel indicating the strong induction of quadruplex structure, whereas the DNAs treated with all the four ligands were retained their positions indicating the presence of nonquadruplex forms (Figure S5, Supporting Information). These results further validate the fact that the ligands are not able to induce quadruplex structures in the telomeric DNA.

CD Melting Studies. Stabilization and selectivity of ligands toward the G-quadruplex over duplex DNAs were evaluated by measuring the ligand induced changes in the melting temperatures at the corresponding wavelengths.[61] The CD melting experiments were performed by following reported procedures; salt and buffer concentrations were adjusted for the DNAs to melt in the range of 40−60 °C.[61] Since the induction of quadruplex structure was saturated after the addition of 5 equiv of ligands in the CD titration spectra, the same amount was used to evaluate ligand induced thermal stabilization.

For the telomeric DNA, the experiments were carried out under 10 mM K^+ conditions by measuring the ellipticity at 295 nm, and this yielded a $T_{1/2}$ of 54 °C (Figure 3A). Addition of ligands (5 equiv) resulted in only a negligible change in the $T_{1/2}$

DOI: 10.1021/acs.biochem.6b00120
Biochemistry 2016, 55, 3571−3585

($\Delta T_{1/2} \sim -0.2-1.4$ °C, Table 1, Figure 3A). Moreover, melting experiments were carried out for the ligand **InEt2** with long telomeric DNA, which can form higher order quadruplex structures.[62] Ellipticity was monitored at 265 nm under K^+ conditions. Addition of **InEt2** resulted in only a slight increase in the $T_{1/2}$ ($\Delta T_{1/2} \sim 2.5$ °C) (Figure S6, Supporting Information). For the duplex DNA, experiments were carried out by measuring the ellipticity at 242 nm, yielding a $T_{1/2}$ of 62 °C (Figure S6, Supporting Information). As expected, the addition of ligands resulted in only a marginal change in the $T_{1/2}$ ($\Delta T_{1/2} \sim 0.7-3.2$ °C, Table 1, Figure S6, Supporting Information). These results show that the ligands are not able to stabilize telomeric quadruplex and duplex DNA structures.

CD melting experiments were monitored at 263 nm for the promoter quadruplex DNAs under 1−10 mM K^+ conditions (Figure 3B and Figure S6, Supporting Information). For the *c-MYC* DNA having a $T_{1/2}$ of 59 °C, a moderate to high increase in $T_{1/2}$ values ($\Delta T_{1/2} \sim 2.9-19.5$ °C, Table 1) were obtained after the addition of ligands (Figure 3B). Similarly, *c-KIT1* DNA yielded $T_{1/2}$ of 45 °C, and an impressive increase in the $T_{1/2}$ values ($\Delta T_{1/2} \sim 4.4-24.3$ °C, Table 1) was observed after the addition of ligands (Figure S6, Supporting Information). In the case of *c-KIT2* DNA having $T_{1/2}$ of 54 °C, a moderate increase in the $T_{1/2}$ values ($\Delta T_{1/2} \sim 2.6-12.4$ °C, Table 1) was observed after the addition of ligands (Figure S6, Supporting Information).

CD melting experiments revealed that irrespective of the length and the number of side chains, the ligands are not able to strongly stabilize the telomeric quadruplex (hybrid and higher order) and the duplex DNA structures. Interestingly, the ligands **InEt2** and **InPr2** showed high thermal stabilization, whereas **InEt1** showed moderate and **InPr1** showed weak stabilization with the *c-MYC* and the *c-KIT* quadruplex DNAs having parallel topologies. Out of the four ligands **InEt2** and **InPr2** with two methylated side chains are found to impart high stability to the *c-MYC* and *c-KIT* quadruplex DNAs than the ligands with single methylated side chains. It should be noted that the differences in side chain length (ethyl or propyl) in **InEt2** and **InPr2** are not reflected in the thermal stabilization properties. However, ligands with a single side chain differed in the thermal stabilization, and the ligand with an ethyl side chain (**InEt1**) is found to be more promising than that with the propyl side chain (**InPr1**).

Electrospray Ionization Mass Spectrometry Studies (ESI-MS). ESI-MS is useful to assess the noncovalent interactions between quadruplex DNAs and small molecules at low concentrations.[63,64] Stoichiometries of ligand−quadruplex interactions, and hence individual binding constants, can indeed be calculated using this technique. Experiments were carried out in a buffer containing NH_4^+ ions as coexisting cations with the ligands **InEt2** and **InPr2**. ESI-MS spectra of *c-MYC* quadruplex DNA (Figure 4A, B) in the absence of ligands showed a sharp signal around m/z 1400 with five negative charges. Upon addition of 2 equiv of ligands, two new signals appeared in the spectra corresponding to 1:1 and 2:1 ligand−quadruplex complexes, in which the former was predominant (Figure 4A,B).

Binding constant values for the interaction of **InEt2** with *c-MYC* quadruplex DNA (K_1 and $K_2 \sim 10^6$ M^{-1}) revealed the high binding affinity with one preferential binding site, whereas **InPr2** showed moderate binding affinity ($K_1 \sim 10^5$ and $K_2 \sim 10^4$ M^{-1}) (Figure 4 and Table 2). Similarly, both the ligands showed moderate to high stabilization (K_1 and $K_2 \sim 10^5$ M^{-1} for **InEt2** and $K_1 \sim 10^6$ and $K_2 \sim 10^5$ M^{-1} for **InPr2**) with *c-KIT1* quadruplex DNA (Figure S7, Supporting Information and Table 2). Control experiments were performed with a tetramolecular parallel quadruplex DNA, $[(dTG_4T)_4]$, and both the ligands showed moderate to weak binding (K_1 and $K_2 \sim 10^5$ M^{-1} for **InEt2** and $K \sim 10^4$ M^{-1} for **InPr2**) with 1:1 and 2:1 stoichiometries (Figure S7 and Table 2).

In order to address the topology specific binding toward *c-MYC* and *c-KIT1* over telomeric quadruplex DNAs, similar experiments were performed with telomeric quadruplex DNA (Figure 4C,D). For **InEt2** and **InPr2** weak signals corresponding to 1:1 and 2:1 stoichiometries as compared to those for *c-MYC* and *c-KIT* quadruplex DNAs were observed. Moreover, high selectivity for the *c-MYC* (up to 56-fold) and moderate selectivity for the *c-KIT1* (up to 9 fold) over telomeric quadruplex DNAs were indicated by the binding constant values (Table 2). These results are in agreement with the results from the CD melting studies, and the ligand **InEt2** with ethyl side chains was found to be highly stabilizing and more

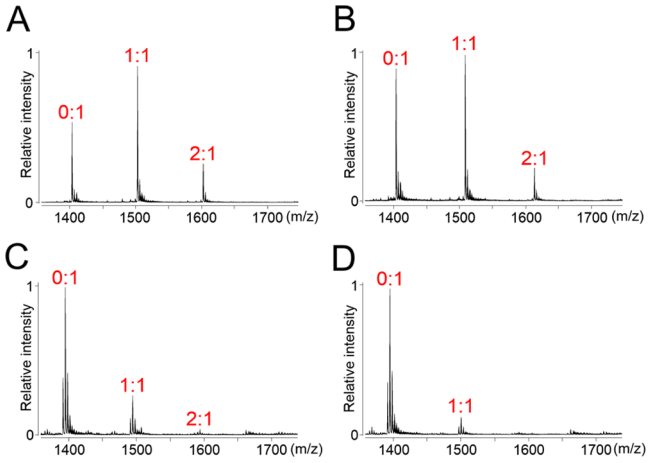

Figure 4. ESI-MS spectra (zoom of the 5− charge state region) of the *c-MYC* and the telomeric quadruplex DNAs (5 μM quadruplex in 100 mM NH_4OAc solution) in the presence 2 equiv of ligands at 22 °C. (A) *c-MYC* + **InEt2**; (B) *c-MYC* + **InPr2**; (C) telomeric DNA + **InEt2**; and (D) telomeric DNA + **InPr2**. Peak annotations indicate the stoichiometry as (number of ligands bound):(target structure).

Table 2. Individual Equilibrium Binding Constants Obtained From ESI-MS Mass Spectrometry (Assuming That the Relative Intensities of Each Stoichiometry Reflect the Relative Concentrations in Solution) in 100 mM NH_4OAc

	ligand			
	InEt2		InPr2	
sequence	$K_1 \times 10^6$ (M^{-1})	$K_2 \times 10^6$ (M^{-1})	$K_1 \times 10^6$ (M^{-1})	$K_2 \times 10^6$ (M^{-1})
c-MYC	5.6	1.3	0.5	0.08
c-KIT1	0.9	0.3	1.2	0.3
telomeric	0.1	0.1	0.28	0.1
$(TGGGGT)_4$	0.9	0.2	0.06	0
DK100[a]	0.2	0.04	0.08	0.02
DK66[a]	0.2	0.06	0.06	0.06
DK33[a]	0.09	0.1	0.08	0.1
DS17[a]	0.6	0.1	0.2	0.04

[a]DK100, DK66, DK33 (self-complementary sequences with varying GC content), and DS17 are the duplex sequences, which are listed in Table S1, Supporting Information.

DOI: 10.1021/acs.biochem.6b00120
Biochemistry 2016, 55, 3571−3585

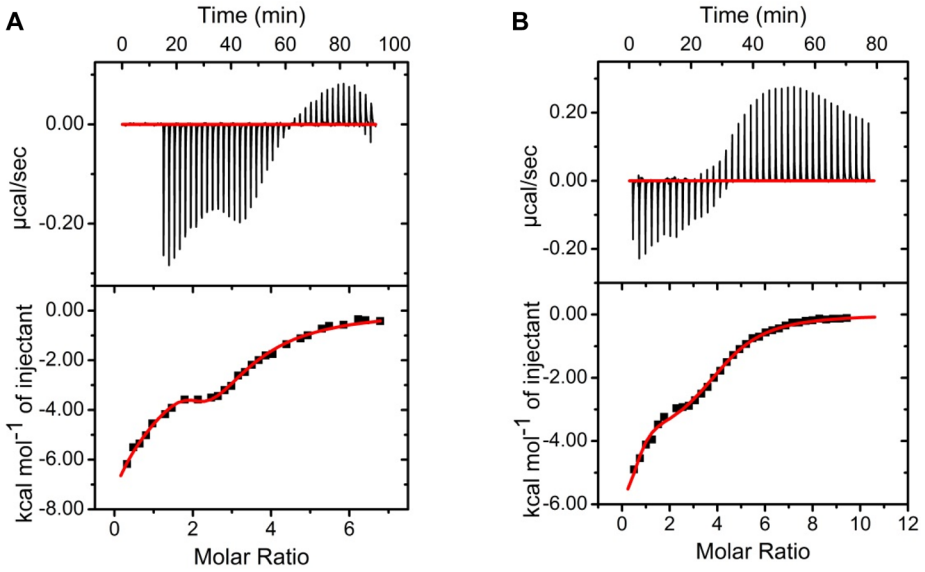

Figure 5. ITC profiles for the interaction of ligand **InEt2** and **InPr2** with *c-MYC* quadruplex DNA (50 μM DNA in 100 mM KCl and 10 mM lithium cacodylate buffer, pH 7.2). (A) **InEt2**; and (B) **InPr2**. Raw data shown in upper panel and curve fit using sequential binding model in the bottom panel with Chi^2 = 8343 and 6988 for **InEt2** and **InPr2** respectively.

Table 3. Thermodynamic Parameters from ITC Experiments for the Interaction of Ligands with *c-MYC* Quadruplex DNA at 25 °C[a]

$K_1 \times 10^6$	ΔH_1	$T\Delta S_1$	$K_2 \times 10^5$	ΔH_2	$T\Delta S_2$	$K_3 \times 10^4$	ΔH_3	$T\Delta S_3$
				InEt2				
1 ± 0.1	−7.1 ± 0.2	0.1	3.8 ± 0.3	−1.8 ± 0.2	0.5	2.1 ± 0.2	−10.8 ± 0.2	−0.4
				InPr2				
0.1 ± 0.0	−6.6 ± 0.2	0.03	0.6 ± 0.01	−6.9 ± 0.1	−0.3	0.7 ± 0.1	−3.5 ± 0.1	0.2

[a]Best fit parameters obtained by sequential binding model with Chi^2 = 8343 and 6988 for **InEt2** and **InPr2** respectively. K values are given in M^{-1} and ΔH, $T\Delta S$ values are given in kcal/mol.

specific toward the *c-MYC* and *c-KIT* quadruplex DNAs as compared to **InPr2** with propyl side chains (Figure 4). ESI-MS analyses were also performed with four duplex sequences (DS17, DK100, DK66, and DK33; Table S1, Supporting Information) having different GC content to ensure the selectivity for quadruplex DNAs over duplex DNAs (Figure S7, Supporting Information). In the case of **InEt2**, as the GC content in the duplex DNAs was increased, and binding affinities were found to be increasing (Table 2). But higher selectivities (up to 62 fold depending on the sequence) reflected in the binding constant values for *c-MYC* quadruplex over duplex DNAs validate the selectivity of ligands. In the case of *c-KIT1* DNA moderate selectivity was achieved by **InPr2** over duplex DNA (6−20 fold), whereas **InEt2** showed poor selectivity (1.5−10 fold) with the duplex DNA depending upon the sequence of duplex DNA.

Isothermal Titration Calorimetry (ITC). ITC experiments enable the thermodynamic profile of ligand−DNA interactions to be derived. We have selected **InEt2** and **InPr2** for the ITC studies and the *c-MYC* as an example from the promoter quadruplex DNAs. In the ITC experiments, both ligands showed a nonlinear isotherm pattern indicating complex multiple binding modes (Figure 5). Integrated heat data were fitted by using a sequential binding model to derive the thermodynamic profile, and the best-fit parameters are listed in Table 3. In the case of **InEt2**, binding of the first and the second molecule were strong enough to get a binding constant of the order of 10^6−10^5 M^{-1}, and the binding of third molecule was weak in nature (~10^4 M^{-1}). Similarly, **InPr2** showed a binding constant of the order of 10^5−10^4 M^{-1} and a weak third binding ~10^3 M^{-1}. As in ESI-MS, the ITC results show that one binding site has higher affinity than the following ones. Both binding interactions are driven by a large favorable negative enthalpy change (Table 3). Among the two ligands, **InEt2** was found to have higher binding affinity with the *c-MYC* quadruplex DNA, which is consistent with the results from ESI-MS. A possible reason for very weak binding of the third molecule may be the formation of nonspecific adducts at high ligand concentrations. To further confirm specificity of the ligands toward *c-MYC* quadruplex DNAs and to support the findings from CD and ESI-MS, similar experiments were conducted with telomeric quadruplex and duplex DNAs (Figure S8, Supporting Information). It was evident from the binding constant values that the ligands showed relatively weak binding (K ~ 10^4−10^3 M^{-1}) with telomeric quadruplex and duplex DNAs (Table S2, Supporting Information).

***Taq* DNA Polymerase Stop Assay.** The Specificity of ligands to stabilize *c-MYC* quadruplex DNAs was further probed with the aid of *Taq* DNA polymerase stop assay. Stop assay was performed with *c-MYC* DNA and with telomeric quadruplex DNAs. The reaction temperatures for the stop assay (50 °C for *c-MYC* and 40 °C for telomeric DNA) were chosen in such a way that there is no formation of stop products in the absence of ligands. At this temperature, partially stable quadruplex structures are easily unwound by the *Taq* DNA polymerase enzyme.[36,37] Control experiments were performed

DOI: 10.1021/acs.biochem.6b00120
Biochemistry 2016, 55, 3571−3585

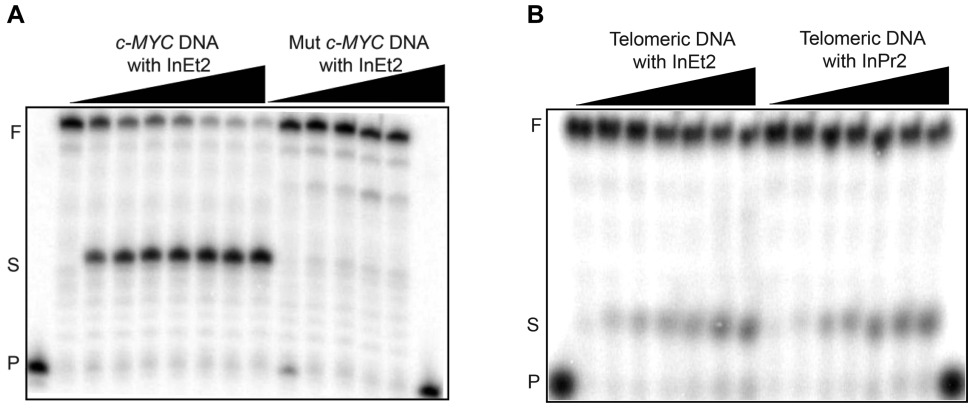

Figure 6. Denaturing PAGE (15%, 7 M urea) for the *Taq* DNA polymerase stop assay in the presence of *c-MYC*, mutated *c-MYC*, and telomeric DNA with increasing ligand concentration. (A) Ligand **InEt2** (0−10 μM) with the *c-MYC* and the mutated *c-MYC* DNA templates; and (B) ligands **InEt2** and **InPr2** (0−120 μM) with the telomeric DNA template. Primer extension reactions were carried out at 50 °C for the *c-MYC* DNA template and at 40 °C for the telomeric template. Conditions: 100 nM template, 50 nM primer, 0.2 mM dNTPs and 0.5 U of *Taq* polymerase in the enzyme buffer (50 mM Tris, 0.5 mM DTT, 0.1 mM EDTA, 5 mM $MgCl_2$, 5 mM KCl for *c-MYC* template and 10 mM KCl for telomeric template). P denotes primer, S denotes stop product, F denotes full length product.

with a template containing mutated *c-MYC* DNA sequences that cannot form quadruplex structure (Figure 6A and Figure S9, Supporting Information). Formation of the stop products were observed for the *c-MYC* DNA (minimum $IC_{50} \sim 1.5$ μM) after incubating with increasing concentration of all the ligands (Figure 6A and Figure S10, Supporting Information). As expected, there was no formation of stop products observed with the mutated *c-MYC* DNA that cannot form a quadruplex structure. There was no significant amount of stop products (~10%) for the telomeric DNAs even at 120 μM ligand concentration (Figure 6B and Figure S9, Supporting Information).

Ligands having double side chains **InEt2** and **InPr2** were very efficient in stabilizing c-*MYC* quadruplex DNA with low IC_{50} values ($IC_{50} \sim 1.5$ and 2.5 μM for respectively). Ligands with single side chains showed moderate IC_{50} values, and the ligand with ethyl side chain, **InEt1** ($IC_{50} \sim 10$ μM) was more effective compared to the other with propyl side chain, **InPr1** ($IC_{50} \sim 34$ μM). However, formation of stop products was not prominent for mutated *c-MYC* and telomeric quadruplex DNAs with all the ligands irrespective of the number and length of the side chains (Figure S9, Supporting Information).

Molecular Modeling and Dynamics Studies. Molecular modeling and dynamics studies were carried out to rationalize the topology specific binding of the ligands **InEt2** and **InPr2** with *c-MYC* and *c-KIT1* G-quadruplex structures over telomeric G-quadruplex topologies. The ligand structures were geometry-optimized in Gaussian09[43] at HF/6-31G* level of theory (Figure S11, Supporting Information). These optimized structures were docked with the G-quadruplex DNA structures from the Protein Data Bank (*c-MYC*: PDB ID 2L7V,[38] *c-KIT1*: PDB ID 2O3M,[39] telomeric parallel: PDB ID 1KF1,[40] telomeric antiparallel: PDB IDB 143D,[41] and telomeric hybrid: 2MB3[42]) using Autodock 4.2.[44] Binding stoichiometry of 2:1 was revealed with both *c-MYC* and *c-KIT1* quadruplex structures, with ligands stacking at the top (5′-end) and at the bottom (3′-end) quartets of the quadruplex DNAs. This binding stoichiometry of the ligands with both *c-MYC* and *c-KIT1* quadruplexes is supported by the ESI-MS results. A similar 5′- and 3′-endstacking mode has also been found for indenopyrimidine ligand **InPy1** with *c-MYC* and *c-KIT1* and for quindoline to *c-MYC* quadruplex DNAs.[33,38] These docked structures were minimized, equilibrated, and 100 ns MD runs in AMBER14[65] (using pmemd module) were carried out.

MM-PBSA analysis using the MM-PB/GBSA[51] module of AMBER14 was carried out to obtain the binding free energy values. The free energy values for the binding of **InEt2** and **InPr2** with *c-MYC*, *c-KIT1* and telomeric quadruplex DNAs are shown in Table 4. The 5′- and 3′-end stacking mode of **InEt2**

Table 4. Binding Energy [ΔG ($\Delta H_{PB} - T\Delta S$)] in kcal/mol of Ligands with Human *c-MYC*, *c-KIT1*, and Telomeric Quadruplex Structures

binding energy (MM-PBSA analysis)	InEt2	InPr2
c-MYC (PDB ID: 2L7V)	Overall: −80 ± 7	Overall: −66 ± 7
	5′-**InEt2**: −39 ± 4	5′-**InPr2**: −36 ± 5
	3′-**InEt2**: −32 ± 7	3′-**InPr2**: −19 ± 5
c-KIT1 (PDB ID: 2O3M)	Overall: −57 ± 7	Overall: −57 ± 7
	5′-**InEt2**: −23 ± 5	5′-**InPr2**: −25 ± 5
	3′-**InEt2**: −26 ± 5	3′-**InPr2**: −24 ± 5
telomeric parallel (PDB ID: 1KF1)	−24 ± 3	−22 ± 3
telomeric antiparallel (PDB ID: 143D)	−19 ± 3	−24 ± 3
telomeric hybrid (PDB ID: 2MB3)	−20 ± 4	−22 ± 4

with *c-MYC* promoter quadruplex structure gives the most favorable binding energy (−80 kcal/mol), while **InPr2**, also in the 5′- and 3′- end stacking mode, showed a slightly reduced affinity (−66 kcal/mol) (Table S5, Supporting Information). With the *c-KIT1*, both **InEt2** and **InPr2** showed very similar binding energies (−58 and −57 kcal/mol respectively) (Table S6, Supporting Information). The specific interactions of the two ligands at the 5′- and 3′-quartet are discussed in detail below (Figures 7 and 8).

The structural stabilities of the systems through the 100 ns MD run were examined using the ptraj module of AMBER14. Root mean square deviation (RMSD) graphs and average values for the heavy atoms in the backbone, quartets, and the two ligands were also derived (Figures S12, S13 and Table S3, Supporting Information). Results indicate that the systems remained relatively stable throughout the run. This was also

DOI: 10.1021/acs.biochem.6b00120
Biochemistry 2016, 55, 3571−3585

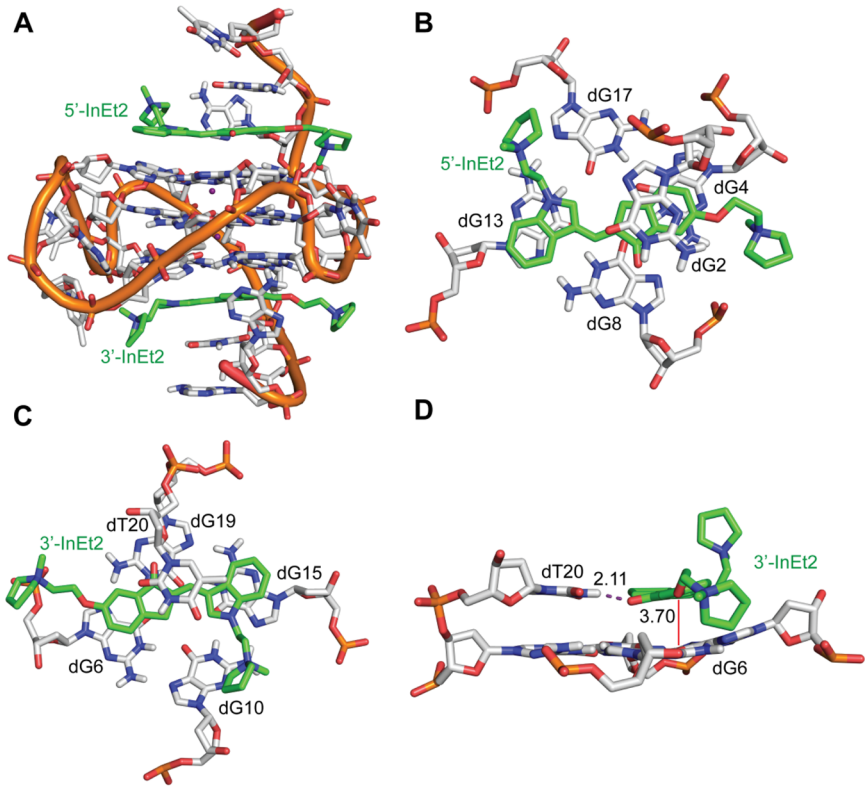

Figure 7. MD snapshot of **InEt2** with *c-MYC* G-quadruplex DNA at 100 ns (A–C) of the MD simulations. (A) **InEt2** and *c-MYC* G-quadruplex DNA (2:1): stacking occurs at both the 5′ and 3′ G-quartets of the G-quadruplex; (B) **InEt2** and 5′ quartet, showing stacking with 5′ quartet guanines as well as flanking nucleotide dG2; (C) **InEt2** and 3′ quartet, where dT20 has moved below the ligand where the hydrogen-bond between ligand and quadruplex is no longer present; and (D) snapshot of 3′-**InEt2** at 23 ns, showing the hydrogen-bonding of the ligand with the flanking nucleotide (dT20) and stacking with 3′ quartet residues. Dashed lines indicate the hydrogen bond distance between the atoms in the ligand and the G-quadruplex DNA, while the red lines indicate stacking distances; all distances are given in Å.

confirmed by the hydrogen bond occupancy for the Hoogsteen hydrogen-bonding within the quartets. The hydrogen-bonds are present through >98.8% of the simulation time for the receptors (Table S4, Supporting Information).

The stability of these complexes results from several factors. In the complex between **InEt2** and *c-MYC*, the 5′-**InEt2** (Figure 7B) stacks its indole ring with the 5′ quartet residue dG13 (average distance: 3.72 ± 0.33 Å), while its indanone ring stacks with the flanking nucleotide dG2 (3.97 ± 0.40 Å) throughout the MD run. Stacking of 3′-**InEt2** with the 3′ quartet (Figure 7C) was observed from both the indole and indanone rings: indole ring with dG15 (stacking distance: 3.63 ± 0.32 Å, 85% of MD run) and indanone ring with dG6, (stacking distance: 3.70 ± 0.32 Å, 77% of run). As seen in Figure 7D, 3′-**InEt2** also showed a strong hydrogen-bonding interaction for the initial 44 ns between the carbonyl oxygen of the ligand and NH of dT20 of the flanking nucleotide (hydrogen-bond distance: 2.11 ± 0.49 Å). After 46 ns, a rearrangement was seen and the dT20 residue moves into a stacking position below the ligand for the rest of the run. Electrostatic interactions involving the positively charged nitrogens in the ligand side chain were found to be short-lived (5′-**InEt2** N^+ with ribose sugar O4′ of dG4; 3′-**InEt2** N^+ with phosphate of dG6). The interactions of the **InPr2** with the *c-MYC* were found to be very similar (Figure S14, Supporting Information). For the 5′-**InPr2**, in addition to stacking of indole with quartet and indanone with flanking dG2, a stacking interaction of indanone with the quartet nucleotide dG17 was also seen (stacking distance: 3.70 ± 0.36 Å). In the case of 3′-**InPr2**, the hydrogen bond of the carbonyl oxygen of the ligand with NH_2 of dA22 persisted for 64% of the run, while for the remaining 32% of the run the oxygen atom was in a hydrogen-bond with NH of dT20 (as seen with 3′-**InEt2**, Figure 7D). During hydrogen-bond contact with dT20, stacking of indole ring with the quartet was disrupted. Again, the electrostatic interactions with pyrrolidine nitrogen (5′-**InPr2** with phosphate of dG8, 3′-**InPr2** with dT7 phosphate) were found to be short-lived. The significant difference between the binding energy of 3′-**InEt2** and 3′-**InPr2** seen in Table 4 could be due to the presence of stacking interaction of 3′-**InEt2** indanone ring with the quartet, which was disturbed for 3′-**InPr2**.

Figure 8 shows a representative structure of the MD run of **InEt2** with the *c-KIT1*. As seen in Table 4, with the *c-KIT1*, both 5′-**InEt2** and 3′-**InEt2** have very similar binding energies, and this is reflected in their stacking interactions which are also very similar. For 5′-**InEt2** (Figure 8B), the indole ring stacks with the 5′-quartet terminal residue dG2 at a distance of 3.98 ± 0.51 Å, and the indanone ring shows stacking with the 5′-quartet residue dG10 (stacking distance: 3.66 ± 0.39 Å). Short-lived electrostatic interactions were seen between the pyrrolidine nitrogen and O4′ of dG9 deoxyribose sugar. The indole ring of 3′-**InEt2** (Figure 8C) was found to have stacking interactions with the 3′-quartet guanine dG4 (stacking distance: 3.81 ± 0.27 Å), while the indanone ring was stacking with another 3′-quartet residue dG8 (stacking distance: 3.79 ± 0.30 Å). In addition, 3′-**InEt2** also showed a strong hydrogen-bond from its carbonyl oxygen to NH of dG20 (average distance: 1.98 ± 0.22 Å), and electrostatic interactions with phosphate of

DOI: 10.1021/acs.biochem.6b00120
Biochemistry 2016, 55, 3571–3585

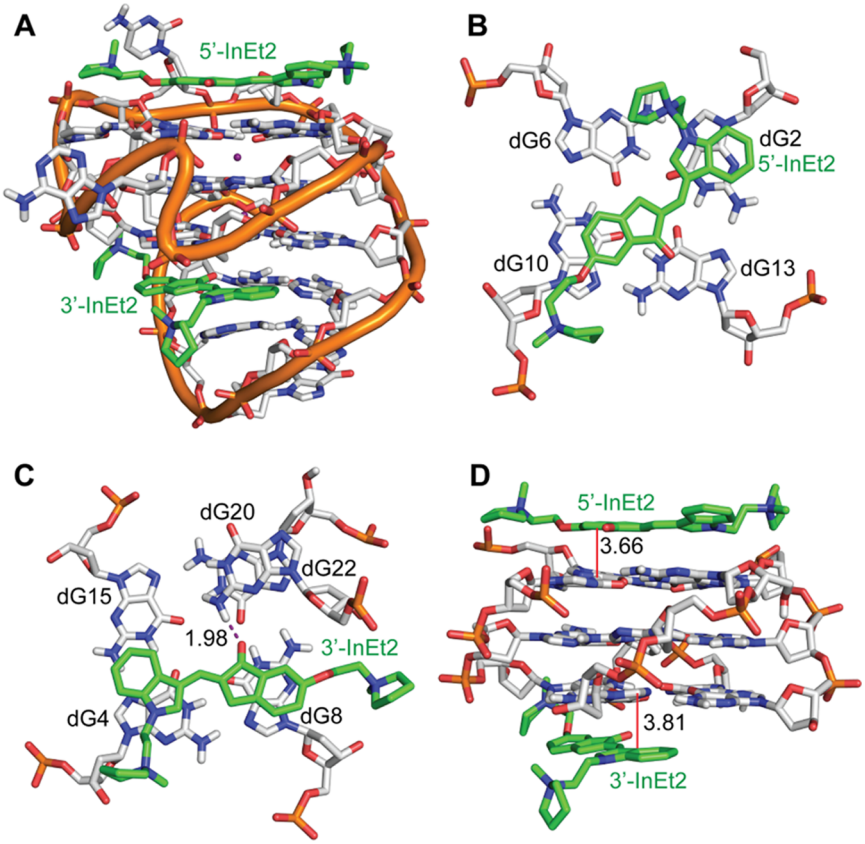

Figure 8. MD snapshot of **InEt2** with *c-KIT1* G-quadruplex DNA at 100 ns of the MD simulation. (A) **InEt2** and *c-KIT1* G-quadruplex DNA (2:1): stacking occurs at both the 5′ and 3′ G-quartets of the G-quadruplex; (B) **InEt2** and 5′ quartet, showing stacking from indanone and indole rings to 5′ quartet residues dG10 and dG2 respectively; (C) **InEt2** and 3′ quartet, showing stacking with 3′ quartet guanines and hydrogen-bonding with flanking dG20; and (D) side view of the complex. Dashed lines indicate the hydrogen bond distance between the atoms in the ligand and the G-quadruplex DNA, while the red lines indicate stacking distances; all the distances are given in Å.

dC9 and O4′ of dA19 deoxyribose ring (Figure 8C). All these interactions were found to be stable throughout the MD simulation. **InPr2** was found to have very similar interactions with *c-KIT1*, as shown in Figure S15, Supporting Information.

In addition, to unravel the topology specific binding of ligands with *c-MYC* and *c-KIT1* G-quadruplex DNAs over telomeric quadruplex topologies, MD simulations (100 ns) of the telomeric parallel, antiparallel, and hybrid topologies in complex with the **InEt2** and **InPr2** ligands were carried out. Docking and MD simulations results revealed that the binding stoichiometries of both the **InEt2** and **InPr2** ligand with telomeric DNA are 1:1 and the ligands stack on the 5′-end of the quartet (Figures S22−S24, Supporting Information). The quadruplex DNAs were quite stable during the 100 ns of MD simulations; however, both the ligands were found to be highly flexible in the complexes (Figures S16−S21, Supporting Information). The binding energy of the ligands with telomeric DNA topologies was found to be in the range of −19 to −24 kcal/mol, which is higher in comparison to the ligand-*c-MYC* and *c-KIT1* quadruplex complexes (Table 4). From the individual binding energy components, it was observed that the ΔE_{MM} in the *c-MYC* and *c-KIT1* quadruplex-ligand complexes (> −950 kcal/mol; for 1:1 binding ratio) was favorable in comparison to that for the complex formed by telomeric topologies (< −750 kcal/mol) (Tables S7 and S8, Supporting Information). This is indeed reflected in the percentage lifetime occupancy of the stacking interactions between ligand and quartet in the promoter (>75) and telomeric topologies (<50) during the MD simulations (Table S9, Supporting Information). These unfavorable stacking interactions may be attributed to the presence of different loop structures in the antiparallel and hybrid topologies, which hinders accommodation of the pyrrolidium side chains of the ligands. In the case of the parallel telomeric DNA, due to the absence of flanking nucleotides as in the *c-MYC* and *c-KIT1* quadruplex, the ligands are flexible to move on the surface of the quartet. However, the percentage lifetime occupancy of stacking interactions was found to be <46% in the 100 ns MD simulations of ligands with parallel telomeric DNA complexes. There were no hydrogen-bonds present between the telomeric quadruplex topologies and the ligands. Also, electrostatic interactions are not observed between the positively charged side chains in the ligands and the negatively charged phosphate backbone of the DNA.

The stacking of the two aromatic groups (indole and indanone) in the ligands **InEt2** and **InPr2** with the G-quartet nucleobases and flanking nucleotides was found to be the main stabilizing interaction for these ligands with the *c-MYC* and *c-KIT1* quadruplex structures. The 2:1 complexes of these ligands with *c-MYC* and *c-KIT1* are possible because of the availability of binding sites at both the top and bottom quartets of these quadruplexes. Overall, the MD simulation results show that along with end stacking, hydrogen bonding between the carbonyl group of ligands with the flanking nucleotides, and electrostatic interactions of the positively charged side chain play a role in the specific recognition of a particular quadruplex

DOI: 10.1021/acs.biochem.6b00120
Biochemistry 2016, 55, 3571−3585

topology. However, the stabilization can be mostly attributed to the stacking interactions of the indolylmethyleneindanone core group with G-quartets as revealed the late stage MD simulation results. Similar stacking interactions were not observed between telomeric quadruplex DNA and the ligands, which is attributed to their specificity toward *c-MYC* and *c-KIT1* quadruplex structures.

CONCLUSIONS

To date, >1000 small molecule ligands have been reported, which show moderate to high affinity toward G-quadruplex structures.[66] Most of them harbor large aromatic core with number of heteroatoms and as a result fall behind the typical drug-like criteria set by medicinal chemists.[16] Though many of them offer target discrimination between quadruplex and duplex structures, there are only a handful of examples which show some preferential target recognition toward a particular quadruplex topology. Since indiscriminate induction and synergic stabilization of multiple quadruplexes can lead to genomic instability,[67,68] for clinical success, the search for a bona fide ligand which specifically targets a particular topology may be desirable. In this line, here we report new indolylmethyleneindanone derivatives **InEt1**, **InEt2**, **InPr1**, and **InPr2**, and confirm their specificity toward *c-MYC* and *c-KIT* quadruplex DNAs having parallel topologies using a variety of biophysical and biochemical techniques. The lead compound **InEt2** bearing a fully conjugated system comprised of indanone and indole moieties along with two positive side chains is able to specifically bind to the parallel topology of oncogenic promoter quadruplexes of *c-MYC* and *c-KIT*. The observed specificity is attributed to the combined effects of number of noncovalent interactions owing to the unique structural elements present in the ligands. Further structural studies are warranted to confirm this. These new unique molecular scaffolds offer opportunities to harness their potential for therapeutic and diagnostic applications centered on promoter quadruplex structures in the genome.

ASSOCIATED CONTENT

Supporting Information

The Supporting Information is available free of charge on the ACS Publications website at DOI: 10.1021/acs.biochem.6b00120.

CD spectra of ligands with telomeric, *c-MYC*, *c-KIT1*, *c-KIT2* DNAs in the absence of added metal ions; nondenaturing gel of telomeric and *c-MYC* DNAs from EMSA; CD melting curves of *c-KIT1*, *c-KIT2*, and duplex DNAs; ESI-MS mass spectra for *c-KIT1*, $(TG_4T)_4$ and duplex DNAs; ITC profiles of ligands with quadruplex and duplex DNAs; PAGE of *Taq* DNA polymerase stop assay with *c-MYC* and telomeric DNAs; IC_{50} plots from *Taq* DNA polymerase stop assay; energy optimized structure of ligands at HF/6-31G* level; time-dependent RMSD graphs of *c-MYC*, *c-KIT1*, and telomeric (parallel, antiparallel, and hybrid) DNAs in complex with **InEt2** and **InPr2**; MD snapshots of **InPr2** with *c-MYC* and *c-KIT1* quadruplex DNAs; MD snapshots of **InEt2** and **InPr2** with telomeric parallel, antiparallel, and hybrid quadruplex DNAs; oligonucleotides used for biophysical and biochemical studies; thermodynamic parameters for telomeric quadruplex and duplex DNAs from ITC; Hoogsteen hydrogen bond occupancies in G-quartet during MD simulations of **InEt2**; binding free energy components of *c-MYC*, *c-KIT1* and telomeric (parallel, antiparallel, and hybrid) DNAs with **InEt2** and **InPr2**; percentage lifetime occupancies of stacking interactions over 100 ns of MD simulations; ^{1}H NMR and ^{13}C NMR spectra of compounds **2**, **3**, **4**, **InEt1**, **InPr1**, **10**, **11**, **12**, **13**, **InEt2**, and **InPr2** (PDF)

AUTHOR INFORMATION

Corresponding Authors

*(V.G.) E-mail: valerie.gabelica@inserm.fr.
*(P.I.P.) E-mail: pradeep@chem.iitb.ac.in.

Funding

This work is financially supported by grants from Department of Biotechnology (DBT)-Government of India (Pilot Project Grants for Young Investigators in Cancer Biology, Grant No. 6242-P4/RGCB/PMD/DBT/PKPI/2015, to P.I.P.), IRCC-IIT Bombay (to P.I.P.), the Inserm (ATIP-Avenir Grant No. R12086GS to V.G.), the Conseil Régional Aquitaine (Grant No. 20121304005 to V.G.), and the EU (FP7-PEOPLE-2012-CIG-333611 to V.G.).

Notes

The authors declare no competing financial interest.

ACKNOWLEDGMENTS

We thank Professor Jean-Louis Mergny, Professor Nand Kishore, and Dr. V. Dhamodharan for fruitful discussions. Computer centre, IIT Bombay is gratefully acknowledged for providing high performance computing facilities. We are also thankful to the central facility supported by IRCC-IIT Bombay for MALDI-MS facility, and the Structural Biophysical Chemistry platform of the IECB Bordeaux for providing access to the mass spectrometers. We are also thankful to Dr. Ruchi Anand for providing access to her laboratory facilities. D.K.V. thanks Council of Scientific and Industrial Research (CSIR), India for the Ph.D. fellowship.

ABBREVIATIONS

ITC, isothermal titration calorimetry; ESI-MS, electrospray ionization mass spectrometry; FDA, Food and Drug Administration; DMF, dimethylformamide; ACN, acetonitrile; AcOH, acetic acid; MeI, methyl iodide; CD, circular dichroism spectroscopy; EMSA, electrophoretic mobility shift assay; PAGE, polyacrylamide gel electrophoresis; MD, molecular dynamics; RMSD, root mean square deviation; **InEt1**, (*E*)-1-methyl-1-(2-(3-((1-oxo-1H-inden-2(3*H*)-ylidene)methyl)-1*H*-indol-1-yl)ethyl)pyrrolidinium iodide; **InPr1**, (*E*)-1-methyl-1-(3-(3-((1-oxo-1*H*-inden-2(3*H*)-ylidene)methyl)-1*H*-indol-1-yl)propyl)pyrolidini-umiodide; **InEt2**, (*E*)-1-methyl-1-(2-(3-((6-(2-(1-methylpyrrolidinium-1-yl)ethoxy)-1-oxo-1*H*-inden-2(3*H*)-ylidene)methyl)-1*H*-indol-1-yl)ethyl)pyrrolidinium iodide; **InPr2**, (*E*)-1-methyl-1-(3-(3-((6-(3-(1-methylpyrrolidinium-1-yl)propoxy)-1-oxo-1*H*-inden-2(3*H*)-ylidene)methyl)-1*H*-indol-1-yl)propyl)pyrrolidinium iodide

REFERENCES

(1) Burge, S., Parkinson, G. N., Hazel, P., Todd, A. K., and Neidle, S. (2006) Quadruplex DNA: sequence, topology and structure. *Nucleic Acids Res. 34*, 5402−5415.

(2) Collie, G. W., and Parkinson, G. N. (2011) The application of DNA and RNA G-quadruplexes to therapeutic medicines. *Chem. Soc. Rev. 40*, 5867−5892.

DOI: 10.1021/acs.biochem.6b00120
Biochemistry 2016, 55, 3571−3585

(3) Meyne, J., Ratliff, R. L., and Moyzis, R. K. (1989) Conservation of the human telomere sequence (TTAGGG)n among vertebrates. *Proc. Natl. Acad. Sci. U. S. A. 86*, 7049−7053.
(4) Wang, Y., and Patel, D. J. (1993) Solution structure of the human telomeric repeat d[AG3(T2AG3)3] G-tetraplex. *Structure 1*, 263−282.
(5) Balasubramanian, S., Hurley, L. H., and Neidle, S. (2011) Targeting G-quadruplexes in gene promoters: a novel anticancer strategy? *Nat. Rev. Drug Discovery 10*, 261−275.
(6) Eddy, J., and Maizels, N. (2007) Conserved elements with potential to form polymorphic G-quadruplex structures in the first intron of human genes. *Nucleic Acids Res. 36*, 1321−1333.
(7) Sen, D., and Gilbert, W. (1988) Formation of parallel four-stranded complexes by guanine-rich motifs in DNA and its implications for meiosis. *Nature 334*, 364−366.
(8) Siddiqui-Jain, A., Grand, C. L., Bearss, D. J., and Hurley, L. H. (2002) Direct evidence for a G-quadruplex in a promoter region and its targeting with a small molecule to repress c-MYC transcription. *Proc. Natl. Acad. Sci. U. S. A. 99*, 11593−11598.
(9) Rankin, S., Reszka, A. P., Huppert, J., Zloh, M., Parkinson, G. N., Todd, A. K., Ladame, S., Balasubramanian, S., and Neidle, S. (2005) Putative DNA quadruplex formation within the human c-kit oncogene. *J. Am. Chem. Soc. 127*, 10584−10589.
(10) Dai, J., Chen, D., Jones, R. A., Hurley, L. H., and Yang, D. Z. (2006) NMR solution structure of the major G-quadruplex structure formed in the human BCL2 promoter region. *Nucleic Acids Res. 34*, 5133−5144.
(11) Sun, D. Y., Guo, K. X., Rusche, J. J., and Hurley, L. H. (2005) Facilitation of a structural transition in the polypurine/polypyrimidine tract within the proximal promoter region of the human VEGF gene by the presence of potassium and G-quadruplex-interactive agents. *Nucleic Acids Res. 33*, 6070−6080.
(12) De Armond, R., Wood, S., Sun, D. Y., Hurley, L. H., and Ebbinghaus, S. W. (2005) Evidence for the presence of a guanine quadruplex forming region within a polypurine tract of the hypoxia inducible factor 1alpha promoter. *Biochemistry 44*, 16341−16350.
(13) Qin, Y., Rezler, E. M., Gokhale, V., Sun, D., and Hurley, L. H. (2007) Characterization of the G-quadruplexes in the duplex nuclease hypersensitive element of the PDGF-A promoter and modulation of PDGF-A promoter activity by TMPyP4. *Nucleic Acids Res. 35*, 7698−7713.
(14) Gonźalez, V., and Hurley, L. H. (2010) The c-MYC NHE III (1): function and regulation. *Annu. Rev. Pharmacol. Toxicol. 50*, 111−129.
(15) Murat, P., and Balasubramanian, S. (2014) Existence and consequences of G-quadruplex structures in DNA. *Curr. Opin. Genet. Dev. 25*, 22−29.
(16) Neidle, S. (2016) Quadruplex Nucleic Acids as Novel Therapeutic Targets. *J. Med. Chem.*, DOI: 10.1021/acs.jmedchem.5b01835.
(17) Risitano, A., and Fox, K. R. (2004) Influence of loop size on the stability of intramolecular DNA quadruplexes. *Nucleic Acids Res. 32*, 2598−2606.
(18) Cevec, M., and Plavec, J. (2005) Role of loop residues and cations on the formation and stability of dimeric DNA G-quadruplexes. *Biochemistry 44*, 15238−15246.
(19) Dai, J., Carver, M., and Yang, D. (2008) Polymorphism of human telomeric quadruplex structures. *Biochimie 90*, 1172−1183.
(20) Hamon, F., Largy, E., Gudin-Beaurepaire, A., Rouchon-Dagois, M., Sidibe, A., Monchaud, D., Mergny, J. L., Riou, J. F., Nguyen, C. H., and Teulade-Fichou, M. P. (2011) An acyclic oligoheteroaryle that discriminates strongly between diverse G-quadruplex topologies. *Angew. Chem., Int. Ed. 50*, 8745−8749.
(21) Sparapani, S., Haider, S. M., Doria, F., Gunaratnam, M., and Neidle, S. (2010) Rational design of acridine-based ligands with selectivity for human telomeric quadruplexes. *J. Am. Chem. Soc. 132*, 12263−12272.
(22) Nicoludis, J. M., Miller, S. T., Jeffrey, P. D., Barrett, S. P., Rablen, P. R., Lawton, T. J., and Yatsunyk, L. A. (2012) Optimized end-stacking provides specificity of N-methyl mesoporphyrin IX for human telomeric G-quadruplex DNA. *J. Am. Chem. Soc. 134*, 20446−20456.
(23) Sabharwal, N. C., Savikhin, V., Turek-Herman, J. R., Nicoludis, J. M., Szalai, V. A., and Yatsunyk, L. A. (2014) N-methylmesoporphyrin IX fluorescence as a reporter of strand orientation in guanine quadruplexes. *FEBS J. 281*, 1726−1737.
(24) Di Leva, F. S., Zizza, P., Cingolani, C., D'Angelo, C., Pagano, B., Amato, J., Salvati, E., Sissi, C., Pinato, O., Marinelli, L., Cavalli, A., Cosconati, S., Novellino, E., Randazzo, A., and Biroccio, A. (2013) Exploring the chemical space of G-quadruplex binders: discovery of a novel chemotype targeting the human telomeric sequence. *J. Med. Chem. 56*, 9646−9654.
(25) Agarwal, T., Roy, S., Chakraborty, T. K., and Maiti, S. (2010) Selective targeting of G-quadruplex using furan-based cyclic homooligopeptides: effect on c-MYC expression. *Biochemistry 49*, 8388−8397.
(26) Brown, R. V., Danford, F. L., Gokhale, V., Hurley, L. H., and Brooks, T. A. (2011) Demonstration that drug-targeted down-regulation of MYC in non-Hodgkins lymphoma is directly mediated through the promoter G-quadruplex. *J. Biol. Chem. 286*, 41018−41027.
(27) Boddupally, P. V. L, Hahn, S., Beman, C., De, B., Brooks, T. A., Gokhale, V., and Hurley, L. H. (2012) Anticancer activity and cellular repression of c-MYC by the G-quadruplex-stabilizing 11-piperazinyl-quindoline is not dependent on direct targeting of the G-quadruplex in the c-MYC promoter. *J. Med. Chem. 55*, 6076−6086.
(28) Ghosh, S., Mendoza, O., Cubo, L., Rosu, F., Gabelica, V., White, A. J. P., and Vilar, R. (2014) Assembly of palladium(II) and platinum(II) metallo-rectangles with a guanosine-substituted terpyridine and study of their interactions with quadruplex DNA. *Chem. - Eur. J. 20*, 4772−4779.
(29) Dash, J., Shirude, P. S., Hsu, S. T. D., and Balasubramanian, S. (2008) Diarylethynyl amides that recognize the parallel conformation of genomic promoter DNA G-quadruplexes. *J. Am. Chem. Soc. 130*, 15950−15956.
(30) Peng, D., Tan, J. H., Chen, S. B., Ou, T. M., Gu, L. Q., and Huang, Z. S. (2010) Bisaryldiketene derivatives: A new class of selective ligands for c-myc G-quadruplex DNA. *Bioorg. Med. Chem. 18*, 8235−8242.
(31) Felsenstein, K. M., Saunders, L. B., Simmons, J. K., Leon, E., Calabrese, D. R., Zhang, S., Michalowski, A., Gareiss, P., Mock, B. A., and Schneekloth, J. S., Jr. (2016) Small Molecule Microarrays Enable the Identification of a Selective,Quadruplex-Binding Inhibitor of MYC Expression. *ACS Chem. Biol. 11*, 139−148.
(32) Chauhan, A., Paladhi, S., Debnath, M., Mandal, S., Das, R. N., Bhowmik, S., and Dash, J. (2014) A small molecule peptidomimetic that binds to *c-KIT1* G-quadruplex and exhibits antiproliferative properties in cancer cells. *Bioorg. Med. Chem. 22*, 4422−4429.
(33) Diveshkumar, K. V., Sakrikar, S., Harikrishna, S., Dhamodharan, V., and Pradeepkumar, P. I. (2014) Targeting promoter G-quadruplex DNAs by indenopyrimidine-based ligands. *ChemMedChem 9*, 2754−2765.
(34) Dhamodharan, V., Harikrishna, S., Bhasikuttan, A. C., and Pradeepkumar, P. I. (2015) Topology specific stabilization of promoter over telomeric G-quadruplex DNAs by bisbenzimidazole carboxamide derivatives. *ACS Chem. Biol. 10*, 821−833.
(35) Dhamodharan, V., Harikrishna, S., Jagadeeswaran, C., Halder, K., and Pradeepkumar, P. I. (2012) Selective G-quadruplex DNA stabilizing agents based on bisquinolinium and bispyridinium derivatives of 1,8-naphthyridine. *J. Org. Chem. 77*, 229−242.
(36) Han, H., Hurley, L. H., and Salazar, M. A. (1999) DNA polymerase stop assay for G-quadruplex-interactive compounds. *Nucleic Acids Res. 27*, 537−542.
(37) Seenisamy, J., Bashyam, S., Gokhale, V., Vankayalapati, H., Sun, D., Siddiqui-Jain, A., Streiner, N., Wilson, W. D., Hurley, L. H., Shinya, K., and White, W. D. (2005) Design and synthesis of an expanded porphyrin that has selectivity for the c-MYC G-quadruplex structure. *J. Am. Chem. Soc. 127*, 2944−2959.
(38) Dai, J., Carver, M., Hurley, L. H., and Yang, D. (2011) Solution structure of a 2:1 quindoline-c-MYC G-quadruplex: insights into G-

DOI: 10.1021/acs.biochem.6b00120
Biochemistry 2016, 55, 3571−3585

quadruplex-interactive small molecule drug design. *J. Am. Chem. Soc. 133*, 17673−17680.
(39) Phan, A. T., Kuryavyi, V., Burge, S., Neidle, S., and Patel, D. J. (2007) Structure of an unprecedented G-quadruplex scaffold in the human c-kit promoter. *J. Am. Chem. Soc. 129*, 4386−4392.
(40) Parkinson, G. N., Lee, M. P. H., and Neidle, S. (2002) Crystal structure of parallel quadruplexes from human telomeric DNA. *Nature 417*, 876−880.
(41) Wang, Y., and Patel, D. J. (1993) Solution structure of the human telomeric repeat d[AG3(T2AG3)3] G-tetraplex. *Structure 1*, 263−282.
(42) Chung, W. J., Heddi, B., Tera, M., Iida, K., Nagasawa, K., and Phan, A. T. (2013) Solution Structure of an Intramolecular (3 + 1) Human Telomeric G-Quadruplex Bound to a Telomestatin Derivative. *J. Am. Chem. Soc. 135*, 13495−13501.
(43) Frisch, M. J., Trucks, G. W., Schlegel, H. B., Scuseria, G. E., Robb, M. A., Cheeseman, J. R., Scalmani, G., Barone, V., Mennucci, B., Petersson, G. A., Nakatsuji, H., Caricato, M., Li, X., Hratchian, H. P., Izmaylov, A. F., Bloino, J., Zheng, G., Sonnenberg, J. L., Hada, M., Ehara, M., Toyota, K., Fukuda, R., Hasegawa, J., Ishida, M., Nakajima, T., Honda, Y., Kitao, O., Nakai, H., Vreven, T., Montgomery, J. A., Jr., Peralta, J. E., Ogliaro, F., Bearpark, M. J., Heyd, J., Brothers, E. N., Kudin, K. N., Staroverov, V. N., Kobayashi, R., Normand, J., Raghavachari, K., Rendell, A. P., Burant, J. C., Iyengar, S. S., Tomasi, J., Cossi, M., Rega, N., Millam, N. J., Klene, M., Knox, J. E., Cross, J. B., Bakken, V., Adamo, C., Jaramillo, J., Gomperts, R., Stratmann, R. E., Yazyev, O., Austin, A. J., Cammi, R., Pomelli, C., Ochterski, J. W., Martin, R. L., Morokuma, K., Zakrzewski, V. G., Voth, G. A., Salvador, P., Dannenberg, J. J., Dapprich, S., Daniels, A. D., Farkas, Ö., Foresman, J. B., Ortiz, J. V., Cioslowski, J., and Fox, D. J. (2013) *Gaussian 09*, Revision D.01, Gaussian, Inc., Wallingford, CT.
(44) Morris, G. M., Huey, R., Lindstrom, W., Sanner, M. F., Belew, R. K., Goodsell, D. S., and Olson, A. J. (2009) AutoDock4 and AutoDockTools4: Automated docking with selective receptor flexibility. *J. Comput. Chem. 30*, 2785−2791.
(45) Trott, O., and Olson, A. J. (2010) AutoDock Vina: improving the speed and accuracy of docking with a new scoring function, efficient optimization, and multithreading. *J. Comput. Chem. 31*, 455−461.
(46) Haider, S., and Neidle, S. (2010) Molecular modeling and simulation of G-quadruplexes and quadruplex-ligand complexes. *Methods Mol. Biol. 608*, 17−37.
(47) Fox, T., and Kollman, P. A. (1998) Application of the RESP Methodology in the Parametrization of Organic Solvents. *J. Phys. Chem. B 102*, 8070−8079.
(48) Wang, J., Wolf, R. M., Caldwell, J. W., Kollman, P. A., and Case, D. A. (2004) Development and testing of a general amber force field. *J. Comput. Chem. 25*, 1157−1174.
(49) Krepl, M., Zgarbova, M., Stadlbauer, P., Otyepka, M., Banas, P., Koca, J., Cheatham, T. E., Jurecka, P., and Sponer, J. (2012) Reference Simulations of Noncanonical Nucleic Acids with Different χ Variants of the AMBER Force Field: Quadruplex DNA, Quadruplex RNA, and Z-DNA. *J. Chem. Theory Comput. 8*, 2506−2520.
(50) Cheatham, T. E., Cieplak, P., and Kollman, P. A. (1999) A Modified Version of the Cornell *et al.* Force Field with Improved Sugar Pucker Phases and Helical Repeat. *J. Biomol. Struct. Dyn. 16*, 845−862.
(51) Kollman, P. A., Massova, I., Reyes, C., Kuhn, B., Huo, S., Chong, L., Lee, M., Lee, T., Duan, Y., Wang, W., Donini, O., Cieplak, P., Srinivasan, J., Case, D. A., and Cheatham, T. E. (2000) Calculating structures and free energies of complex molecules: combining molecular mechanics and continuum models. *Acc. Chem. Res. 33*, 889−897.
(52) Humphrey, G. R., and Kuethe, J. T. (2006) Practical methodologies for the synthesis of indoles. *Chem. Rev. 106*, 2875−2920.
(53) Nakano, H., Saito, N., Parker, L., Tada, Y., Abe, M., Tsuganezawa, K., Yokoyama, S., Tanaka, A., Kojima, H., Okabe, T., and Nagano, T. (2012) Rational evolution of a novel type of potent and selective proviral integration site in Moloney murine leukemia virus kinase 1 (PIM1) inhibitor from a screening-hit compound. *J. Med. Chem. 55*, 5151−5164.
(54) Bansal, R., Narang, G., Zimmer, C., and Hartmann, R. (2011) Synthesis of some imidazolyl-substituted 2-benzylidene indanone derivatives as potent aromatase inhibitors for breast cancer therapy. *Med. Chem. Res. 20*, 661−669.
(55) Meng, F. C., Mao, F., Shan, W. J., Qin, F., Huang, L., and Li, X. S. (2012) Design, synthesis, and evaluation of indanone derivatives as acetylcholinesterase inhibitors and metal-chelating agents. *Bioorg. Med. Chem. Lett. 22*, 4462−4466.
(56) Kanagarajan, V., Thanusu, J., and Gopalakrishnan, M. (2010) Synthesis and in vitro microbiological evaluation of an array of biolabile 2-morpholino-N-(4,6-diarylpyrimidin-2-yl)acetamides. *Eur. J. Med. Chem. 45*, 1583−1589.
(57) Paramasivan, S., Rujan, I., and Bolton, H. P. (2007) Circular dichroism of quadruplex DNAs: applications to structure, cation effects and ligand binding. *Methods 43*, 324−331.
(58) Randazzo, A., Spada, G., and da Silva, M. W. (2012) Circular dichroism of quadruplex structures. *Top. Curr. Chem. 330*, 67−86.
(59) Karsisiotis, A. I., Hessari, N. M., Novellino, E., Spada, G. P., Randazzo, A., and Webba da Silva, M. (2011) Topological characterization of nucleic acid G-quadruplexes by UV absorption and circular dichroism. *Angew. Chem., Int. Ed. 50*, 10645−10648.
(60) Kim, M. Y., Vankayalapati, H., Shin-ya, K., Wierzba, K., and Hurley, L. H. (2002) Telomestatin, a potent telomerase inhibitor that interacts quite specifically with the human telomeric intramolecular g-quadruplex. *J. Am. Chem. Soc. 124*, 2098−2099.
(61) Guedin, A., Lacroix, L., and Mergny, J. L. (2010) Thermal melting studies of ligand DNA interactions. *Methods Mol. Biol. 613*, 25−35.
(62) Petraccone, L., Spink, C., Trent, J. O., Garbett, N. C., Mekmaysy, C. S., Giancola, C., and Chaires, J. B. (2011) Structure and stability of higher-order human telomeric quadruplexes. *J. Am. Chem. Soc. 133*, 20951−20961.
(63) Gabelica, V. (2010) Determination of equilibrium association constants of ligand-DNA complexes by electrospray mass spectrometry. *Methods Mol. Biol. 613*, 89−101.
(64) Marchand, A., Granzhan, A., Iida, K., Tsushima, Y., Ma, Y., Nagasawa, K., Teulade-Fichou, M. P., and Gabelica, V. (2015) Ligand-induced conformational changes with cation ejection upon binding to human telomeric DNA G-quadruplexes. *J. Am. Chem. Soc. 137*, 750−756.
(65) Case, D. A., Cheatham, T. E., Darden, T. O. M., Gohlke, H., Luo, R. A. Y., Merz, K. M., Onufriev, A., Simmerling, C., Wang, B., and Woods, R. J. (2005) The Amber biomolecular simulation programs. *J. Comput. Chem. 26*, 1668−1688.
(66) Li, Q., Xiang, J. F., Yang, Q. F., Sun, H. X., Guan, A. J., and Tang, Y. L. G4LDB: a database for discovering and studying G-quadruplex ligands. *Nucleic Acids Res.* 2013, *41*, D1115−D1123.10.1093/nar/gks1101
(67) Piazza, A., Boule, J. B., Lopes, J., Mingo, K., Largy, E., Teulade-Fichou, M. P., and Nicolas, A. (2010) Genetic instability triggered by G-quadruplex interacting Phen-DC compounds in Saccharomyces cerevisiae. *Nucleic Acids Res. 38*, 4337−4348.
(68) Hale, T. K., Norris, G. E., Jameson, G. B., and Filichev, V. V. (2014) Helicases, G4-DNAs, and drug design. *ChemMedChem 9*, 2031−2034.

DOI: 10.1021/acs.biochem.6b00120
Biochemistry 2016, 55, 3571−3585

Specific Stabilization of *c-MYC* and *c-KIT* G-Quadruplex DNA Structures by Indolylmethyleneindanone Scaffolds

K. V. Diveshkumar,[†] Saaz Sakrikar,[†] Frédéric Rosu,[‡,§] S. Harikrishna,[†]

Valérie Gabelica*[,§,⊥] and P. I. Pradeepkumar*[,†]

[†]*Department of Chemistry, Indian Institute of Technology Bombay, Mumbai-400076, India*

[‡]*CNRS, UMS3033/US001, Institut Européen de Chimie et Biologie, 33607 Pessac, France*

[§]*Univ. Bordeaux, U869 ARNA Laboratory, 33600 Pessac, France*

[⊥]*Inserm, U869 ARNA Laboratory, 33000 Bordeaux, France*

E-mail: valerie.gabelica@inserm.fr and pradeep@chem.iitb.ac.in

TABLE OF CONTENTS

CD spectra of ligands with telomeric DNA in the absence of added metal ions

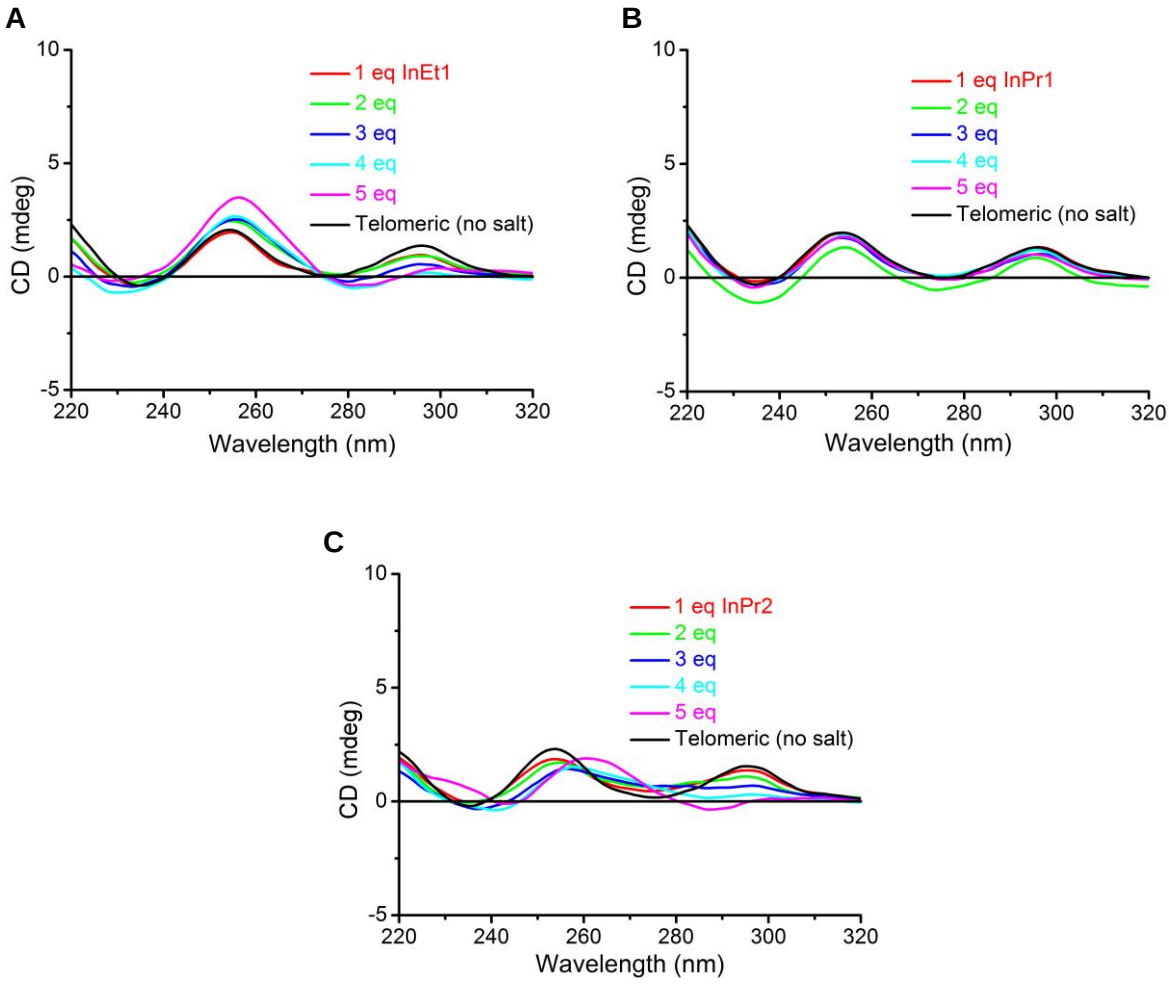

Figure S1. CD titration spectra of ligands with telomeric DNA (12.5 µM DNA in 50 mM Tris-HCl, pH 7.2) in the absence of added metal ions. (A) **InEt1**; (B) **InPr1**; and (C) **InPr2**.

CD spectra of ligands with *c-MYC* DNA in the absence of added metal ions

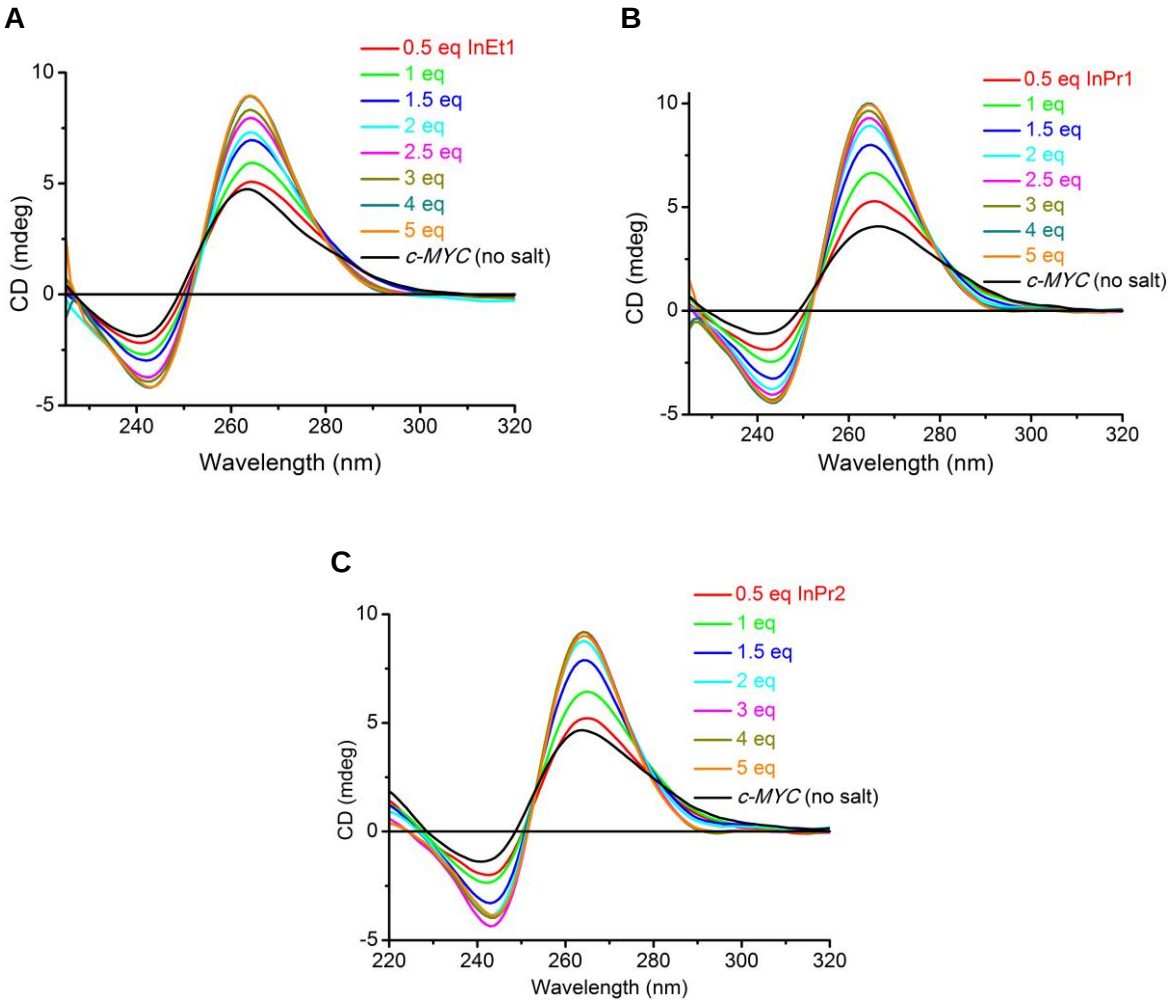

Figure S2. CD titration spectra for ligands with *c-MYC* DNA (12.5 µM DNA in 50 mM Tris-HCl, pH 7.2) in the absence of added metal ions. (A) **InEt1**; (B) **InPr1**; and (C) **InPr2**.

CD spectra of ligands with *c-KIT1* DNA in the absence of added metal ions

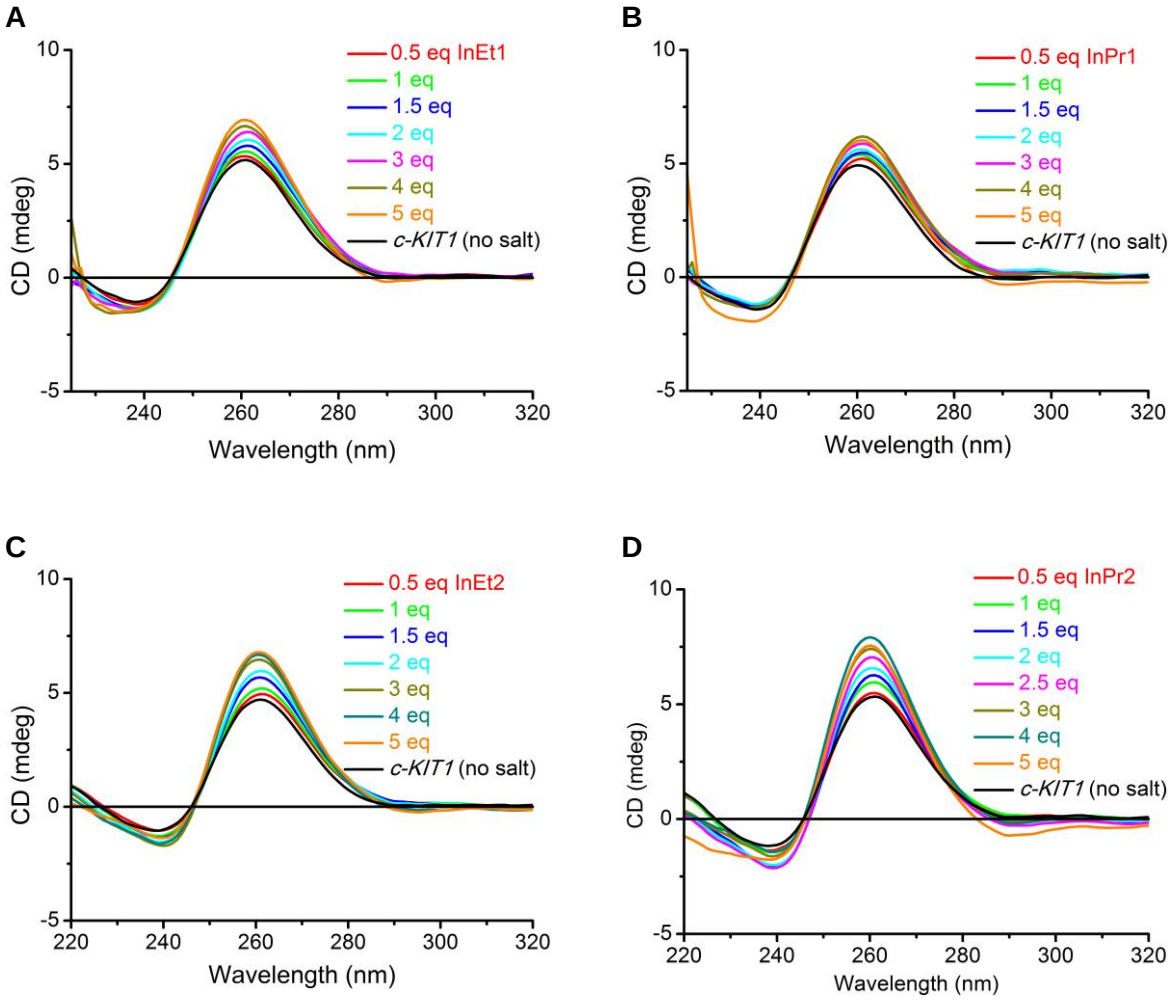

Figure S3. CD titration spectra of ligands with *c-KIT1* DNA (12.5 µM DNA in 50 mM Tris-HCl, pH 7.2) in the absence of added metal ions. (A) **InEt1**; (B) **InPr1**; (C) **InEt2**; and (D) **InPr2**.

CD spectra of ligands with *c-KIT2* DNA in the absence of added metal ions

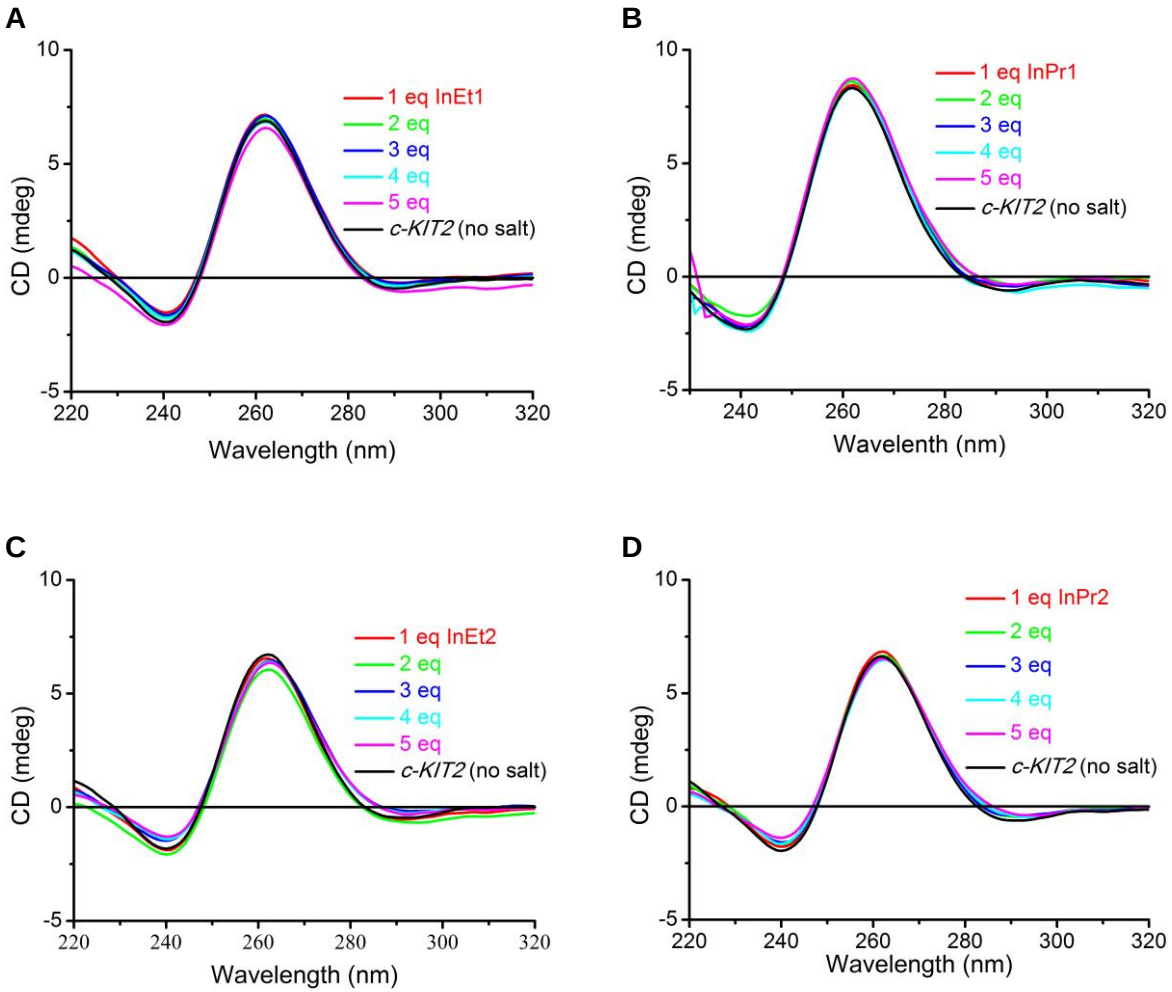

Figure S4. CD titration spectra of ligands with *c-KIT2* DNA (12.5 µM DNA in 50 mM Tris-HCl, pH 7.2) in the absence of added metal ions. (A) **InEt1**; (B) **InPr1**; (C) **InEt2**; and (D) **InPr2**.

Nondenaturing gel of telomeric DNA from EMSA

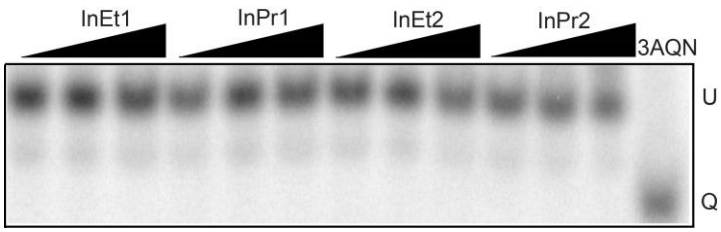

Figure S5. Nondenaturing PAGE of telomeric DNA (5 µM in 10 mM Tris-HCl, pH 7.2) with increasing molar equivalents of ligands (0, 5 and 10) in the absence of added monovalent cations at 22 °C. Induction of stable compact quadruplex structure by the control ligand 3AQN (5 equivalents) resulted in accelerated mobility of telomeric DNA and no acceleration observed for the telomeric DNA bands after titration with the ligands. **U** denotes non-quadruplex forms and **Q** denotes quadruplex forms.

CD melting curves of *c-KIT1*, *c-KIT2* quadruplex, duplex and long telomeric DNAs

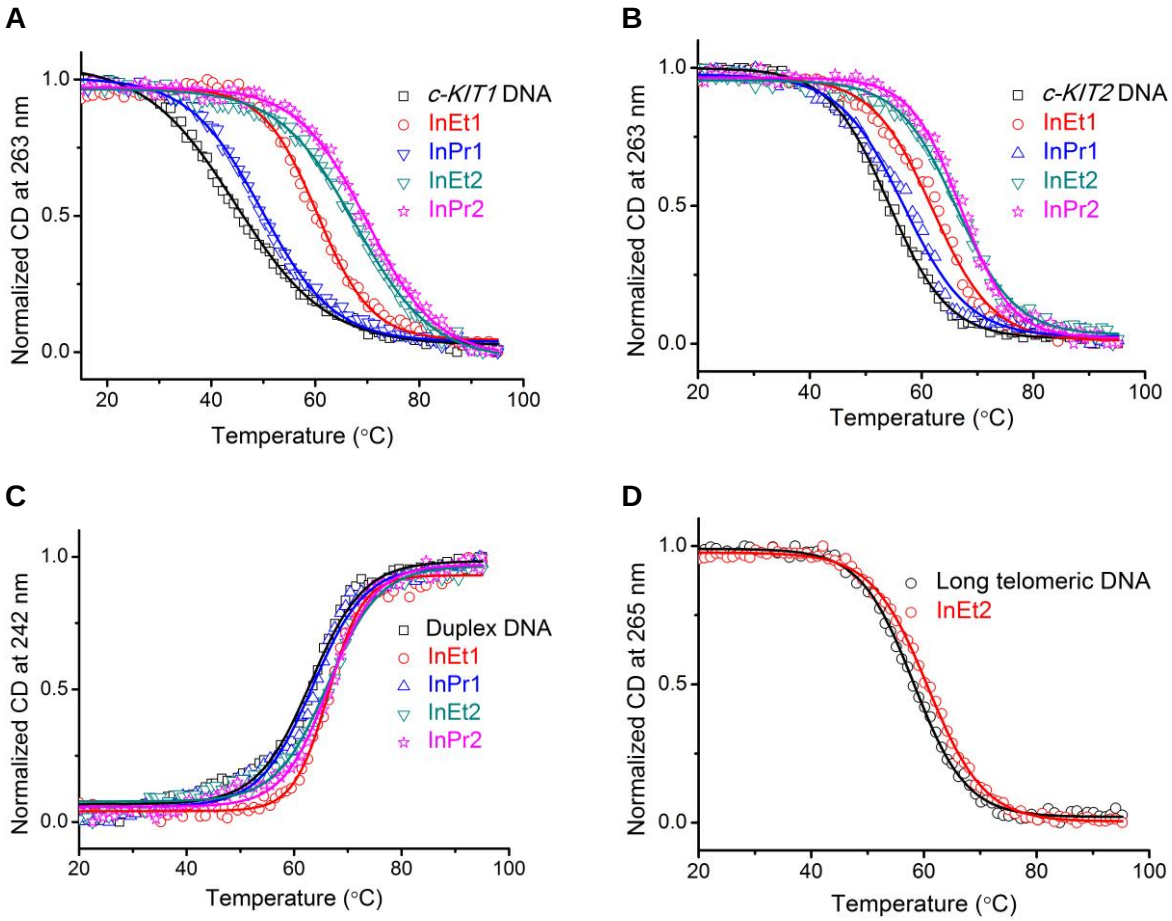

Figure S6. CD melting curves of *c-KIT*, duplex and long telomeric DNAs (10 mM lithium cacodylate buffer, pH 7.2) in the absence and presence of 5 equivalents of ligands. (A) *c-KIT1* (10 µM in 10 mM KCl and 90 mM LiCl); (B) *c-KIT2* DNA (10 µM in 1mM KCl, 99 mM LiCl); (C) Duplex DNA (15 µM in 10 mM KCl and 90 mM LiCl); and (D) Long telomeric DNA (10 µM in 100 mM KCl)

ESI-MS mass spectra of *c-KIT1*, $(TG_4T)_4$ and duplex DNAs with ligands

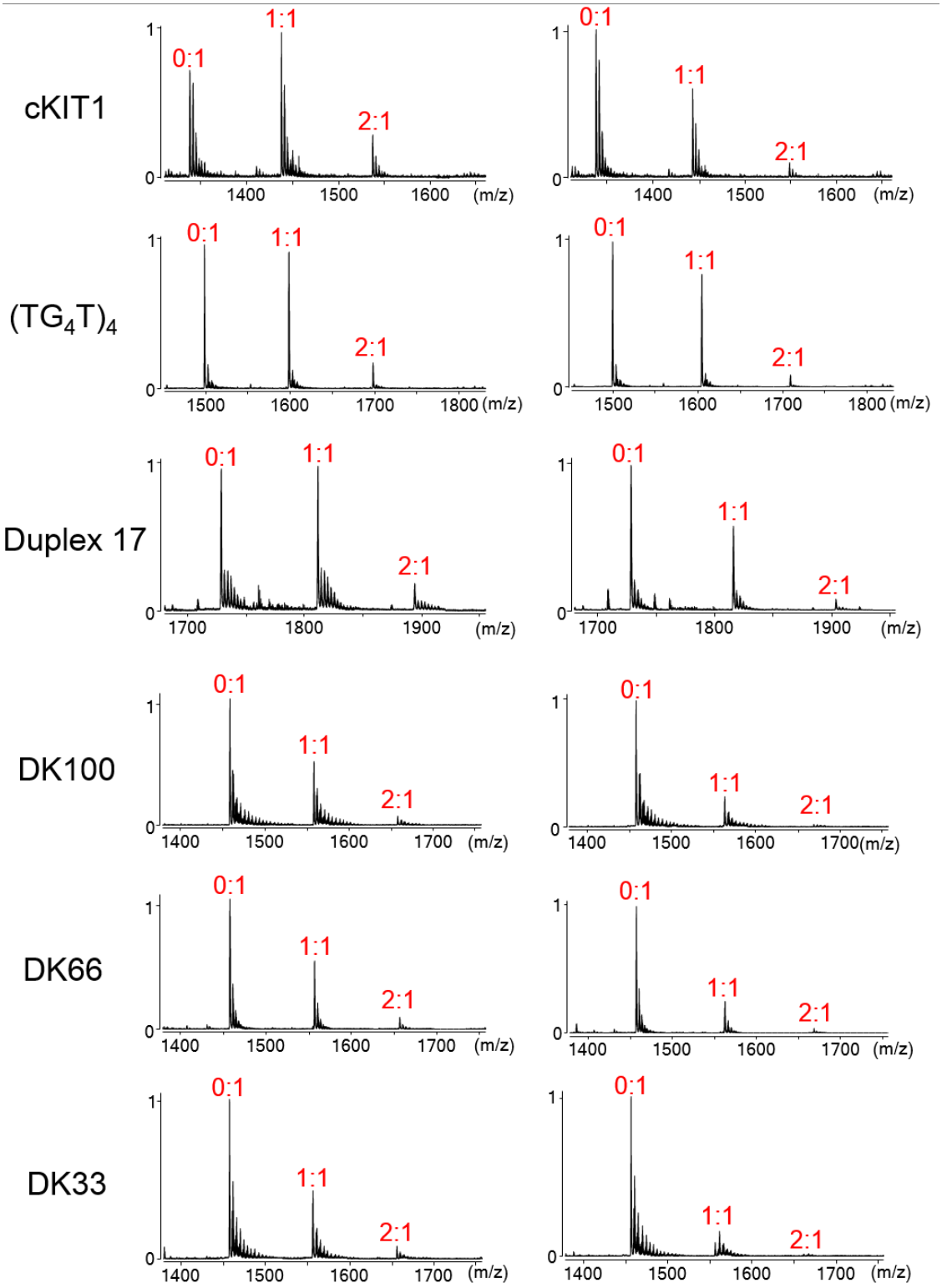

Figure S7. ESI-MS spectra with zoom on the 5- charge state of *c-KIT1*, $(TG_4T)_4$, telomeric quadruplex and duplex DNAs of different GC content (5 µM DNA, 10 µM ligands in 100 mM NH_4OAc solution) at 22 °C. Left column: **InEt2** ligand. Right column: **InPr2** ligand. Peak annotations indicate the stoichiometry as (number of ligands bound):(target structure).

ITC profiles of ligands with quadruplex and duplex DNAs

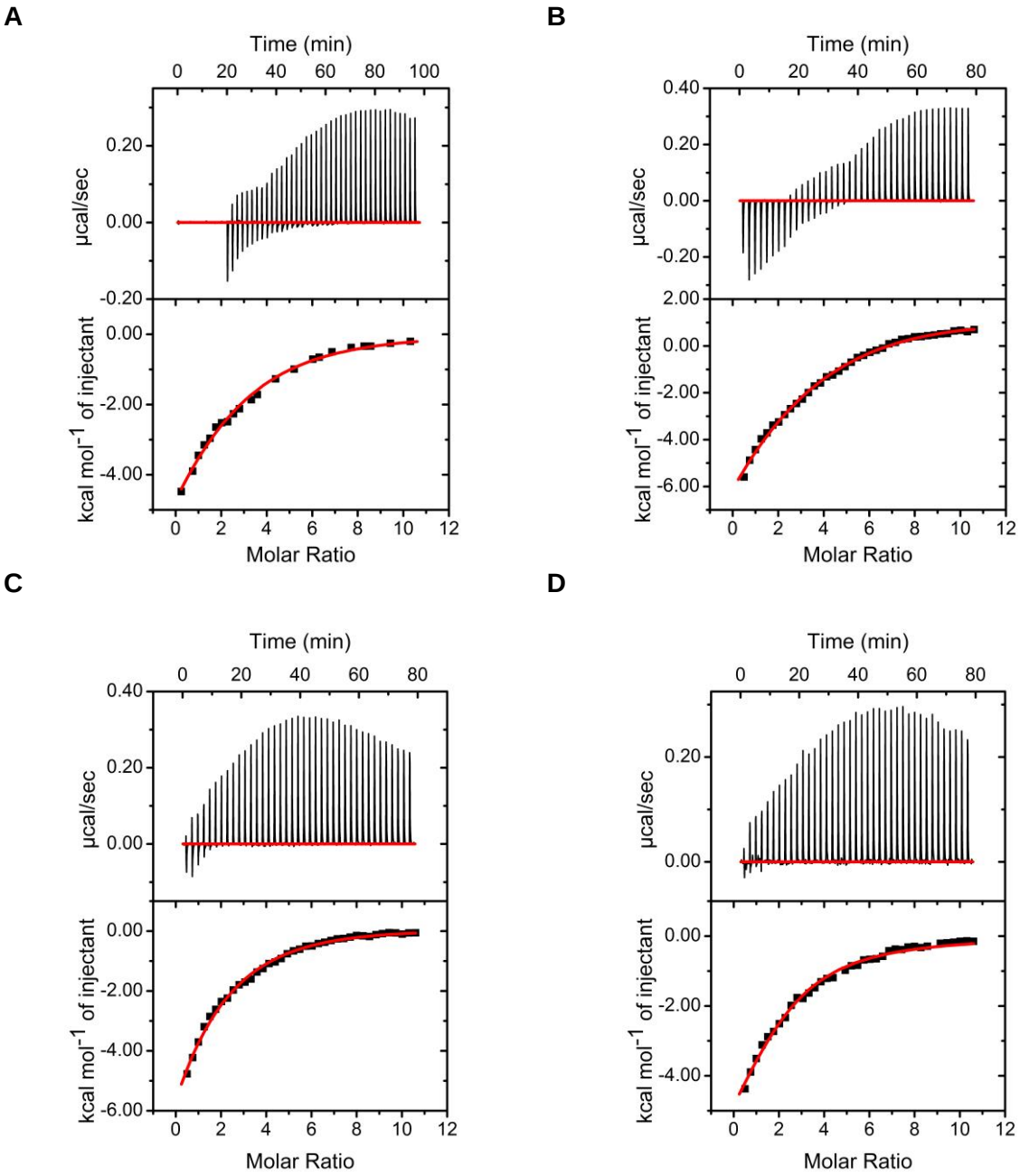

Figure S8. ITC profiles for the interaction of ligand **InEt2** and **InPr2** with quadruplex and duplex DNAs (50 µM DNA in 100 mM KCl and 10 mM lithium cacodylate buffer, pH 7.2). (A) Telomeric DNA with **InEt2**; (B) Duplex DNA with **InEt2**; (C) Telomeric DNA with **InPr2**; and (D) Duplex DNA with **InPr2**. Raw data shown in upper panel and curve fit by using sequential binding mode after subtracting the heats of dilution is shown in the bottom panel.

PAGE of *Taq* DNA polymerase stop assay

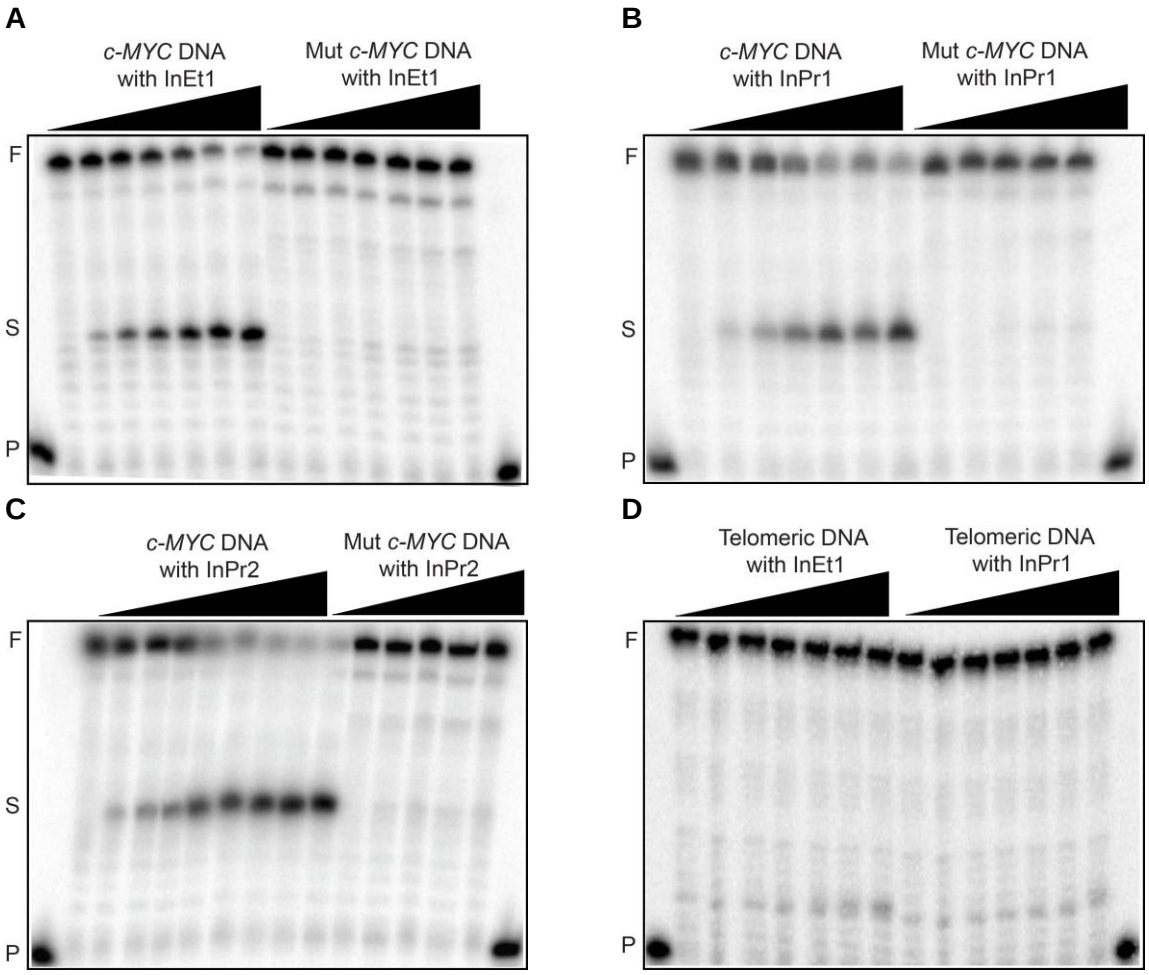

Figure S9. Denaturing PAGE (15%, 7M urea) of *Taq* DNA polymerase stop assay of ligands with *c-MYC* (A-C) and telomeric quadruplex (D) DNAs. (A) **InEt1** (0-80 µM); (B) **InPr1** (0-160 µM); (C) **InPr2** (0-10 µM); and (D) **InEt1** and **InPr1** (0-120 µM). Primer extension reactions were carried out at 50 °C for *c-MYC* DNA and at 40 °C for telomeric DNA. Conditions: 100 nM template, 50 nM primer, 0.2 mM dNTPs in *Taq* polymerase buffer (50 mM Tris, 0.5 mM DTT, 0.1 mM EDTA, 5 mM $MgCl_2$, 5mM KCl for *c-MYC* template and 10 mM KCl for telomeric template).

IC_{50} plots from *Taq* DNA polymerase stop assay

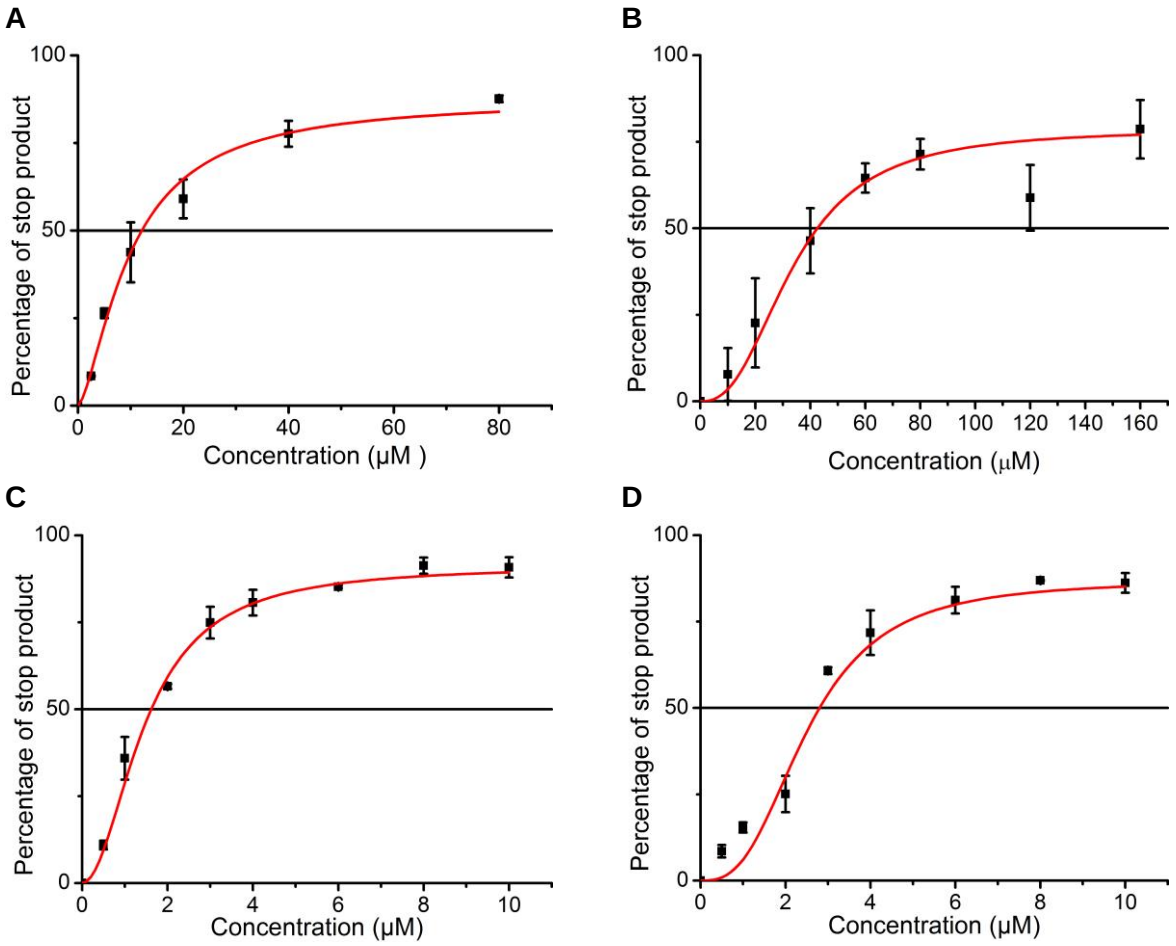

Figure S10. Plots of *Taq* DNA polymerase stop products versus ligand concentration. Normalized percentage of stop products in each lane was plotted against concentration of ligand. (A) **InEt1** (0-80 μM); (B) **InPr1** (0-160 μM); (C) **InEt2** (0-10 μM); and (D) **InPr2** (0-10 μM). Error bar represents standard deviation from 3 independent experiments.

Energy optimized structures of ligands at HF/6-31G* level

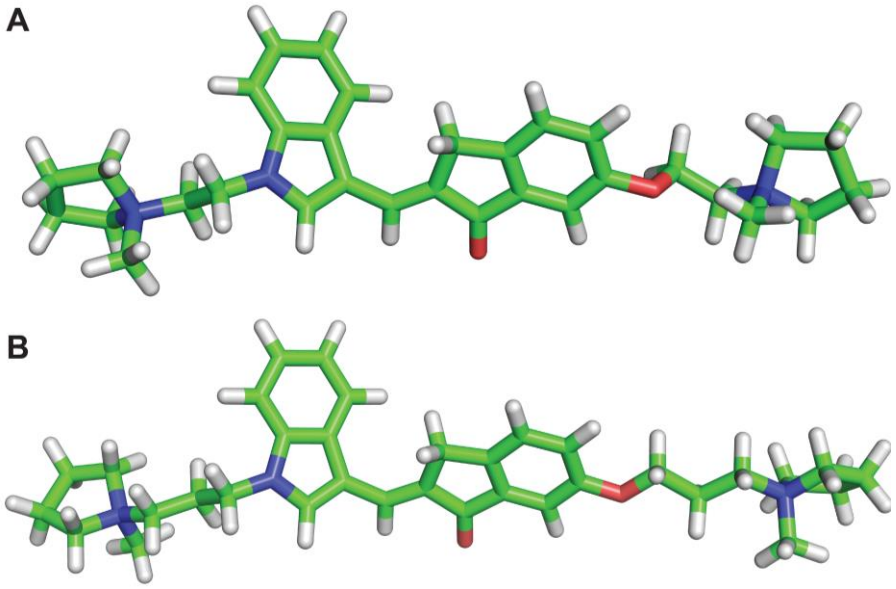

Figure S11. Energy optimized structures of (A) **InEt2**; and (B) **InPr2** using HF/6-31G* level in Gaussian 09. RESP charges were calculated at same level in Gaussian 09. Figures were rendered using PyMOL.

Time dependent RMSD graphs of *c-MYC* DNA and InEt2

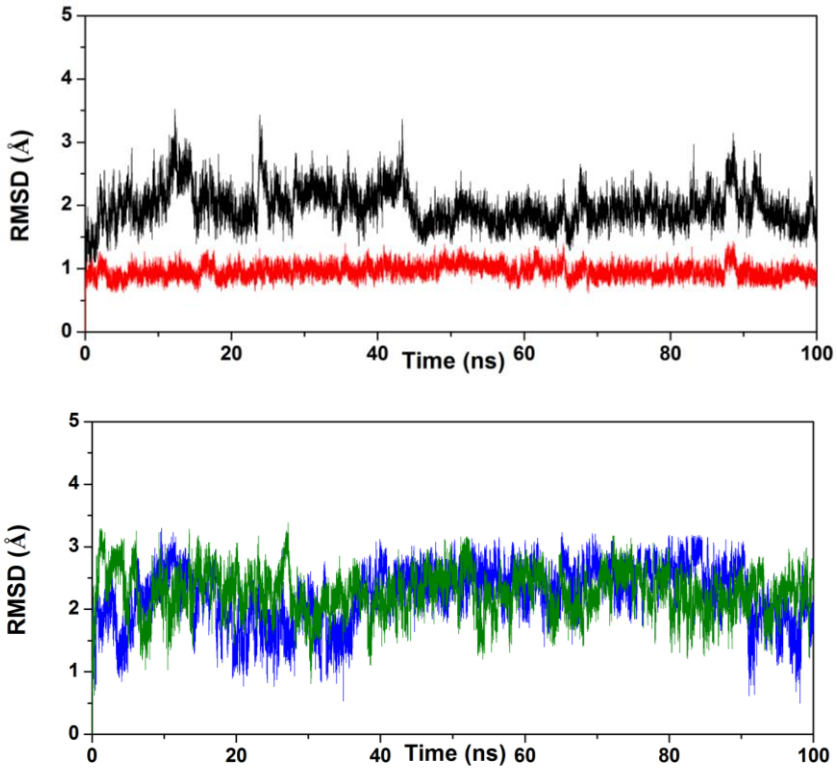

Figure S12. Time dependent root mean square deviation graphs (RMSD) of *c-MYC* G-quadruplex DNA complexed with **InEt2**. RMSD of backbone (black), G-quartet (red), 5'-**InEt2** (blue) and 3'-**InEt2** (green) were plotted against time. RMSDs were calculated at each ps during 100 ns of MD simulations using ptraj module in AMBER 14.

Time dependent RMSD graphs of *c-KIT1* DNA and InEt2

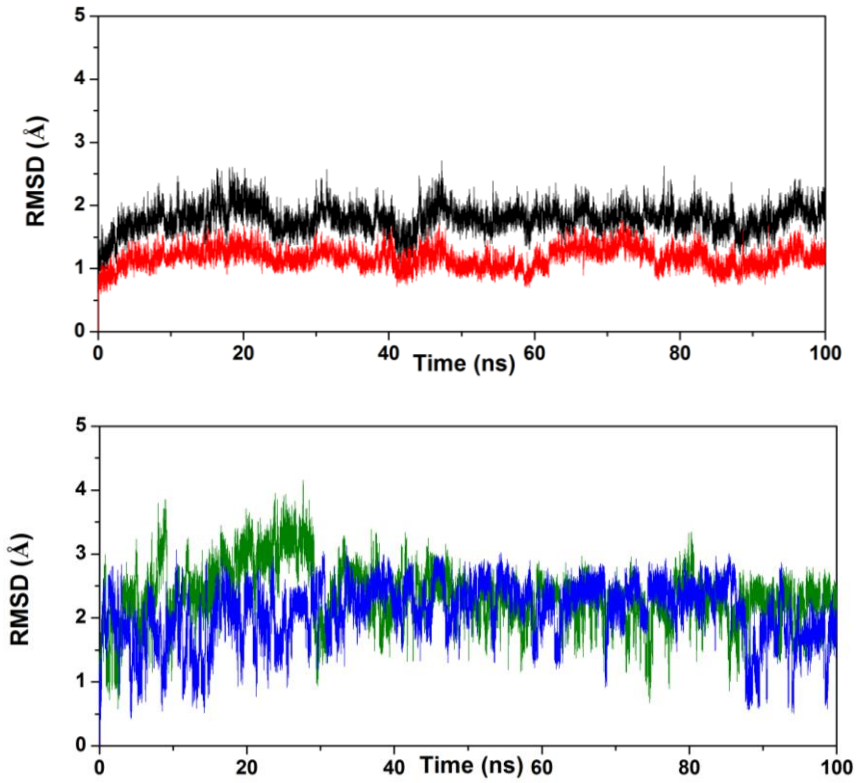

Figure S13. Time dependent root mean square deviation graphs (RMSD) of *c-KIT1* G-quadruplex DNA complexed with **InEt2**. RMSD of backbone (black), G-quartet (red), 5'-**InEt2** (blue) and 3'-**InEt2** (green) were plotted against time. RMSDs were calculated at each ps during 100 ns of MD simulations using ptraj module in AMBER 14.

MD snapshots of InPr2 with *c-MYC* quadruplex DNA

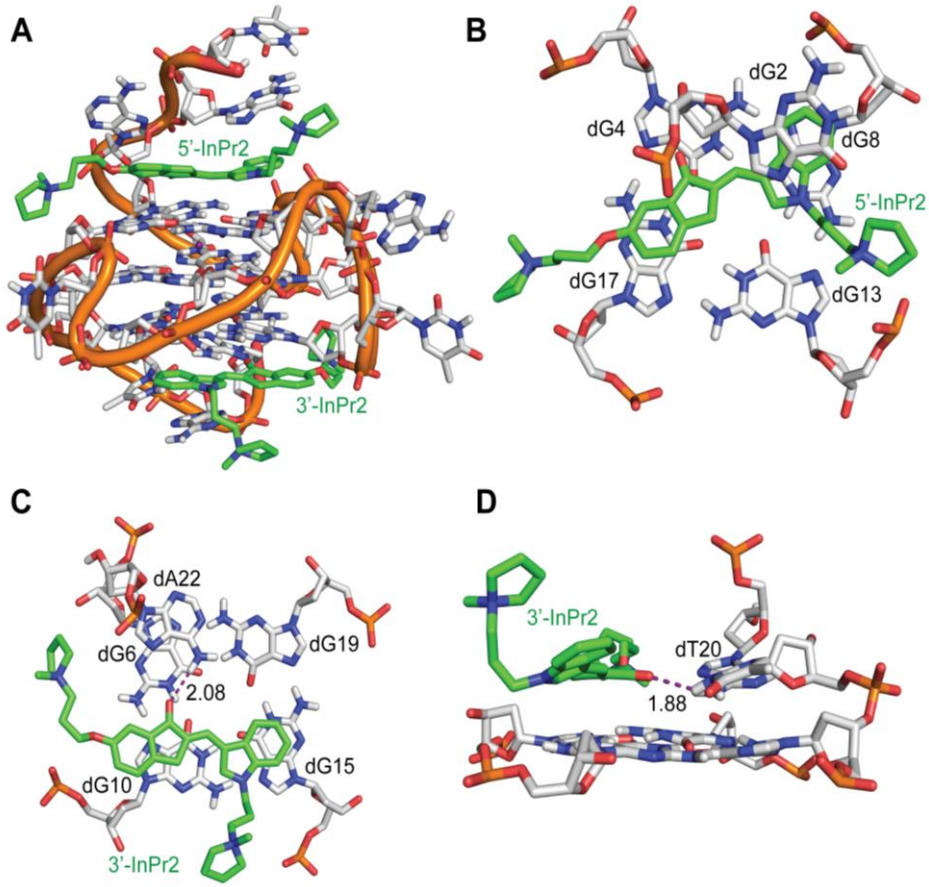

Figure S14. MD snapshots of **InPr2** with *c-MYC* G-quadruplex DNA at 100 ns of the MD simulation. (A) **InPr2** and *c-MYC* G-quadruplex DNA (2:1): stacking occurs at both the 5' and 3' G-quartets of the G-quadruplex DNA; (B) **InPr2** and 5' quartet, showing stacking with 5' quartet guanines as well as flanking nucleotide; (C) **InPr2** and 3' quartet, showing the hydrogen bonding with the flanking nucleotide (dA22) and stacking with 3' quartet residues; and (D) Snapshot of 3'-**InPr2** at 60 ns, where the ligand has moved into a position where the H-bond is with dT20 and stacking of indole ring with the quartet is disrupted. This position is seen for 34% of the MD run. Dashed lines indicate the hydrogen bond distance between the atoms in ligand and G-quadruplex DNA while red lines indicate stacking distances; all distances are given in Å.

MD snapshots of InPr2 with *c-KIT1* quadruplex DNA

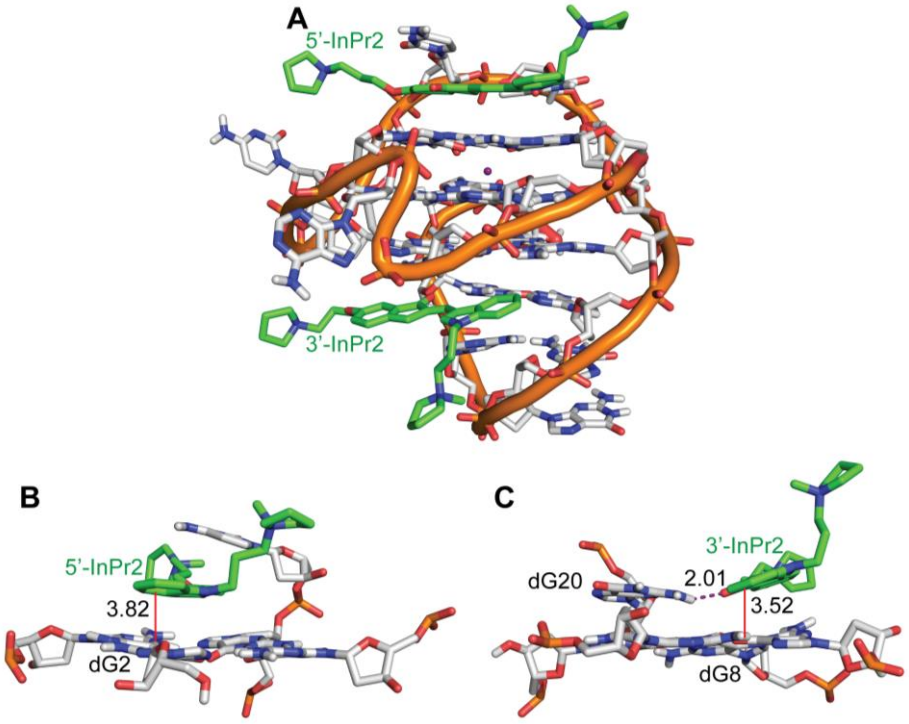

Figure S15. MD snapshots of **InPr2** with *c-KIT1* G-quadruplex DNA at 100 ns of the MD simulation. (A) **InPr2** and *c-KIT1* G-quadruplex DNA (2:1): stacking occurs at both the 5' and 3' G-quartets of the G-quadruplex; (B) **InPr2** and 5' quartet, showing stacking from indanone and indole rings to 5' quartet residues dG10 and dG2 respectively; and (C) **InPr2** and 3' quartet, showing stacking with 3' quartet guanines and H-bonding with flanking dG20. Dashed lines indicate the hydrogen bond distance between the atoms in ligand and G-quadruplex DNA, while red lines indicate stacking distances; all the distances are given in Å.

Time dependent RMSD graphs of telomeric antiparallel quadruplex and InEt2

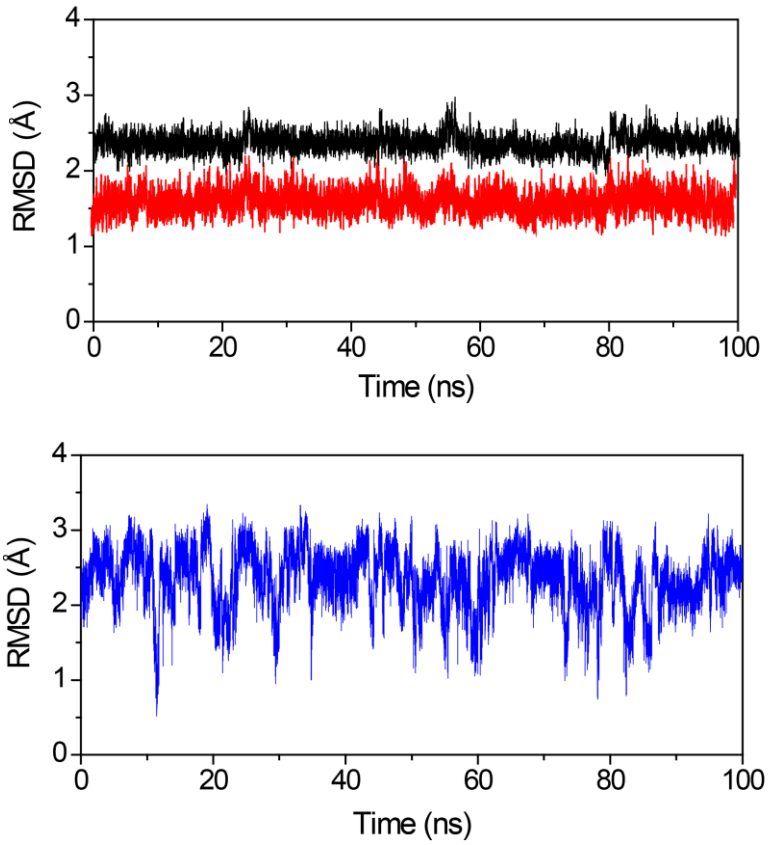

Figure S16. Time dependent root mean square deviation graphs (RMSD) of telomeric antiparallel G-quadruplex DNA complexed with **InEt2**. RMSD of backbone (black), G-quartet (red), **InEt2** (blue) were plotted against time. RMSDs were calculated at each ps during the 100 ns of MD simulations using ptraj module in AMBER 14.

Time dependent RMSD graphs of telomeric antiparallel quadruplex and InPr2

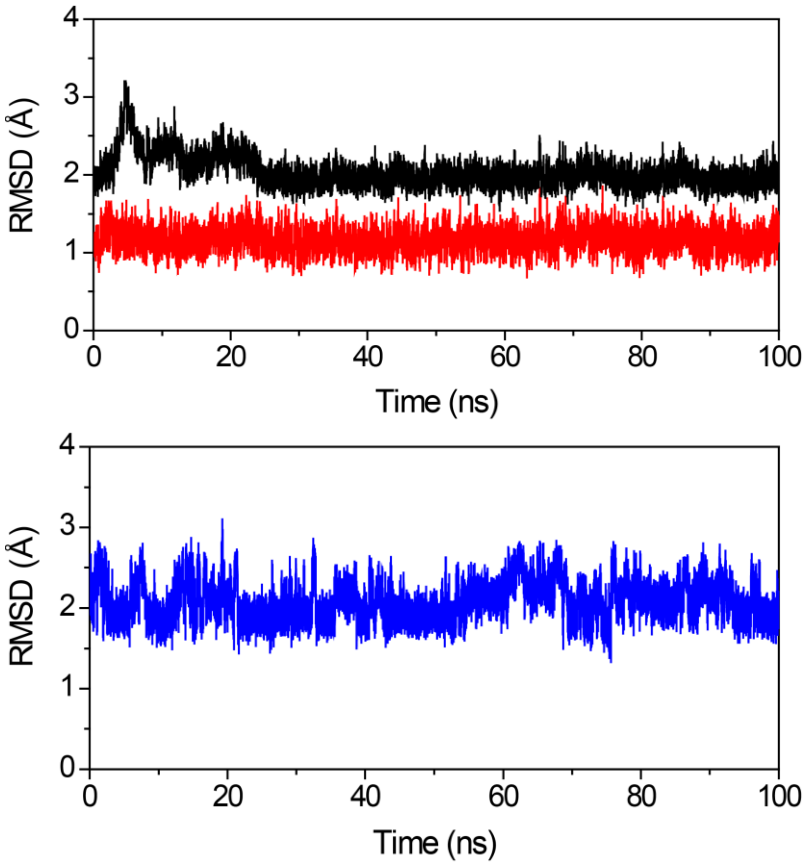

Figure S17. Time dependent root mean square deviation graphs (RMSD) of telomeric antiparallel G-quadruplex DNA complexed with **InPr2**. RMSD of backbone (black), G-quartet (red), **InPr2** (blue) were plotted against time. RMSDs were calculated at each ps during the 100 ns of MD simulations using ptraj module in AMBER 14.

Time dependent RMSD graphs of telomeric hybrid quadruplex and InEt2

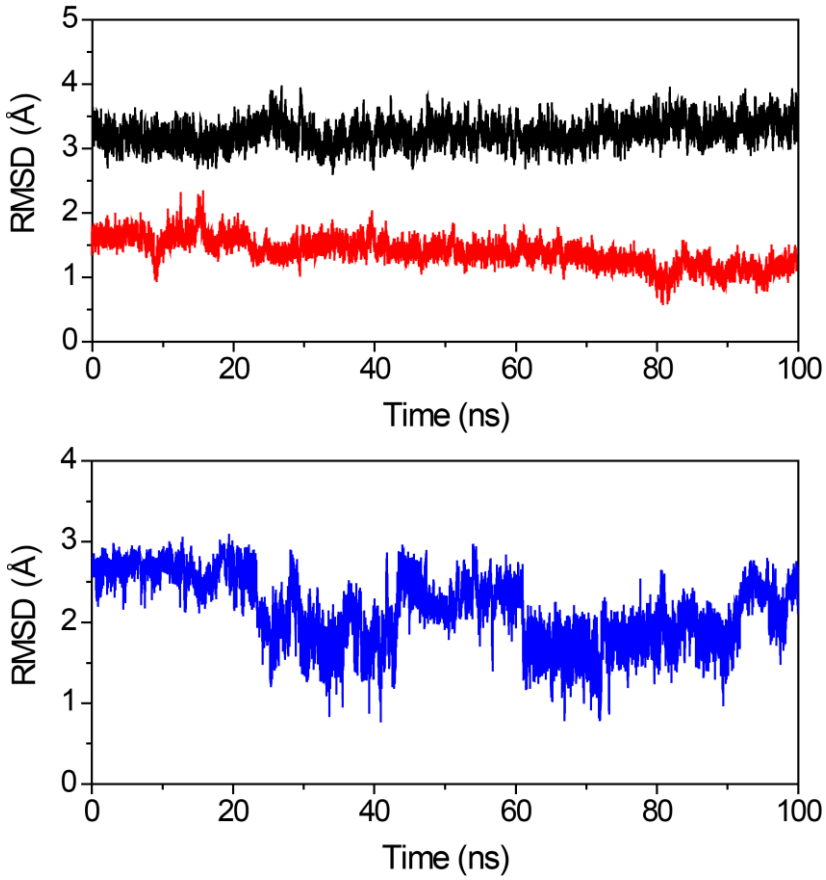

Figure S18. Time dependent root mean square deviation graphs (RMSD) of telomeric hybrid G-quadruplex DNA complexed with **InEt2**. RMSD of backbone (black), G-quartet (red), **InEt2** (blue) were plotted against time. RMSDs were calculated at each ps during the 100 ns of MD simulations using ptraj module in AMBER 14.

Time dependent RMSD graphs of telomeric hybrid quadruplex and InPr2

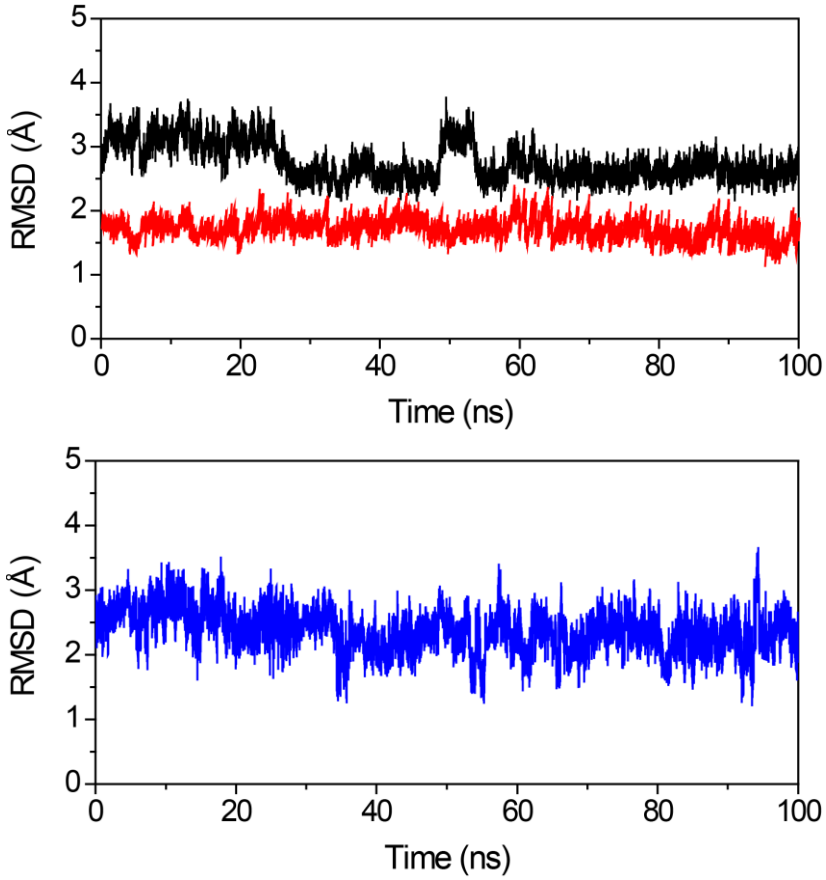

Figure S19. Time dependent root mean square deviation graphs (RMSD) of telomeric hybrid G-quadruplex DNA complexed with **InPr2**. RMSD of backbone (black), G-quartet (red), **InPr2** (blue) were plotted against time. RMSDs were calculated at each ps during the 100 ns of MD simulations using ptraj module in AMBER 14.

Time dependent RMSD graphs of telomeric parallel quadruplex and InEt2

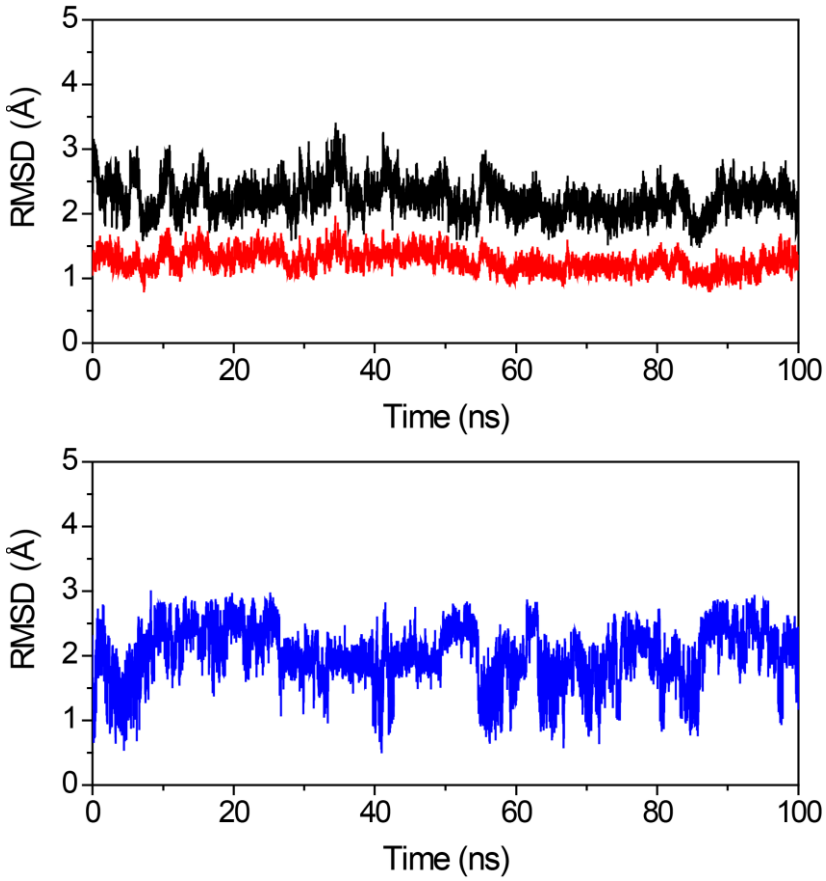

Figure S20. Time dependent root mean square deviation graphs (RMSD) of telomeric parallel G-quadruplex DNA complexed with **InEt2**. RMSD of backbone (black), G-quartet (red), **InEt2** (blue) were plotted against time. RMSDs were calculated at each ps during the 100 ns of MD simulations using ptraj module in AMBER 14.

Time dependent RMSD graphs of telomeric parallel quadruplex and InPr2

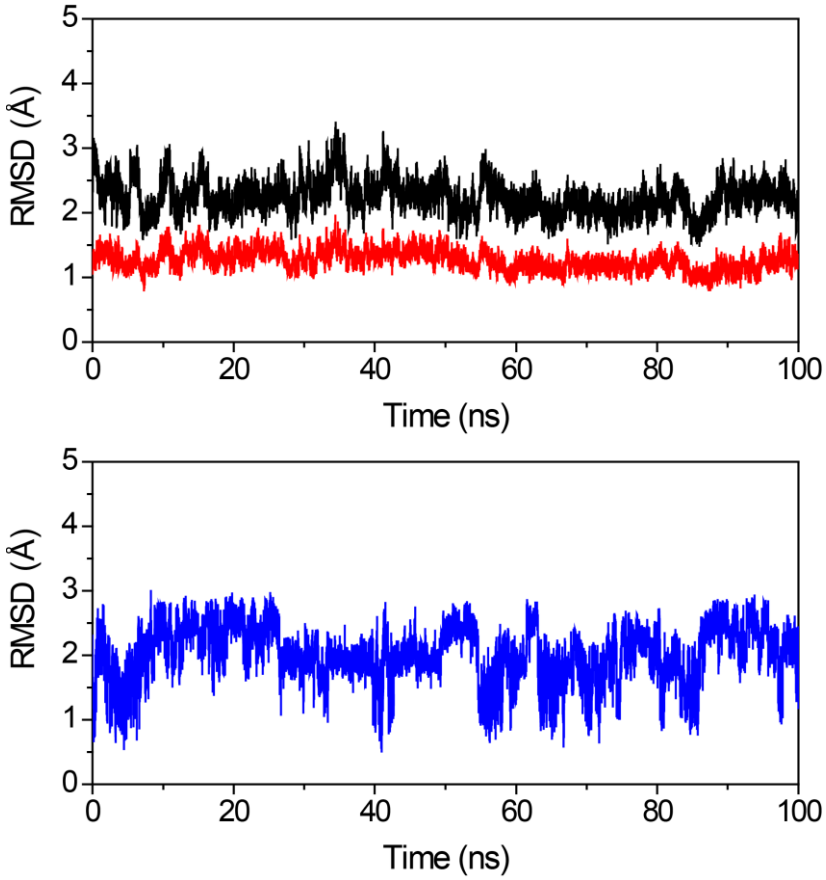

Figure S21. Time dependent root mean square deviation graphs (RMSD) of telomeric parallel G-quadruplex DNA complexed with **InPr2**. RMSD of backbone (black), G-quartet (red), **InPr2** (blue) were plotted against time. RMSDs were calculated at each ps during the 100 ns of MD simulations using ptraj module in AMBER 14.

MD snapshots of InEt2 and InPr2 with telomeric parallel quadruplex DNA

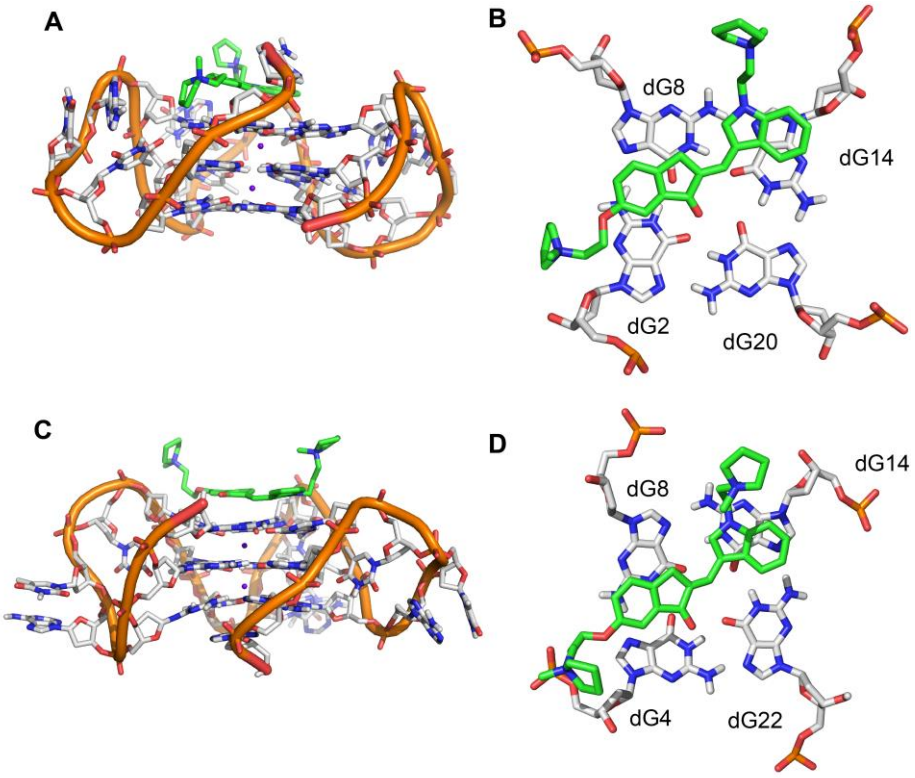

Figure S22. MD snapshots of **InEt2** and **InPr2** with telomeric parallel G-quadruplex DNA at 100 ns of the MD simulation. (A) Snapshot of **InEt2** and telomeric parallel G-quadruplex DNA (full view); (B) Top G-quartet view of **InEt2** and telomeric parallel G-quadruplex DNA; (C) MD snapshot of **InPr2** and telomeric parallel G-quadruplex DNA (full view); and (D) Top G-quartet view of **InPr2** and telomeric parallel G-quadruplex DNA.

MD snapshots of InEt2 and InPr2 with telomeric antiparallel quadruplex DNA

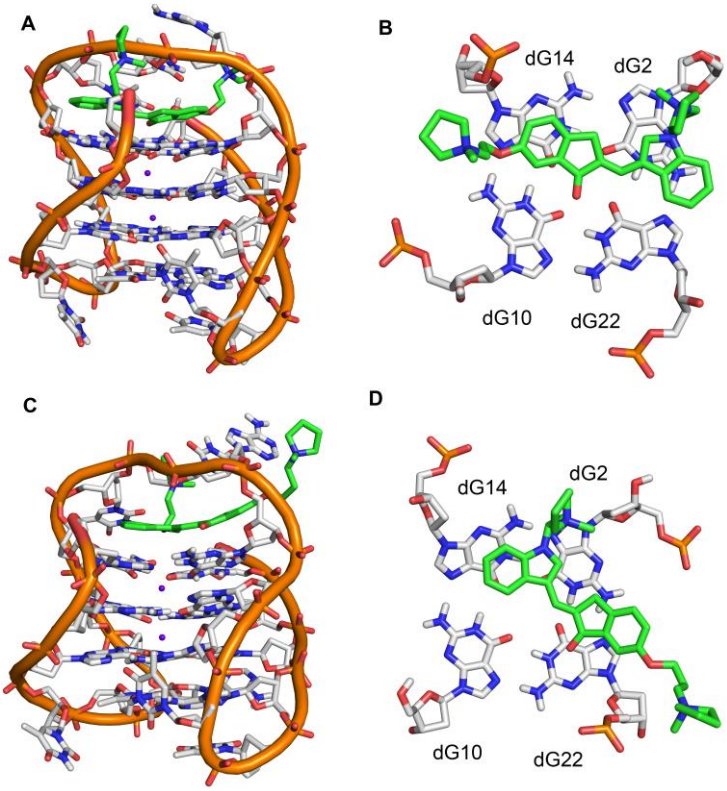

Figure S23. MD snapshots of **InEt2** and **InPr2** with telomeric antiparallel G-quadruplex DNA at 100 ns of the MD simulation. (A) Snapshot of **InEt2** and telomeric antiparallel G-quadruplex DNA (full view); (B) Top G-quartet view of **InEt2** and telomeric antiparallel G-quadruplex DNA; (C) MD snapshot of **InPr2** and telomeric antiparallel G-quadruplex DNA (full view); and (D) Top G-quartet view of **InPr2** and telomeric antiparallel G-quadruplex DNA.

MD snapshots of InEt2 and InPr2 with telomeric hybrid quadruplex DNA

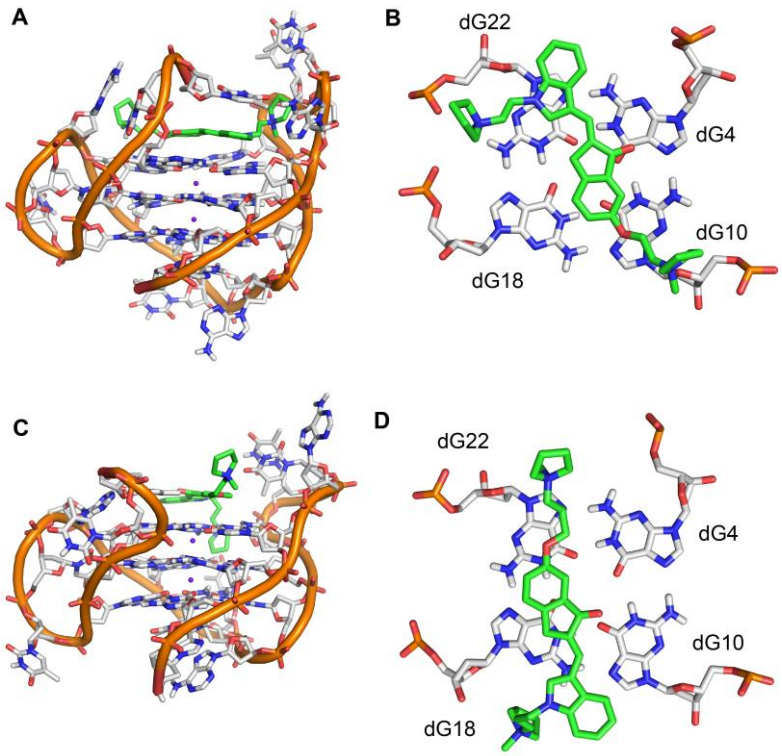

Figure S24. MD snapshots of **InEt2** and **InPr2** with telomeric hybrid G-quadruplex DNA at 100 ns of the MD simulation. (A) Snapshot of **InEt2** and telomeric hybrid G-quadruplex DNA (full view); (B) Top G-quartet view of **InEt2** and telomeric hybrid G-quadruplex DNA; (C) MD snapshot of **InPr2** and telomeric hybrid G-quadruplex DNA (full view); and (D) Top G-quartet view of **InPr2** and telomeric hybrid G-quadruplex DNA.

Oligonucleotides used for biophysical and biochemical studies

Description	Sequence
Telomeric DNA	5'-AGGGTTAGGGTTAGGGTTAGGG-3'
Long telomeric DNA	5'-AGGGTTAGGGTTAGGGTTAGGG-TT-AGGGTTAGGGT TAGGGTTAGGG-3'
c-MYC DNA	5'-TGAGGGTGGGTAGGGTGGGGAA-3'
c-KIT1 DNA	5'-GGGAGGGCGCTGGGAGGAGGG-3'
c-KIT2 DNA	5'-GGGCGGGCGCGAGGGAGGGG-3'
Parallel quadruplex DNA	$(5'\text{-TGGGGT-}3')_4$
DS17	5'-CCAGTTCGTAGTAACCC-3'
	5'-GGGTTACTA CGAACTGG-3'
DK33	$(5'\text{-CGTAAATTTACG-}3')_2$
DK66	$(5'\text{-CGCGAATTCGCG -}3')_2$
DK100	$(5'\text{-CGCGGGCCCGCG-}3')_2$
Primer for stop assay	5'-ACGACTCACTATAGCAATTGCG-3'
Template with *c-MYC*	5'-TGAGGGTGGGGAGGGTGGGGAAGCCACCGCAATTG
DNA	CTATAGTGAGTCGT-3'
Template with mutated *c-*	5'-TGAGGGTGGGTAGAGTGGGTAAGCCACCGCAATTG
MYC DNA	CTATAGTGAGTCGT-3'
Template with telomeric	5'-AGGGTTAGGGTTAGGGTTAGGGGCCACCGCAATTG
DNA	CTATAGTGAGTCGT-3'

Table S1. List of oligonucleotides used for the experiments.

Thermodynamic parameters of telomeric quadruplex and duplex DNAs from ITC

Ligand	K_1 (M^{-1}) × 10^4	ΔH_1 (kcal/mol)	$T\Delta S_1$ (kcal/mol)	K_2 (M^{-1}) × 10^4	ΔH_2 (kcal/mol)	$T\Delta S_2$ (kcal/mol)
Telomeric DNA						
InEt2	0.6 ± 0.05	−20.6 ± 1.5	−1.3	0.4 ± 0.03	5.8± 2.0	0.1
InPr2	0.7 ± 0.05	−20.6 ± 0.9	−1.3	0.3 ± 0.03	10.3 ± 1.6	1.3
Duplex-17 (DS17)						
InEt2	1.2 ± 0.05	−100 ± 3.9	8.1	2.3 ± 0.2	153.6 ± 5.4	13.3
InPr2	2.2 ± 0.2	−8.9 ± 0.3	−0.2	0.6 ± 0.04	−7.7 ± 0.6	−0.2

Table S2. Thermodynamic parameters obtained from ITC experiment for the interaction of ligands with telomeric quadruplex and duplex DNAs at 25 °C. Best fit parameters obtained by sequential binding model with Chi^2 = 8173 and 6293 for **InEt2** and **InPr2** with telomeric DNA and Chi^2 = 8124 and 7860 for **InEt2** and **InPr2** with duplex DNA respectively

Average RMSDs of G-Quadruplex DNAs and InEt2 complex

Heavy atoms of DNA and ligand	*c-MYC* G-quadruplex DNA	*c-KIT1* G-quadruplex DNA
G-quartet	0.96 ± 0.11	1.17 ± 0.16
DNA backbone	1.98 ± 0.29	1.80 ± 0.20
InEt2	2.22 ± 0.45 (5'-**InEt2**)	2.09 ± 0.46 (5'-**InEt2**)
	2.27 ± 0.35 (3'-**InEt2**)	2.35 ± 0.44 (3'-**InEt2**)

Table S3. Average RMSD values (Å) of the heavy atoms in the backbone, G-quartet of G-quadruplex DNA complexed with **InEt2**. RMSDs were calculated at each ps from 100 ns of MD simulations using ptraj module in AMBER 14. Errors indicate the standard deviation.

Hoogsteen H-bond occupancies in G-quartet during MD simulations of InEt2

G-quartet	Percentage occupancy (*c-MYC)*	Percentage occupancy (*c-KIT1)*
5' quartet	99.59%	99.92%
Middle quartet	99.09%	98.84%
3' quartet	99.83%	99.67%

Table S4. The percentage occupancy of Hoogsteen hydrogen bond between the guanine bases present in each G-quartet. The occupancies were calculated at each ps during 100 ns of MD simulations using ptraj module in AMBER 14.

Binding free energy components of InEt2-*c-MYC* quadruplex DNA complex

MD Simulations (100 ns)	***c-MYC* G-quadruplex DNA (PDB entry: 2L7V)**		
	Dual	**5'-InEt2**	**3'-InEt2**
ΔE_{ELEC}	−1765 ± 26	−875 ± 19	−990 ± 22
ΔE_{VDW}	−126 ± 6	−64 ± 3	−61 ± 5
$\Delta E_{MM}(\Delta E_{Elec}+\Delta E_{VDW})$	−1891 ± 29	−940 ± 20	−951 ± 25
ΔPB_{np}	−13 ± 0.5	−7 ± 0.3	−7 ± 0.5
ΔPB_{cal}	1798 ± 27	890 ± 19	908 ± 23
ΔPB_{solv} ($\Delta PB_{np}+\Delta PB_{cal}$)	1785 ± 27	883 ± 19	902 ± 23
$\Delta H_{PB}(\Delta E_{MM}+\Delta PB_{solv})$	**−106 ± 6**	**−57 ± 4**	**−50 ± 4**
ΔGB_{np}	−13 ± 0.5	−7 ± 0.3	−7 ± 0.5
ΔGB_{cal}	1779 ± 26	881 ± 18	898 ± 22
ΔGB_{solv} ($\Delta GB_{np}+\Delta GB_{cal}$)	1766 ± 25	875 ± 18	891 ± 22
$\Delta H_{GB}(\Delta E_{MM}+\Delta GB_{solv})$	−126 ± 5	−65 ± 3	−60 ± 4
ΔS_{TRANS}	−13.85 ± 0.00	−13.28 ± 0.00	−13.29 ± 0.00
ΔS_{ROTA}	−13.19 ± 0.02	−11.64 ± 0.03	−11.62 ± 0.04
ΔS_{VIBR}	−0.55 ± 7.86	7.50 ± 6.39	7.08 ± 6.59
$T\Delta S$	−26 ± 8	−17 ± 6	−18 ± 7
ΔG ($\Delta H_{PB} - T\Delta S$)	**−80 ± 10**	**−39 ± 7**	**−30 ± 8**

Table S5. Binding free energy components of *c-MYC* G-quadruplex DNA in complex with **InEt2** calculated from last 15 ns of 100 ns MD simulations. The molecular mechanical energy calculations are calculated using MM/PB-GBSA and entropy calculations are carried using nmode in AMBER 14. ΔE_{ELEC} is the electrostatic interaction, ΔE_{VDW} is the Vander Waals contribution, ΔE_{MM} is the total molecular-mechanical energy (ΔE_{ELEC} + ΔE_{VDW} + ΔE_{ini} (zero for all)). ΔGB_{np} is the nonpolar contribution to the solvation energy. ΔH_{PB} and ΔH_{GB} are the electrostatic contributions to the solvation energy calculated; ΔPB_{solv} and ΔGB_{solv} are the total solvation energy. $T\Delta S$ is solute entropic contribution, where T = temperature and ΔS is the sum of translational, rotational, and vibrational entropies. ΔG is the estimated binding free energy with solute entropic contribution ($\Delta H_{GB} - T\Delta S$). All the values are reported in kcal mol^{-1}.

Binding free energy components of InEt2-*c-KIT1* quadruplex DNA complex

MD Simulations (100 ns)	***c-KIT1* G-quadruplex DNA (PDB entry: 2O3M)**		
	Dual	**5'-InEt2**	**3'-InEt2**
ΔE_{ELEC}	−1662 ± 35	−750 ± 27	−912 ± 26
ΔE_{VDW}	−100 ± 6	−47 ± 4	−53 ± 4
$\Delta E_{MM}(\Delta E_{Elec}+\Delta E_{VDW})$	−1762 ± 39	−797 ± 30	−964 ± 29
ΔPB_{np}	−11 ± 0.5	−5 ± 0.4	−6 ± 0.3
ΔPB_{cal}	1688 ± 36	762 ± 27	926 ± 28
ΔPB_{solv} ($\Delta PB_{np}+\Delta PB_{cal}$)	1677 ± 35	756 ± 27	921 ± 28
$\Delta H_{PB}(\Delta E_{mm}+\Delta PB_{solv})$	**−85 ± 7**	**−40 ± 5**	**−43 ± 5**
ΔGB_{np}	−11 ± 0.5	−5 ± 0.4	−6 ± 0.3
ΔGB_{cal}	1671 ± 35	755 ± 26	916 ± 26
ΔGB_{solv} ($\Delta GB_{np}+\Delta GB_{cal}$)	1660 ± 34	750 ± 26	910 ± 26
$\Delta H_{GB}(\Delta E_{MM}+\Delta GB_{solv})$	−102 ± 6	−47 ± 5	−54 ± 5
ΔS_{TRANS}	−13.84 ± 0.00	−13.28 ± 0.00	−13.28 ± 0.00
ΔS_{ROTA}	−13.21 ± 0.03	−11.61 ± 0.04	−11.63 ± 0.06
ΔS_{VIBR}	−0.38 ± 7.16	7.87 ± 5.87	7.35 ± 5.74
$T\Delta S$	−27 ± 7	−17 ± 6	−18 ± 6
ΔG ($\Delta H_{PB} - T\Delta S$)	**−58 ± 7**	**−23 ± 5**	**−26 ± 5**

Table S6. Binding free energy components of *c-KIT1* G-quadruplex DNA in complex with **InEt2** calculated from last 15 ns of 100 ns MD simulations. The molecular mechanical energy calculations are calculated using MM/PB-GBSA and entropy calculations are carried using nmode in AMBER 14. ΔE_{ELEC} is the electrostatic interaction, ΔE_{VDW} is the Vander Waals contribution, ΔE_{MM} is the total molecular-mechanical energy (ΔE_{ELEC} + ΔE_{VDW} + ΔE_{ini} (zero for all)). ΔGB_{np} is the nonpolar contribution to the solvation energy. ΔH_{PB} and ΔH_{GB} are the electrostatic contributions to the solvation energy calculated; ΔPB_{solv} and ΔGB_{solv} are the total solvation energy. $T\Delta S$ is solute entropic contribution, where T = temperature and ΔS is the sum of translational, rotational, and vibrational entropies. ΔG is the estimated binding free energy with solute entropic contribution ($\Delta H_{GB} - T\Delta S$). All the values are reported in kcal mol^{-1}.

Binding free energy components of InEt2-telomeric G-quadruplex DNA complexes

MD Simulations (100 ns)	Telomeric G-quadruplex DNA		
	Parallel	**Antiparallel**	**Hybrid**
ΔE_{ELEC}	−747 ± 22	−742 ± 25	−722 ± 26
ΔE_{VDW}	−43 ± 3	−39 ± 5	−37 ± 4
$\Delta E_{MM}(\Delta E_{Elec}+\Delta E_{VDW})$	−790 ± 26	−781 ± 23	−759 ± 29
ΔPB_{np}	−6 ± 0.3	−7 ± 0.5	−5 ± 0.3
ΔPB_{cal}	752 ± 27	749 ± 29	726 ± 28
ΔPB_{solv} ($\Delta PB_{np}+\Delta PB_{cal}$)	746 ± 27	742 ± 24	719 ± 28
$\Delta H_{PB}(\Delta E_{mm}+\Delta PB_{solv})$	−44 ± 5	−39 ± 5	−40 ± 5
ΔS_{TRANS}	−13.28 ± 0.00	−13.28 ± 0.00	−13.28 ± 0.00
ΔS_{ROTA}	−12.61 ± 0.04	−12.61 ± 0.04	−12.63 ± 0.06
ΔS_{VIBR}	5.7 ± 1.2	5.8 ± 1.2	3.8 ± 1
$T\Delta S$	−20 ± 4	−20 ± 4	−22 ± 5
ΔG ($\Delta H_{PB} - T\Delta S$)	**−24 ± 3**	**−19 ± 3**	**−20 ± 4**

Table S7. Binding free energy components of telomeric G-quadruplex DNA toplogies in complex with **InEt2** calculated from last 15 ns of 100 ns MD simulations. The molecular mechanical energy calculations are calculated using MM/GBSA and entropy calculations are carried using nmode in AMBER 14. All the values are reported in kcal mol^{-1}.

Binding free energy components of InPr2-telomeric G-quadruplex DNA complexes

MD Simulations (100 ns)	Telomeric G-quadruplex DNA		
	Parallel	**Antiparallel**	**Hybrid**
ΔE_{ELEC}	−745 ± 22	−739 ± 25	−732 ± 24
ΔE_{VDW}	−41 ± 3	−39 ± 5	−38 ± 4
$\Delta E_{MM}(\Delta E_{Elec}+\Delta E_{VDW})$	−786 ± 26	−768 ± 23	−770 ± 27
ΔPB_{np}	−5 ± 0.3	−6 ± 0.5	−6 ± 0.5
ΔPB_{cal}	748 ± 27	730 ± 29	736 ± 25
ΔPB_{solv} $(\Delta PB_{np}+\Delta PB_{cal})$	743 ± 27	724 ± 24	730 ± 24
$\Delta H_{PB}(\Delta E_{mm}+\Delta PB_{solv})$	−43 ± 5	−44 ± 5	−40 ± 5
ΔS_{TRANS}	−13.62 ± 0.00	−13.62 ± 0.00	−13.28 ± 0.00
ΔS_{ROTA}	−12.82 ± 0.04	−12.85 ± 0.04	−12.63 ± 0.06
ΔS_{VIBR}	5.7 ± 1.2	6.8 ± 1.2	3.8 ± 1
$T\Delta S$	−21 ± 4	−20 ± 4	−22 ± 5
ΔG $(\Delta H_{PB} - T\Delta S)$	**−22 ± 3**	**−24 ± 3**	**−22 ± 4**

Table S8. Binding free energy components of telomeric G-quadruplex DNA toplogies in complex with **InPr2** calculated from last 15 ns of 100 ns MD simulations. The molecular mechanical energy calculations are calculated using MM/PBSA and entropy calculations are carried using nmode in AMBER 14. All the values are reported in kcal mol^{-1}.

Percentage Life time occupancies of stacking interactions over 100 ns of MD simulations

	Telomeric G-quadruplex DNA		
	Parallel	**Antiparallel**	**Hybrid**
InEt2	42%	31%	30%
InPr2	46%	29%	23%

Table S9. Percentage life-time occupancies of stacking interaction between G-quartet and the ligand over the 100 ns time of MD simulations. This analysis was carried out using CPPTRAJ in AMBER 14. The cut-off distance between the center of mass is < 3.7 Å and the angle between the planes of the residues is < 30°.

^{1}H & ^{13}C spectra of compound 2 (G - Grease)

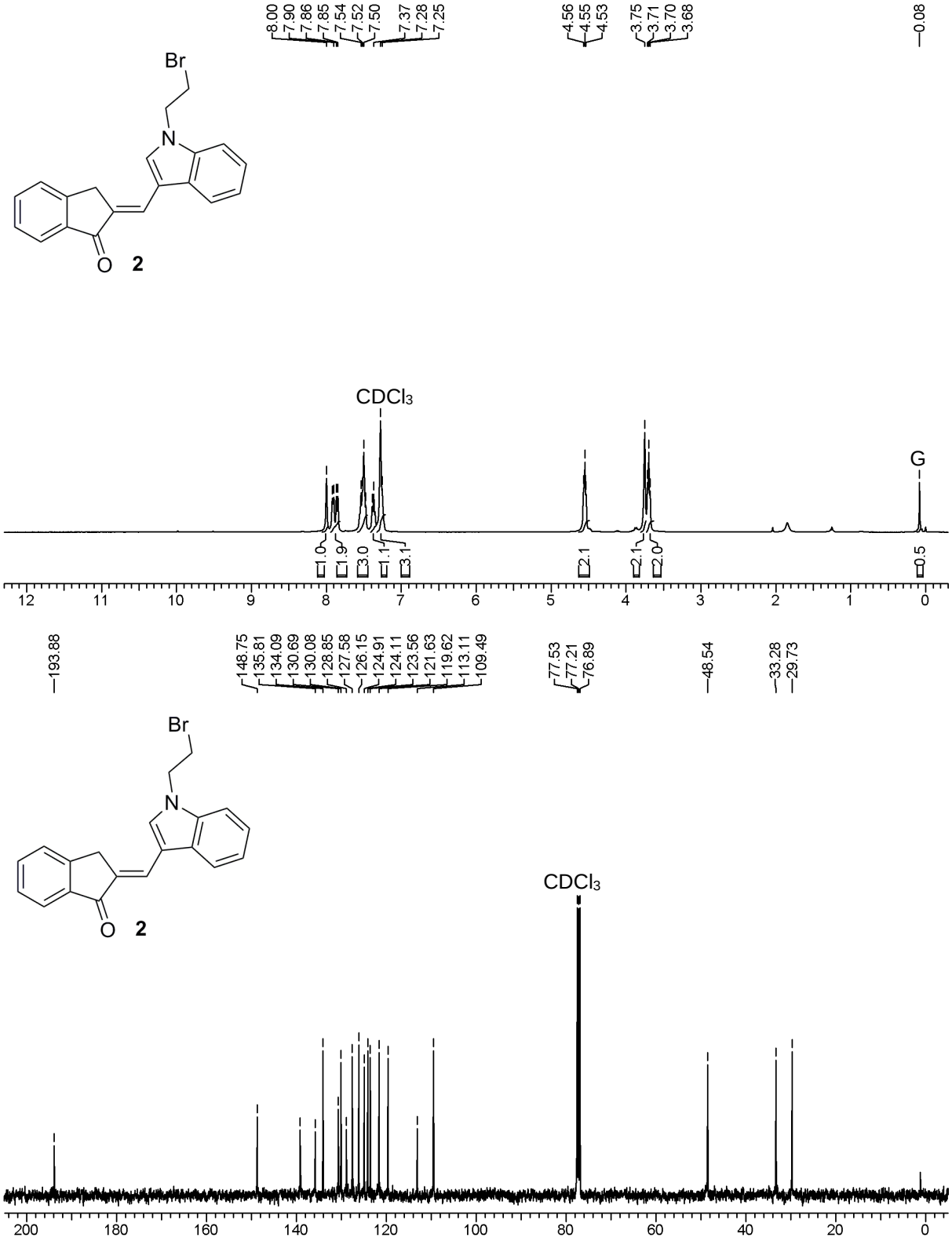

^{1}H & ^{13}C spectra of compound 3

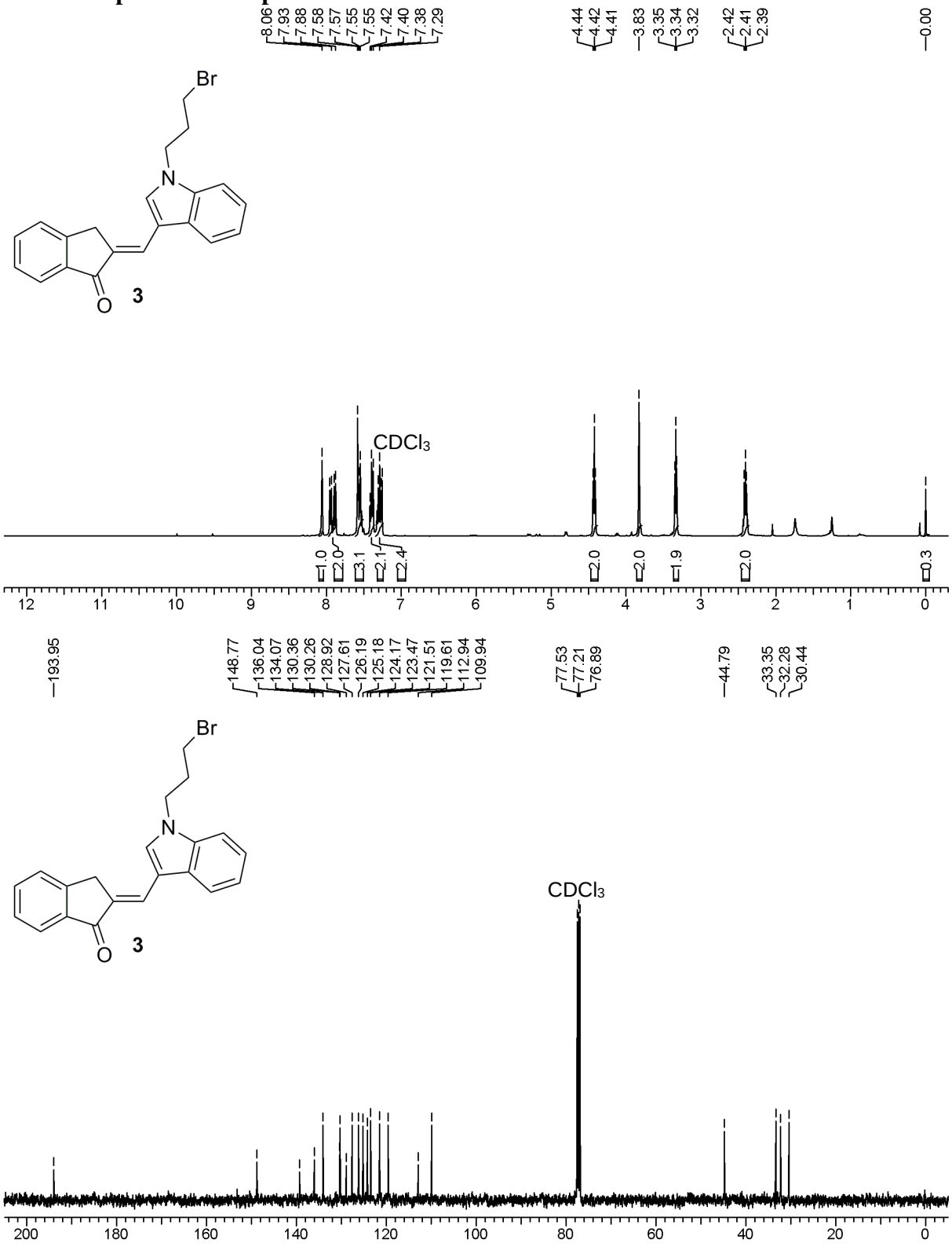

^{1}H & ^{13}C spectra of compound 4

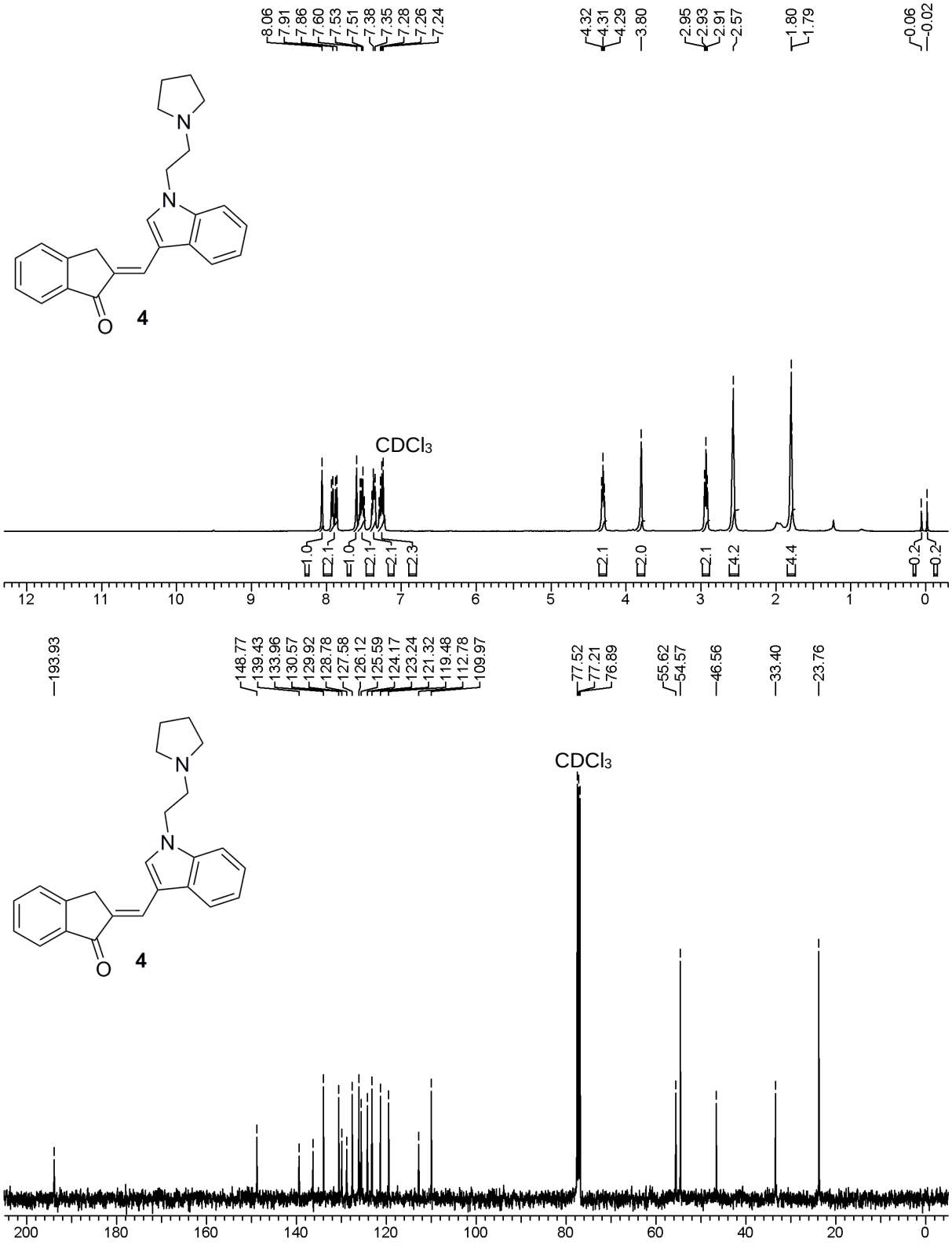

^{1}H & ^{13}C spectra of compound 5 (G - Grease)

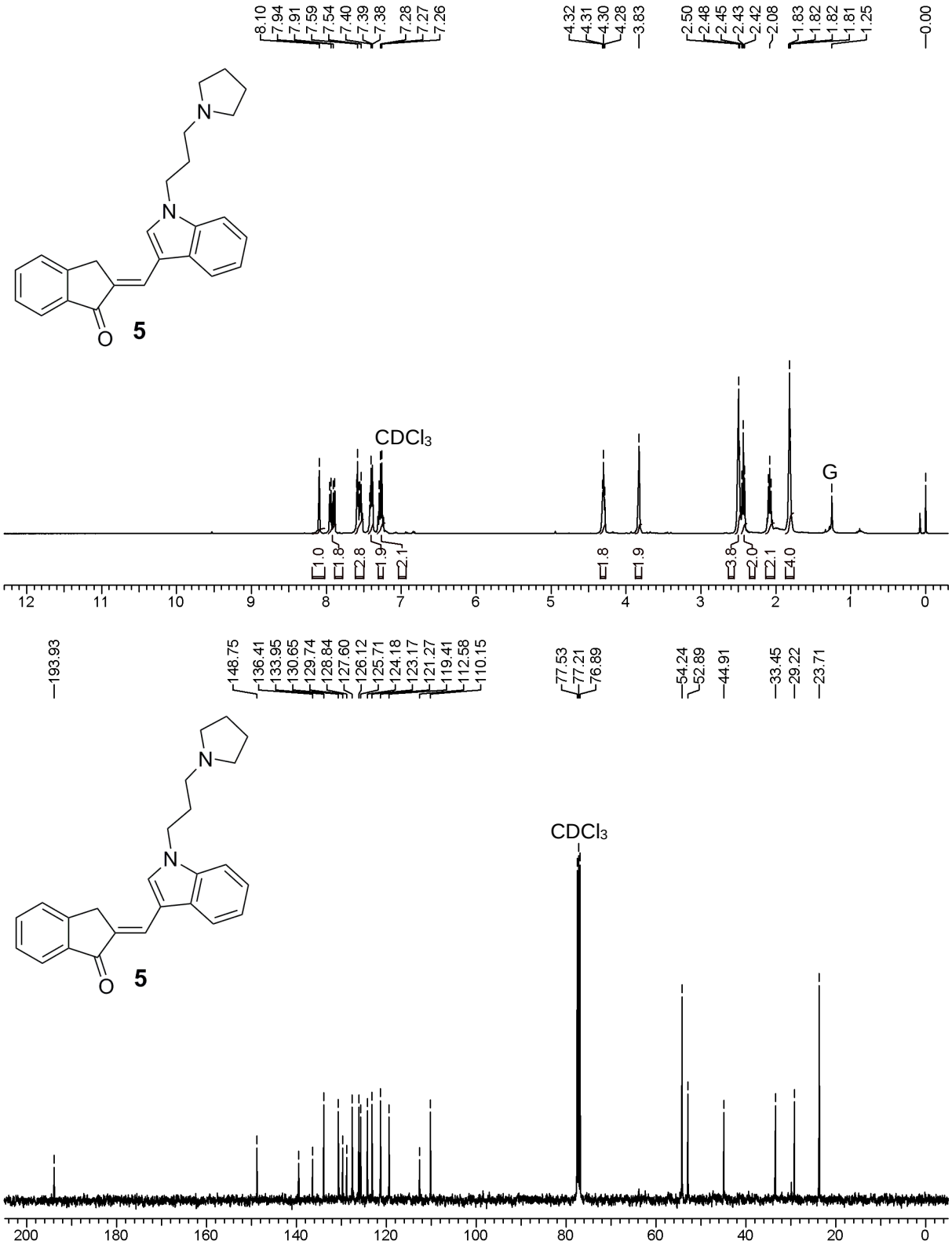

^{1}H & ^{13}C spectra of compound InEt1

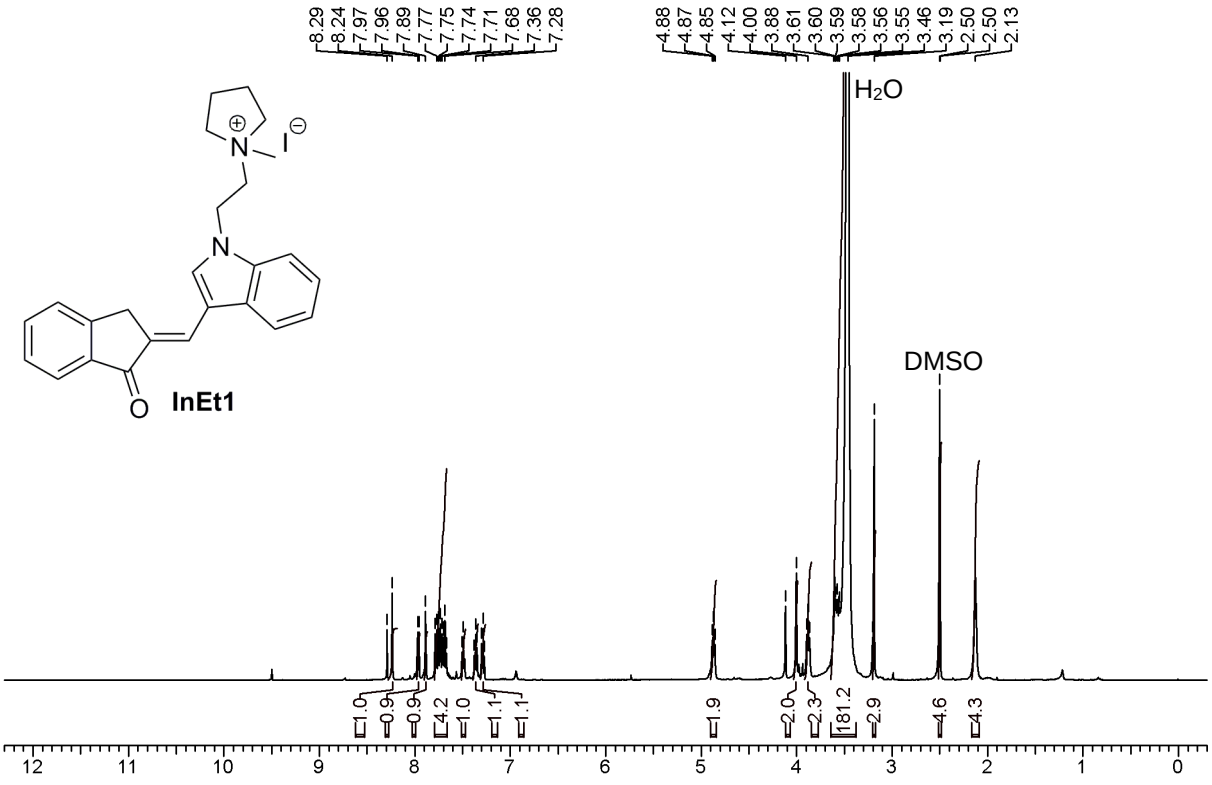

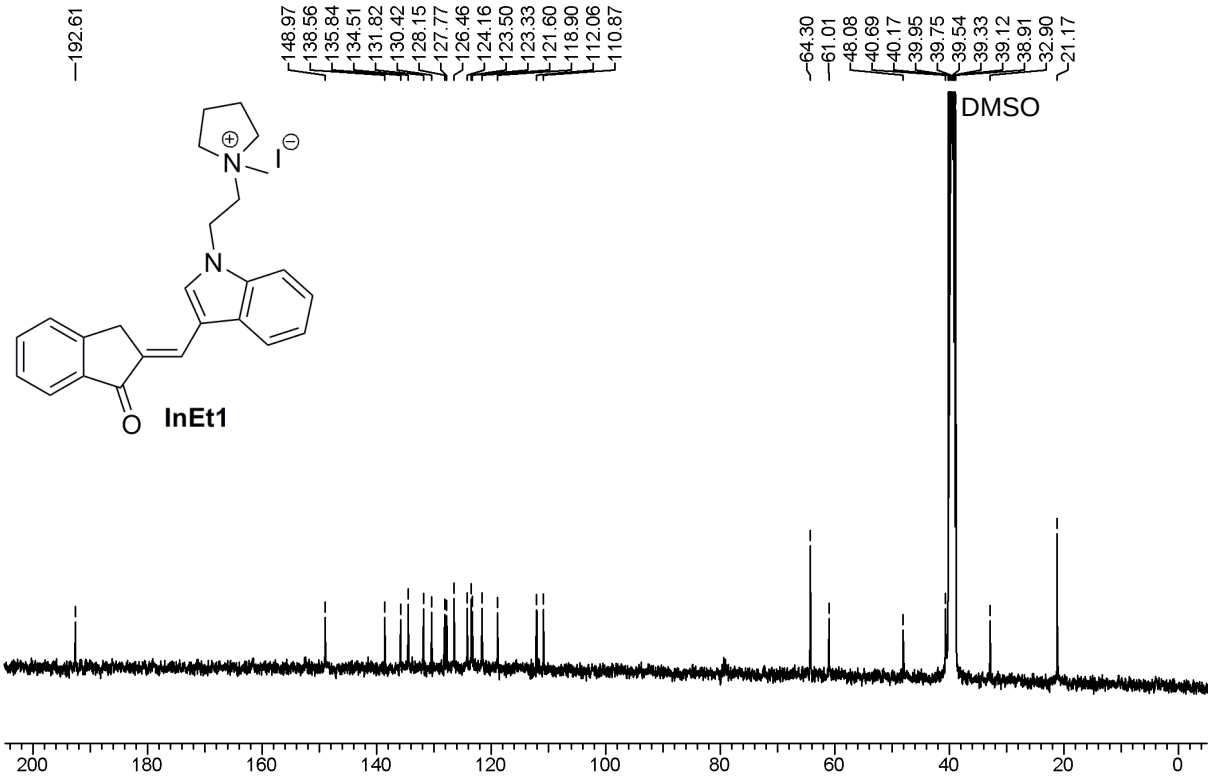

^{1}H & ^{13}C spectra of compound InPr1

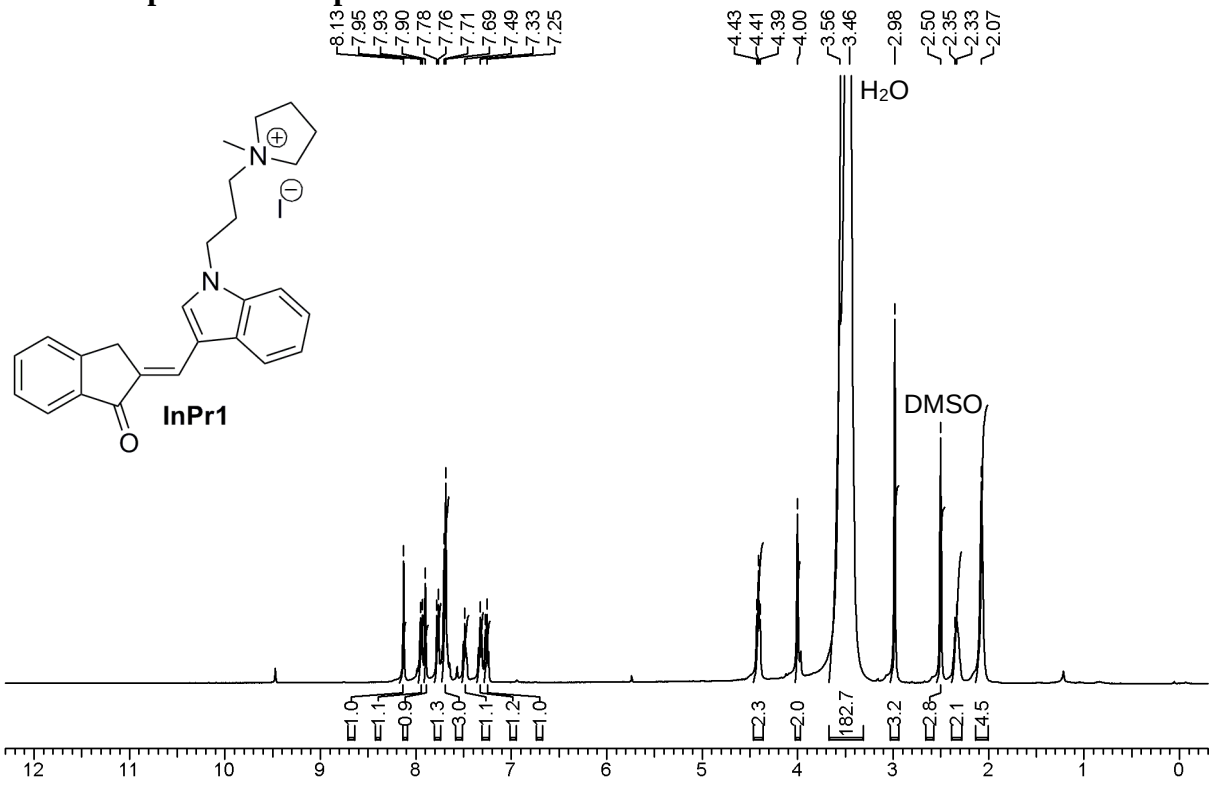

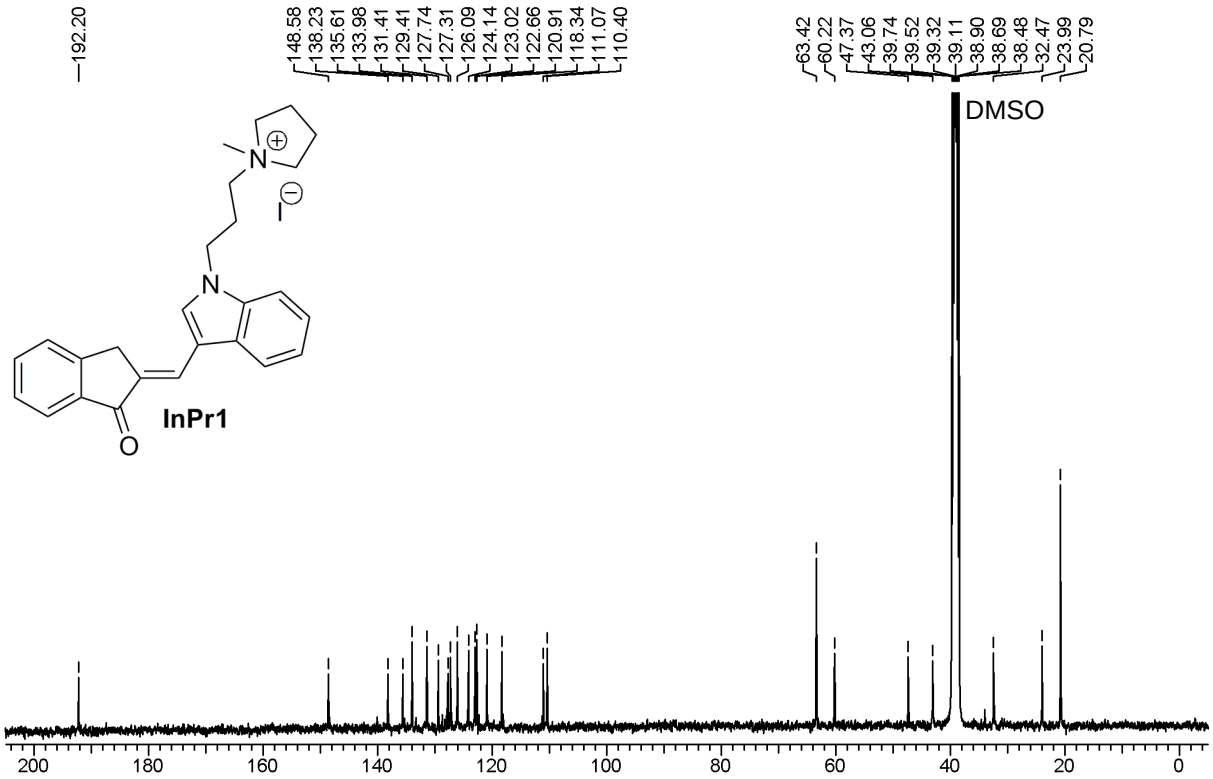

^{1}H & ^{13}C spectra of compound 10 (G - Grease)

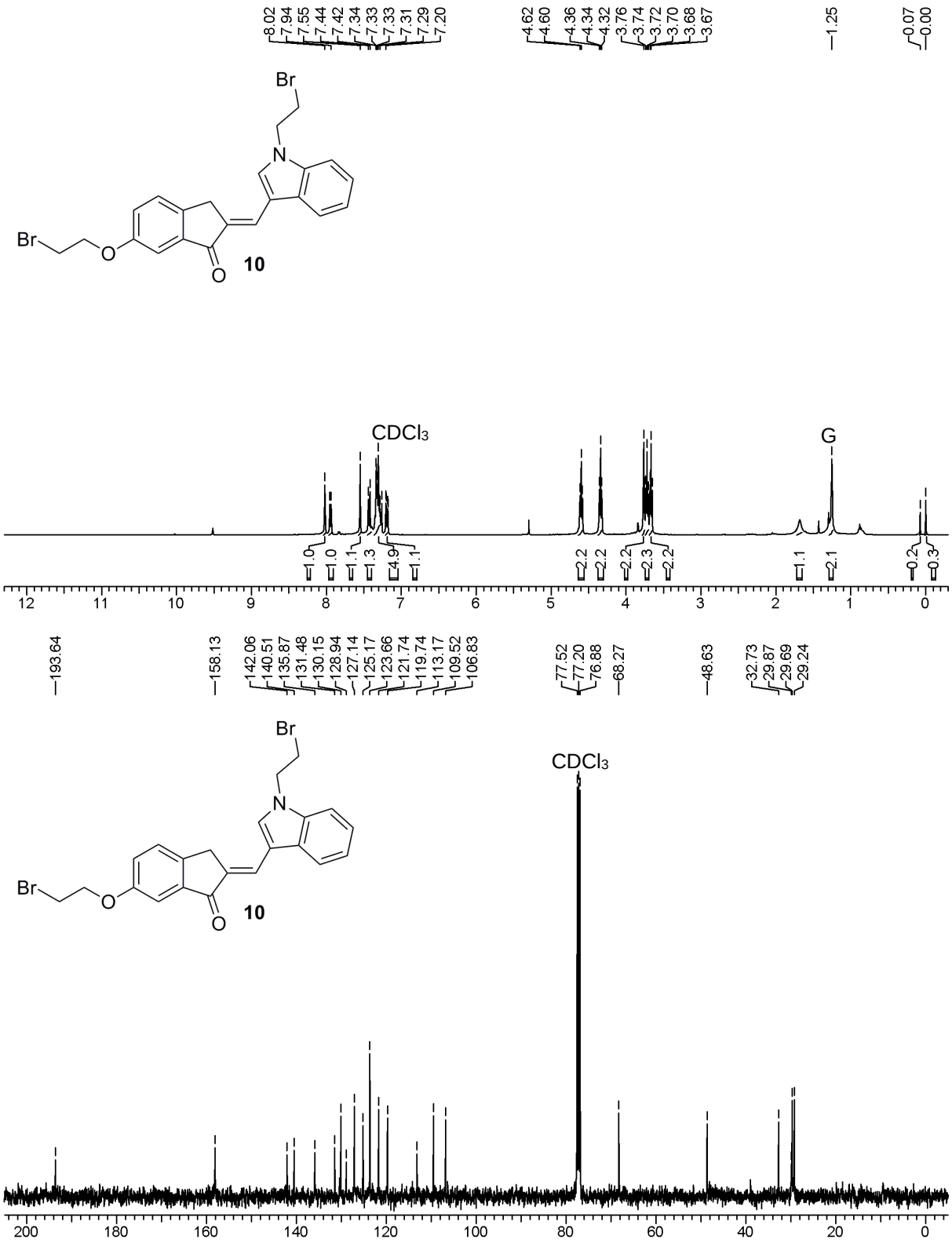

^{1}H & ^{13}C spectra of compound 11

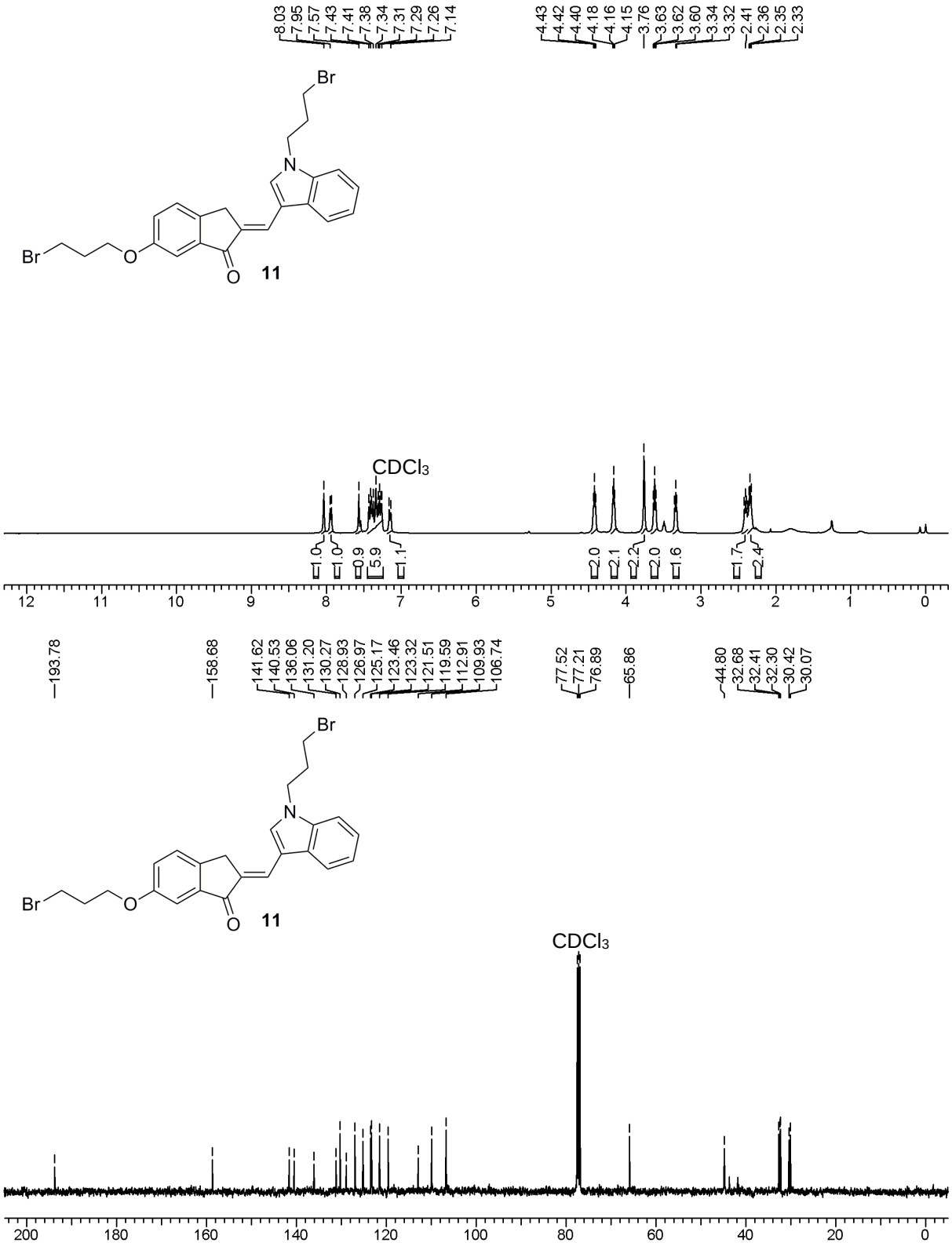

^{1}H & ^{13}C spectra of compound 12 (G - Grease)

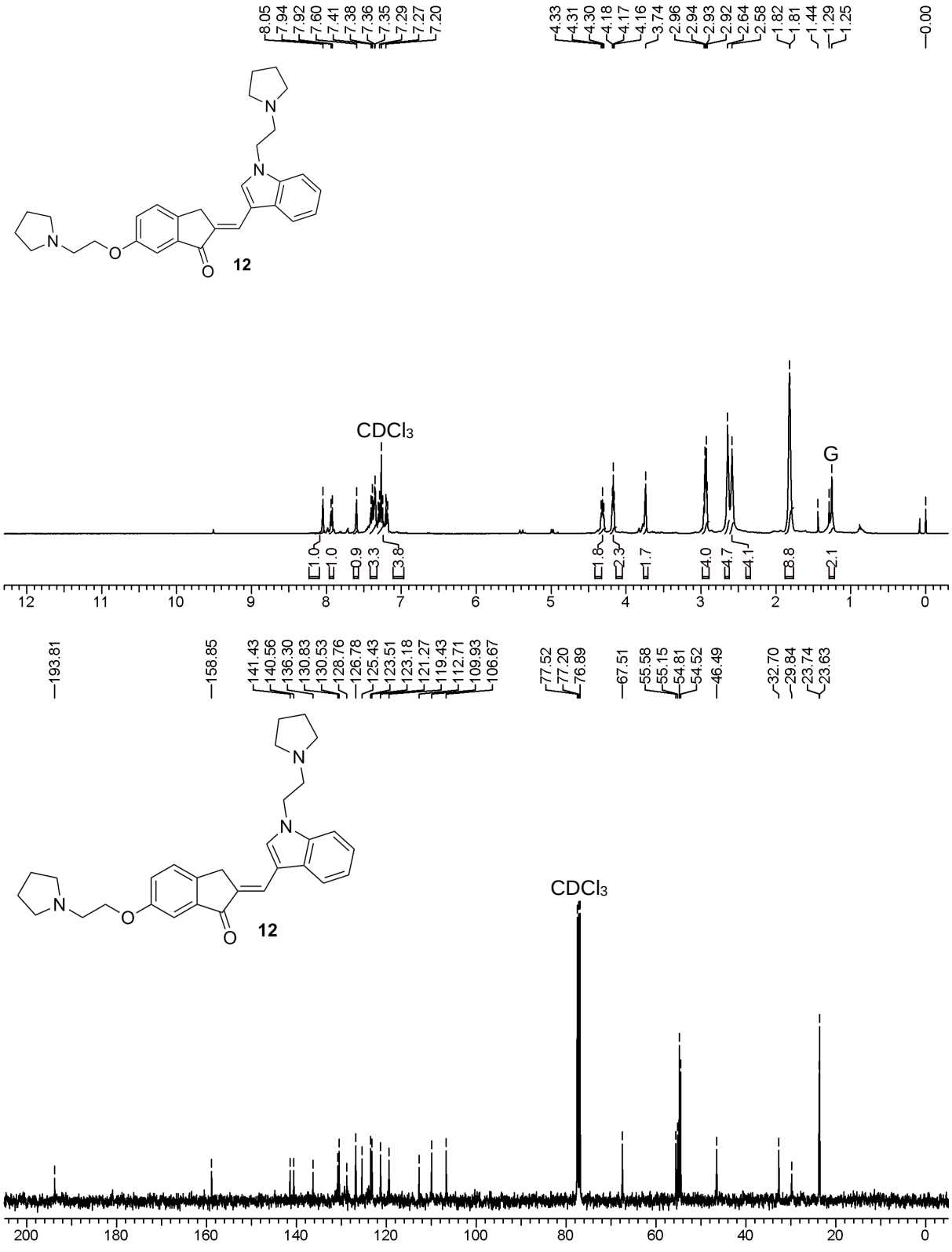

^{1}H & ^{13}C spectra of compound 13

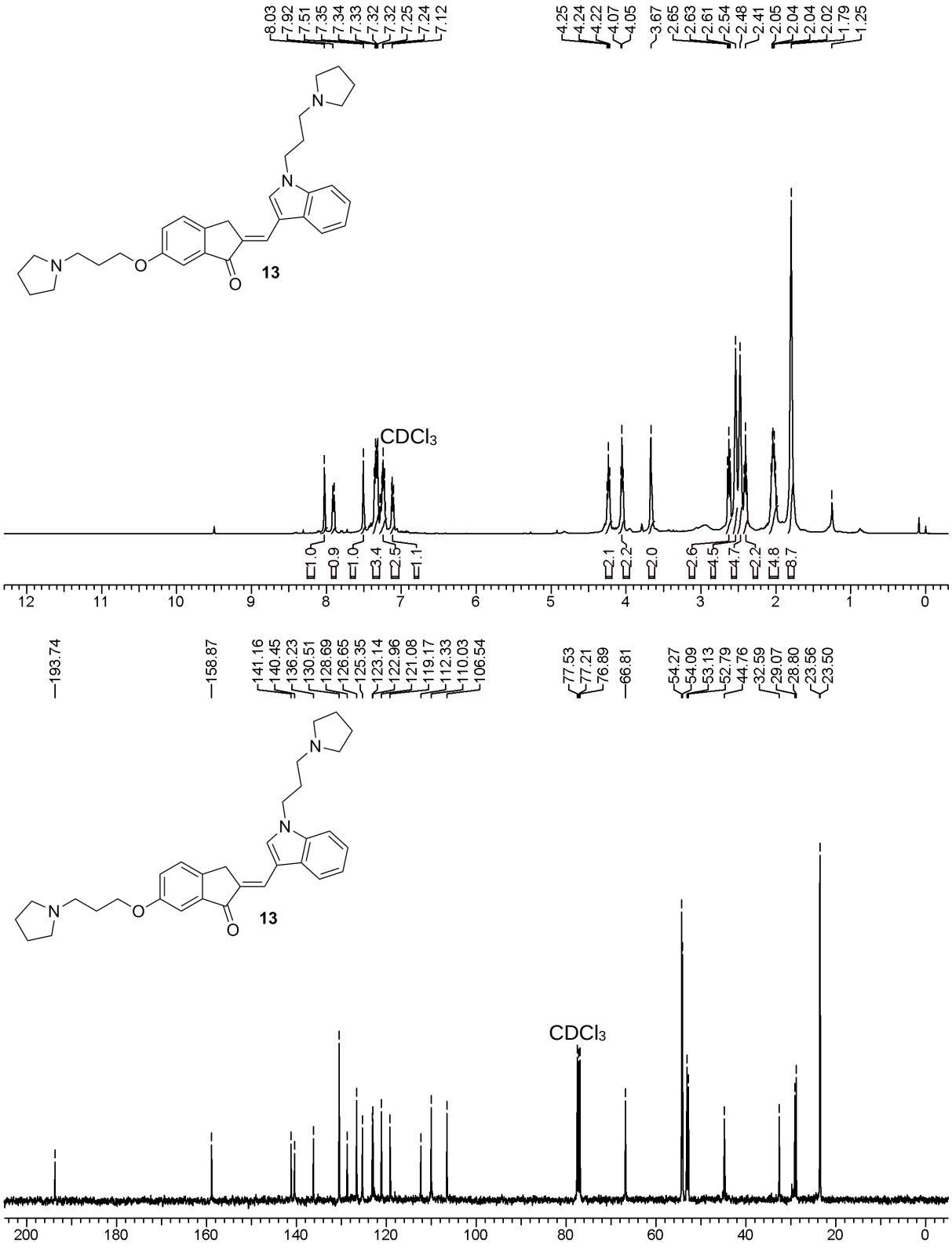

^{1}H & ^{13}C spectra of compound InEt2

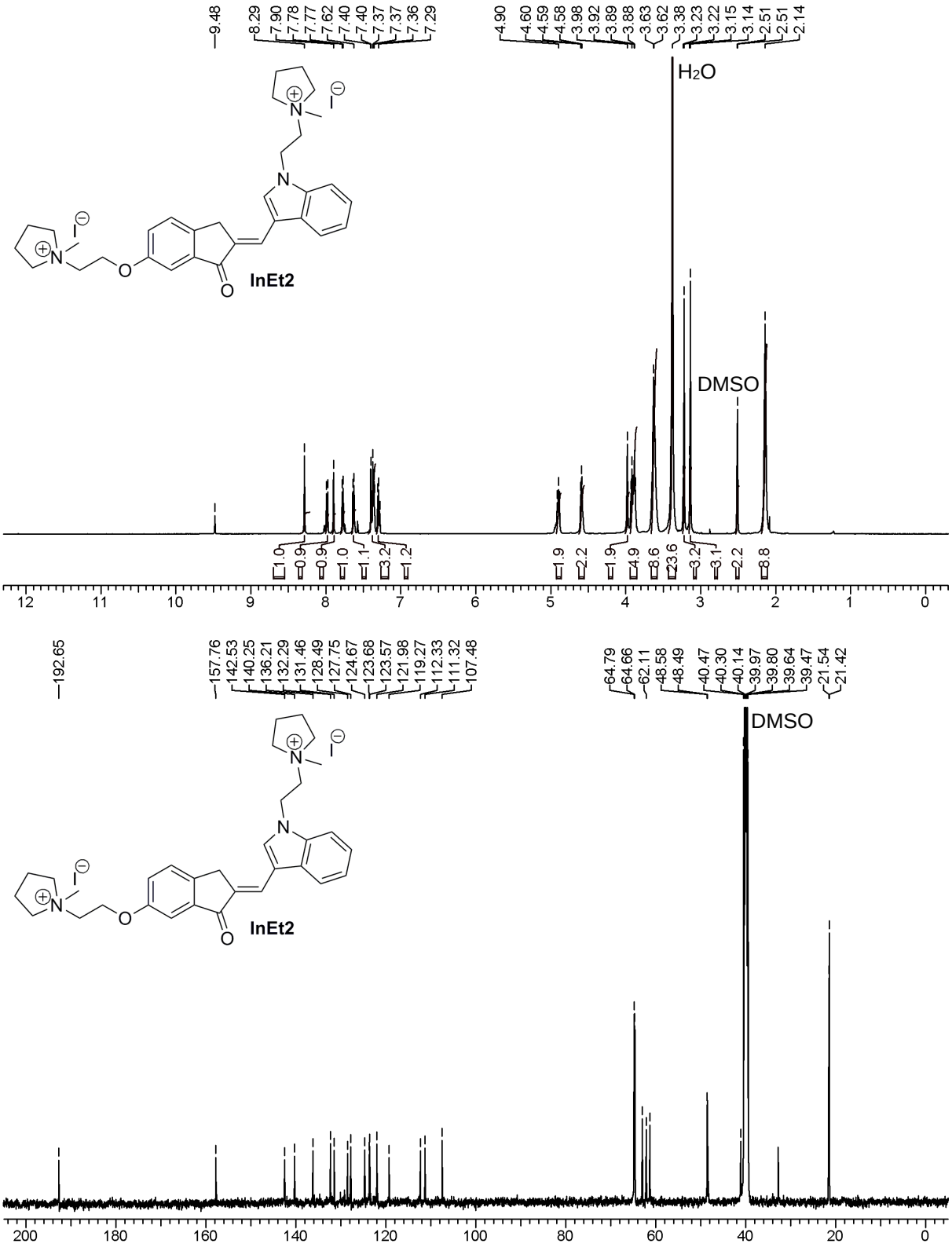

^{1}H & ^{13}C spectra of compound InPr2